

A FOURIER TRANSFORM SPECTROMETER FOR
MILLIMETER AND SUBMILLIMETER WAVELENGTHS

by

DAVID HOPKINS SHOEMAKER

SUBMITTED IN PARTIAL FULFILLMENT
OF THE REQUIREMENTS FOR THE
DEGREE OF

MASTER OF SCIENCE

at the

MASSACHUSETTS INSTITUTE OF TECHNOLOGY

August 1980

© Massachusetts Institute of Technology 1980

Signature of Author _____ Department of Physics
August 8, 1980

Certified by _____ Rainer Weiss
Thesis Supervisor

Accepted by _____ George Koster

ARCHIVES Chairman, Department Committee
MASSACHUSETTS INSTITUTE
OF TECHNOLOGY

SEP 24 1980

LIBRARIES

A FOURIER TRANSFORM SPECTROMETER FOR
MILLIMETER AND SUBMILLIMETER WAVELENGTHS

by

DAVID HOPKINS SHOEMAKER

Submitted to the Department of Physics
on August 15, 1980 in partial fulfillment of the
requirements for the Degree of Master of Science in
Physics

ABSTRACT

The design and testing of an interferometer for the range from 1 to 100 inverse centimeters is described. The apparatus is a polarizing Michelson interferometer in a symmetrized design, used in the rapid scan mode. It has an optical throughput of $.5 \text{ cm}^2\text{-sr}$, and a resolution of $.1 \text{ cm}^{-1}$ at 20 cm^{-1} .

The interferometric and geometric properties of the design are discussed. The experimental results include the measurement of the efficiency, high and low frequency response, frequency distortions, and resolution. The instrument transfer function is close to theoretical performance. Appendices describe a technique for constructing large free standing wire grid polarizers, alignment and operating procedures, and computer models of sampling errors.

Thesis Supervisor: Dr. Rainer Weiss

Title: Professor of Physics

TABLE OF CONTENTS

| | |
|---|------------|
| Introduction | 3 |
| The Nature of the Instrument | 6 |
| Specifics of the Design | 13 |
| Interferotometric Properties | 13 |
| Geometric Optical Design | 20 |
| The Instrument Transfer Function | 35 |
| Measurement of the Efficiency | 35 |
| High Frequency Response | 71 |
| Low Frequency Response | 97 |
| Frequency Distortions | 109 |
| Resolution | 115 |
| | |
| Appendices | 117 |
| Sampling Errors | 117 |
| Individual Optics Tests | 131 |
| Polarizer Construction | 132 |
| Alignment of the Interferometer | 139 |
| Instruction Manual | 144 |

INTRODUCTION

The instrument to be discussed is designed to measure the cosmic background radiation in the range from 1.5-100 inverse centimeters (icm) from an earth satellite. Quite a number of ground and balloon based measurements have been made; however, the opacity of the atmosphere prevents ground based measurements above a few icm, and the brief observing times and difficult experimental conditions prevent balloon measurements from achieving high absolute accuracy. The Cosmic Background Explorer satellite will provide a stable platform for a precise measurement. The FIRAS (for Far Infrared Absolute Spectrometer) will measure the background to one part in one thousand over one thousand angular resolution elements in the sky in the period of one year, with a resolution of .2 icm.

There are some novel aspects of the design, which is based on suggestions from John Mather of NASA. The first of this kind of interferometer is described here. The spectrometer must operate satisfactorily well into the diffraction regime and with a large etendue. The difficulty in diffraction calculations and with predicting the response in general made the construction and testing of a breadboard of the instrument imperative. This document is primarily a report of the results of these measurements.

Because the spectrum of the CBR (Cosmic Background Radiation) has already been determined to be close to a thermal spectrum of temperature 2.8 degrees K, the new measurement is best made by finding the difference between the CBR and a black body reference whose temperature can be varied around 2.8 degrees K to minimize the difference. To achieve this end the spectrometer has two inputs which are differential; one input will be fed by the reference and the other by a horn looking at the CBR or a BB calibrator. To ensure that the differencing be as free as possible of errors, the spectrometer is completely symmetric with respect to the inputs. There are a number of advantages to this arrangement. First, since most of the frequency distortions introduced by the interferometer are proportional to the net power at the detectors, the influence of these distortions is minimized by looking at the small difference signal, which will be on the order of a few percent of either signal alone. Secondly, the detector system dynamic range need only be as large as the difference signal and not the total signal. The symmetry yields two outputs. The difference in the two outputs is the difference signal desired. The sum of the two outputs is the difference signal desired. The sum of the two outputs is a measure of the total power through the interferometer; this can be used as a broadband photometer signal to keep track of the total flux through the device.

The connection to absolute quantities and the final measurement of the instrument response is made with a calibrator BB which is the primary reference for the experiment. During the flight the calibrator can be placed to fill the input sky horn, and a calibration made of the instrument and its reference. The instrument and reference then must remain stable from calibration to calibration. It is the accuracy to which this calibrator is known that ultimately determines the accuracy of the COBE measurement.

Because the CBR has such a small absolute intensity ($1 \times 10^{-11} \text{ W/cm}^2\text{-sr}$) and the state of the art bolometers operating at the COBE dewar design temperatures of 1.6 to 1.8 degrees K have NEP's in the range of 1×10^{-14} , the spectrometer must have a large throughput if the measurement to the desired precision is to be made in the available amount of time. This instrument is designed to have an etendue of $.5 \text{ cm}^2\text{-sr}$, sufficient for the required sensitivity of $\nabla I_\nu = 1 \times 10^{-13} \text{ watts/cm}^2\text{-sr}$.

1) THE NATURE OF THE INSTRUMENT

The spectrometer is an interferometer: the spectrum is obtained by fourier transformation of the interferogram. Why an interferometer rather than, say, a grating spectrometer? An interferometer collects information over the entire range of input frequencies throughout a scan, in contrast to a grating spectrometer which with one detector can only measure the intensity in one frequency resolution element at a time. This so called multiplex advantage is necessary to obtain the desired signal to noise; the advantage is $n^{1/2}$, where n is the number of spectral points. Furthermore, the throughput of a grating spectrometer must go down as the resolution is increased (i.e. as the input slit is narrowed); the resolution of an interferometer depends on the amount of path length difference that can be achieved, until the shear condition that is exceeded. To get a similar resolution and throughput from a grating instrument would require multiple detectors. These features allow a high resolution wide frequency range measurement to be made without sacrificing throughput. Most importantly, the broad frequency range (roughly 7 octaves) required for this measurement would be impossible to achieve in a grating instrument without order sorting.

There are some dangers in using Fourier transform spectroscopy. Since small deviations from a black body spectrum

are being measured, very little frequency distortion by the spectrometer is tolerable. Stray reflections from surfaces in or near the spectrometer, producing spurious signals. Any electrical signals out of the detectors which are correlated with the change in optical path in the interferometer appears as signal in the interferogram, and are not averaged out: if there is microphonic pickup, or defocussing of the beam, there will be false spectral information. However, the symmetry of the design minimizes these problems, and careful measurements with a known calibrator should allow remaining distortions to be removed.

Once FTS has been chosen, the decision to step and chop or rapid scan must be made. In the former mode, each point in the interferogram is measured by comparing the CBR signal with a reference by the use of a chopper. This chopper frequency is chosen to be at the optimum frequency for the detector: above 1/f noise and below the cutoff imposed by the detector thermal time constant. Thus only half of the measurement time is spent looking at the CBR. When rapid scanning, the carriage is moved at a constant speed such that the modulation of the beam interferometrically produces an A.C signal containing the spectral information. All of the observation time is spent collecting data in this mode of operation except for a short time at the end of the scan. Also, the time for a scan is reduced

significantly from the slow scan mode. If, for instance, an object swings through the field of view, or a brief electrical problem distorts the detector output, the disturbance can be edited without throwing away much data. Any noise before the detector whose amplitude grows at lower frequency is attenuated; the temperature fluctuations on the interferometer surfaces are an example. There are also fewer moving parts.

The drawbacks in rapid scanning lie primarily with the way the detector system is used. There is a linear relationship between optical input frequency and audio output frequency from the interferometer. At low audio frequencies the $1/f$ noise in the detector-amplifier combination becomes significant; at high frequencies the detector thermal time constant will attenuate the signal. Consequently, there is a limited range of audio frequencies and hence optical frequencies that are detectable with a good signal to noise. Another problem is that jitter or speed variations in the transport for the mirrors will cause distortions in the spectrum, and scan synchronous microphonic pickup is more likely. Despite these problems, the speed of data collection and the greater optical efficiency suggests RS FTS for the COBE instrument.

A polarizing Michelson interferometer is chosen because of its smooth response over a broad band. The efficiency of an interferometer goes as the reflection times the transmission of

the beamsplitter; the beam must be evenly split for high efficiency. With a conventional pellicle beamsplitter (BS) the reflection at low frequency approaches zero and varies cyclically as the frequency increases. This means that the efficiency is poor for wavelengths long compared with the optical thickness of the BS, and is uneven throughout. In contrast, wire grid polarizers for the far infrared are most efficient at long wavelengths and have a smoothly varying response over many octaves. This is particularly important for the CBR measurement because the power of the BB is very small at long wavelengths.

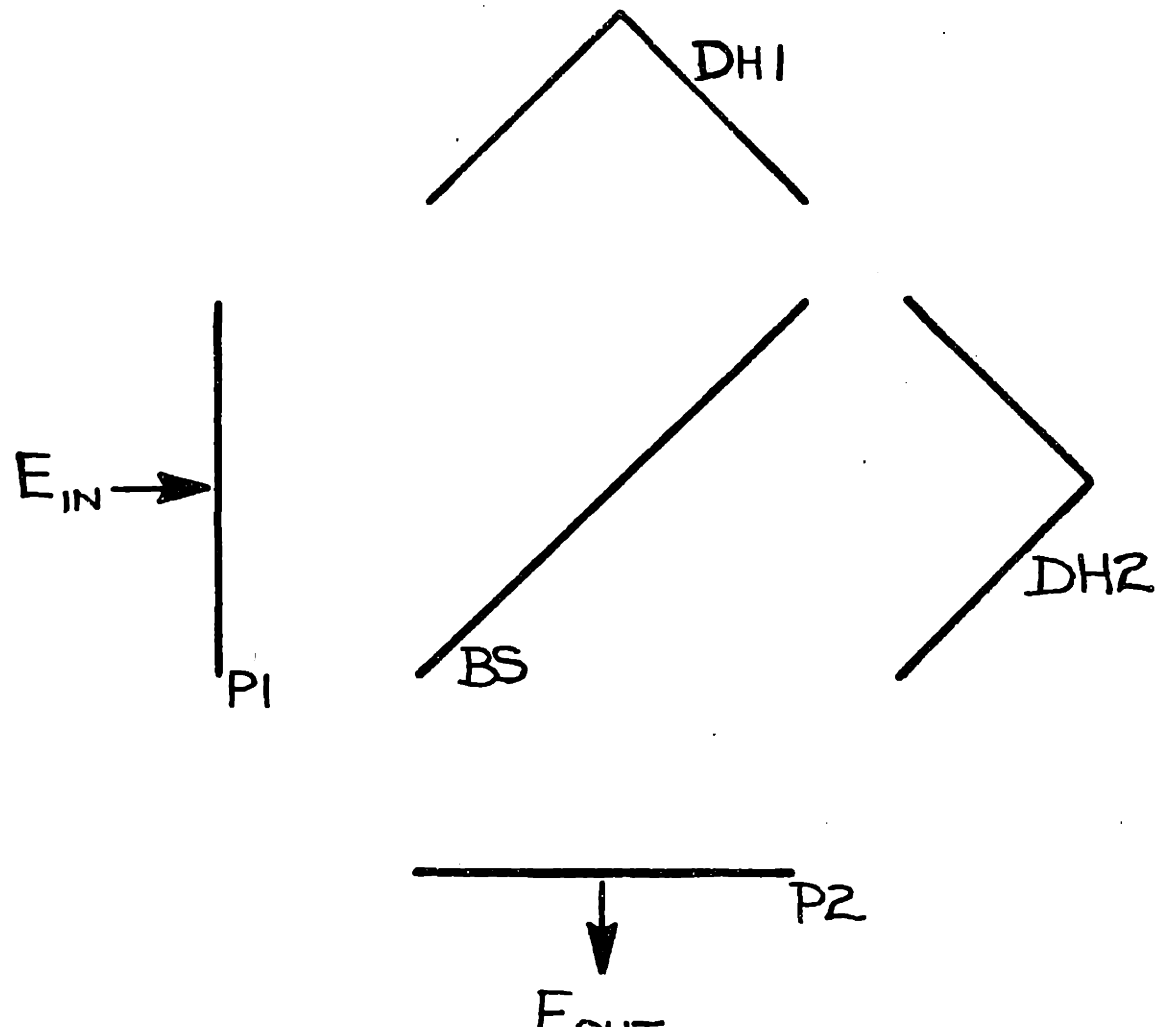
To illustrate the functioning of a PMI, consider the simple Martin-Puplett design (figure 1). P1 and P2 are polarizers at 45 degrees to the normal \hat{n} of the paper; call their axis \hat{p} . The beamsplitter is also a polarizer, with its wires normal to the paper. Call the perpendicular in the paper to the direction of propagation \hat{s} . Then after P1 we have

$$\begin{aligned} E &= A \hat{p} \cos(\omega t) \\ &= A/\sqrt{2} * (\hat{n} + \hat{s}) \cos(\omega t) \end{aligned}$$

After reflection from the dihedrals and recombining at the beamsplitter,

$$\begin{aligned} E_{\text{delayed}} &= A/\sqrt{2} (\hat{n} \cos(\omega t + 2\pi x_1/\lambda) \\ &\quad + \hat{s} \cos(\omega t + 2\pi x_2/\lambda)) \end{aligned}$$

where x_1 and x_2 are the distances from the BS to DH₁ to BS and BS to DH₂ to BS respectively. When reanalyzed by p2, one has



POLARIZING MICHELSON
INTERFEROMETER

Figure 1

$$\begin{aligned}\vec{E}_{\text{out}} &= \hat{p} (\vec{E}_{\text{delayed}} \cdot \hat{p}) \\ &= \hat{p} A \cos(\omega t + 2\pi(x_1 + x_2)/\lambda) * \cos(\pi(x_1 - x_2)/\lambda)\end{aligned}$$

so

$$\langle E_{\text{out}} \rangle^2 = A^2/2 (1 + \cos(2\pi(x_1 - x_2)/\lambda))$$

So the device acts as an interferometer. When there is constructive interference, an interesting property appears.

Because the dihedrals rotate the axis of polarization by 90 degrees, the beam that made it through the beamsplitter before now reflects, and the previously reflected one now is along the easy axis, so that all of the input that made it past the first beamsplitter appears at the output. When the interference is destructive, all of the input is returned to the input port.

There is the disadvantage that only one polarization of the input beam is accepted; this makes the instrument only 50 % efficient for an input of random polarization, and polarization sensitive to the instrument orientation for a polarized source.

2) SPECIFICS OF THE DESIGN

INTERFEROTOMETRIC PROPERTIES:

To overcome the loss of the other polarization and to allow differential inputs and outputs, a symmetrized version of the PMI was designed (figure 2). The light from an input is collimated by $M1_+$. It is divided into x and y polarizations at the IPOP, focussed by the two $M2$'s onto the two DH after having been analyzed into components at 45 degrees to x and y by the BS. The two beams are recombined after experiencing the delay of the difference in path to $DH+$ and $DH-$ at the BS, recollimated by $M2$, analyzed into x and y by the IPOP, and focussed by $M1$ onto the outputs. To separate the inputs and outputs, the input and output signal are injected 4.8 degrees on either side of the focal point of the input mirror $M1$. This causes the collimated beam to be directed down. When it reaches the DH, it bounces from the lower mirror to the upper mirror, and returns eventually to the other side of the focal point of $M1$, thus achieving the input--output separation.

The device has two symmetries: one about the dividing line between plus and minus sides (horizontally) and one about the dividing line between upper and lower beams (vertically). One can exploit these symmetries in this unfolded drawing of figure 3. The interferometer is labeled so that signals above the vertical

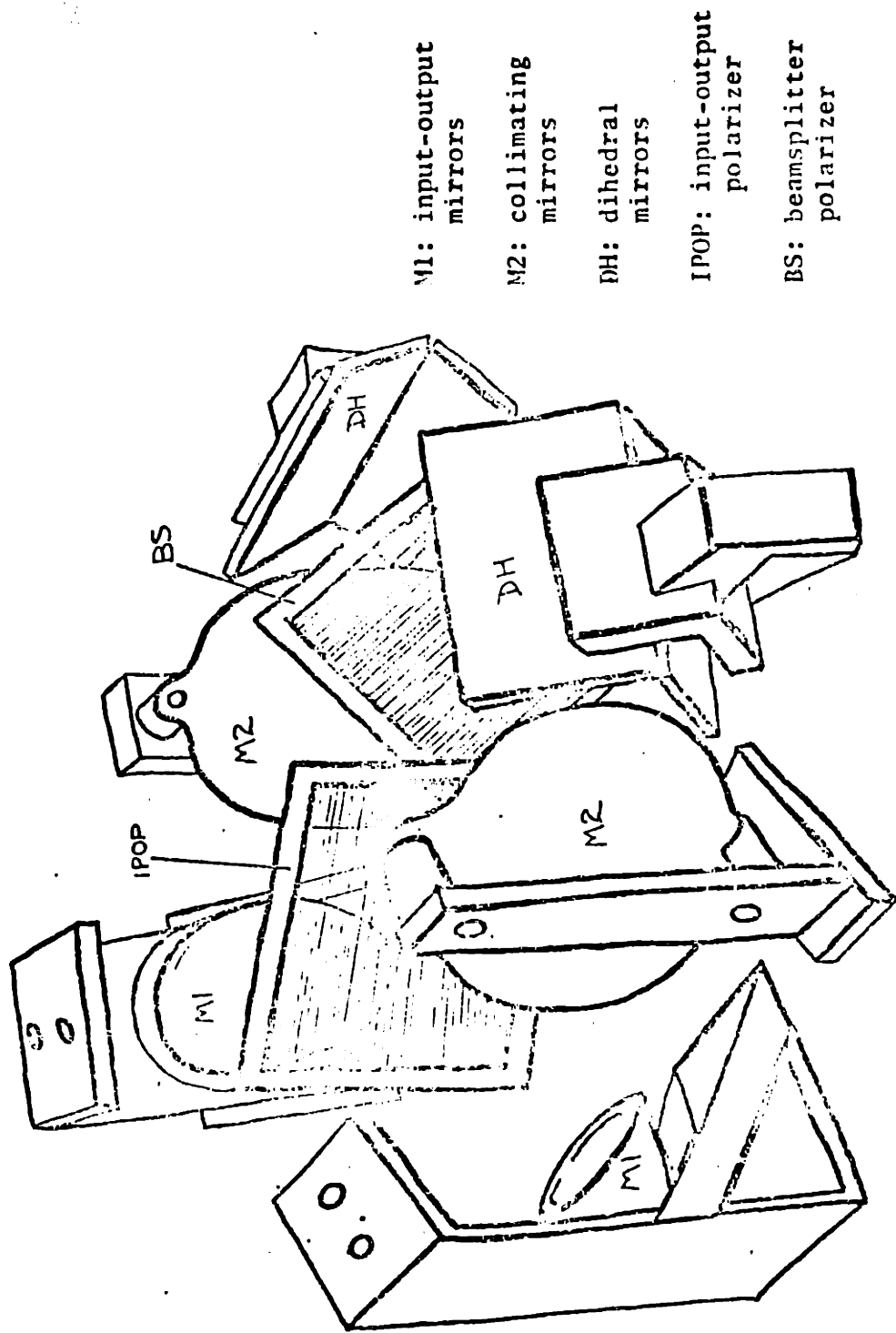
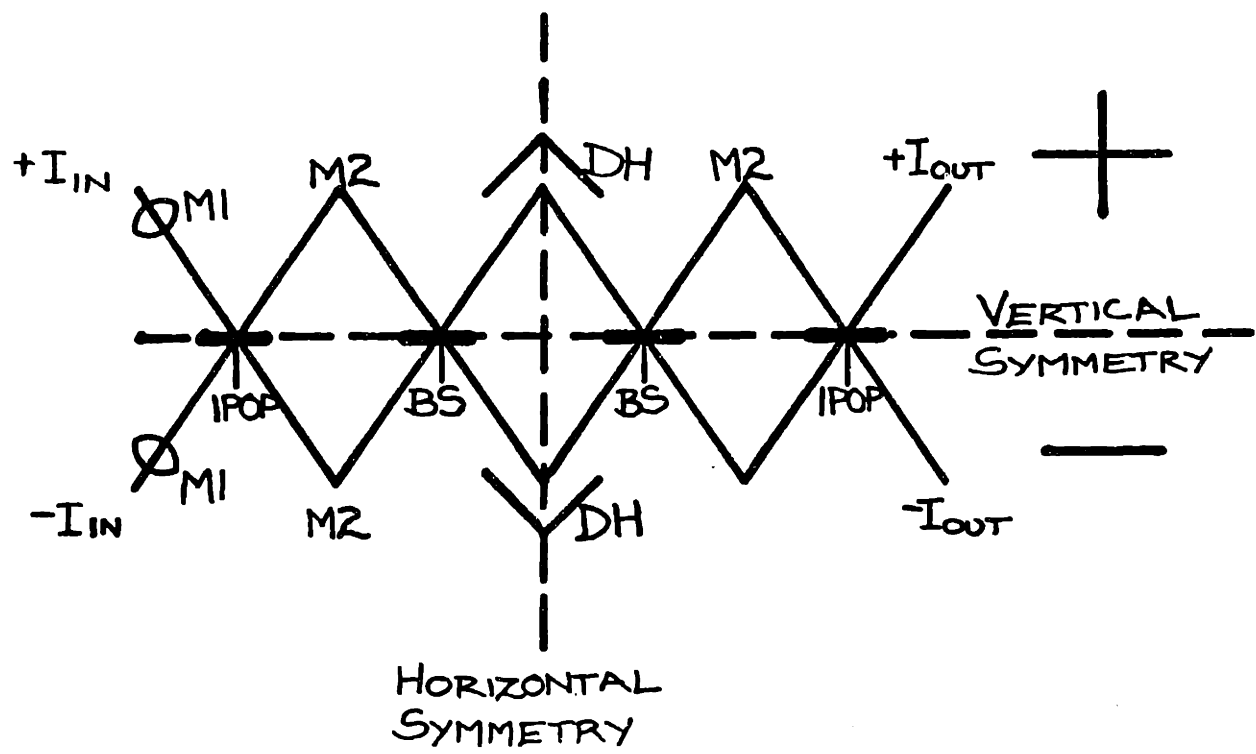


Figure 2



UNFOLDED DRAWING OF
COBE INTERFEROMETER

Figure 3

line of symmetry carry the subscript + and those below -.

The two polarizations of the electric field are subscripted x and y.

One can qualitatively see how the device captures both polarizations. For a single unpolarized input, say I+, the beam impinges on IPOP and is split into X and Y polarizations. From here on in, the instrument looks like the simple PMI discussed earlier, only now there is an interferometer for each polarization. When there is no delay, all the signal appears at the - output as in the simple PMI; if the delay is $\lambda/2$, all of the signal returns to the + side but appears at the + output rather than the + input because of the 9.5 degree shift.

A convenient technique for a more complete analysis uses matrix methods. Initially, the optical components will be assumed to be perfect so that the basic features of the instrument can be illustrated. When later discussing imperfections, the method will be expanded to encompass some analytically tractable problems.

The input vector will be written

$$E_{in} = \begin{pmatrix} E_{+x} \\ E_{+y} \\ E_{-x} \\ E_{-y} \end{pmatrix}$$

so that the two polarizations of the two inputs can be accounted for.

To generate a matrix for an optical element, the coefficient relating each input direction and polarization to each output direction and polarization must be known. Then the first row is the set of coefficients for E_{+xout} in the order of the input vector:

$$\alpha_{11} = E_{+xout}/E_{+xin}$$

$$\alpha_{12} = E_{+xout}/E_{+yin}$$

$$\alpha_{13} = E_{+xout}/E_{-xin}$$

$$\alpha_{14} = E_{+xout}/E_{-yin}$$

The next row is for E_{+yout} , and so on.

The DH are set up with the vertex of the two mirrors in the x plane, causing x polarized radiation to be returned as it was incident; y polarized radiation returns flipped in phase:

$$DH = \begin{pmatrix} 1 & 0 & 0 & 0 \\ 0 & -1 & 0 & 0 \\ 0 & 0 & 1 & 0 \\ 0 & 0 & 0 & -1 \end{pmatrix}$$

A polarizer with its wires along the Y axis has a reflectivity of -1 (minus for the change in phase upon reflection) for Y (parallel) radiation, and a transmission of 1 for x (perpendicular) radiation. This leads to a matrix:

IPOP=

$$\begin{pmatrix} 0 & 0 & 1 & 0 \\ 0 & -1 & 0 & 0 \\ 1 & 0 & 0 & 0 \\ 0 & 0 & 0 & -1 \end{pmatrix}$$

Notice that here E_{-xin} is returned to E_{tout} ; transmission through the polarizer puts radiation on the other side of the vertical symmetry.

If the polarizer is at 45 degrees, as the BS is, the matrix must be rotated with a coordinate transformation. The result is

BS= 1/2

$$\begin{pmatrix} -1 & 1 & 1 & 1 \\ 1 & -1 & 1 & 1 \\ 1 & 1 & -1 & 1 \\ 1 & 1 & 1 & -1 \end{pmatrix}$$

Since the paths for all radiation are the same except for the delay between the DH and the BS, the only propagator that needs to be retained is the one that represents that path. If x is the total path length difference for a displacement of the carriage, for $\delta = 2\pi x/\lambda$ the propagator is

PROP=

$$\begin{pmatrix} e^{i\delta/2} 0 & 0 & 0 \\ 0 & e^{i\delta/2} 0 & 0 \\ 0 & 0 & e^{-i\delta/2} 0 \\ 0 & 0 & 0 & e^{-i\delta/2} \end{pmatrix}$$

If now the input vector is put through the interferometer

$$E_{out} = (IPOP)(BS)(PROP)(DH)(PROP)(BS)(IPOP)(E_{in})$$

One finds that

$$E_{out} = \begin{cases} E_{-x}\cos\delta - iE_{+y}\sin\delta \\ -E_{-y}\cos\delta - iE_{+x}\sin\delta \\ E_{+x}\cos\delta + iE_{-y}\sin\delta \\ -E_{+y}\cos\delta + iE_{-x}\sin\delta \end{cases}$$

The intensity at the output as detected by a polarization insensitive detector is

$$\begin{aligned} I_{+out} &= (E_{-x}^2 + E_{-y}^2)\cos^2\delta + (E_{+x}^2 + E_{+y}^2)\sin^2\delta \\ &= 1/2(I_+ + I_-) + 1/2(I_- - I_+)\cos 2\delta \end{aligned}$$

$$I_{-out} = 1/2(I_+ + I_-) - 1/2(I_- - I_+)\cos 2\delta$$

$$\text{where } I_+ = (E_{+x} \text{ in})^2 + (E_{+y} \text{ in})^2$$

$$\text{and } I_- = (E_{-x} \text{ in})^2 + (E_{-y} \text{ in})^2$$

If there are detectors at both output ports, and their sum and difference are obtained, one sees

$$I_{\text{common mode}} = I_{+out} + I_{-out} = I_+ + I_-$$

$$I_{\text{differential}} = (I_- - I_+)\cos 2\delta$$

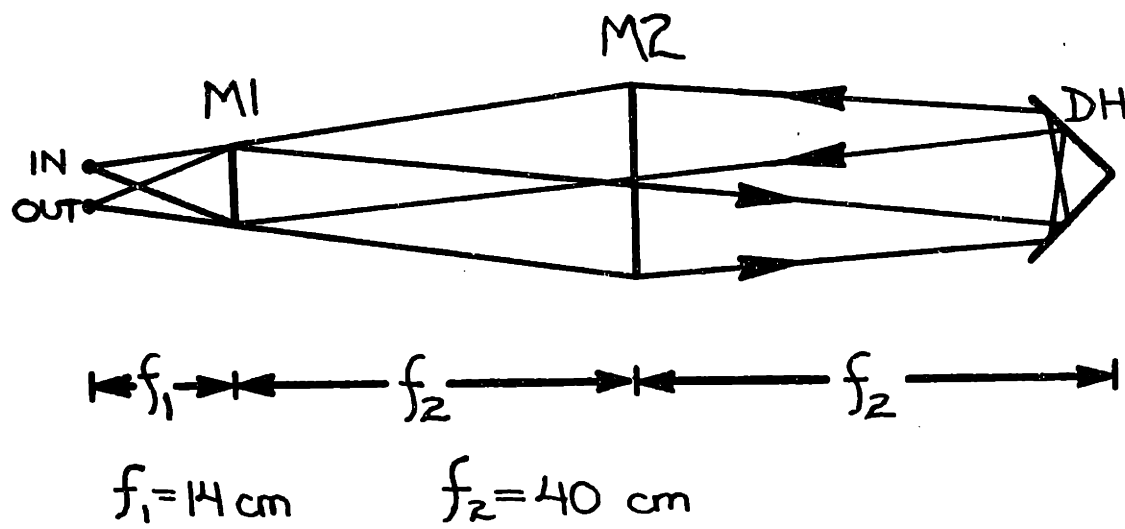
This illustrates the previously mentioned features: a monitor on the total power through the device, and a differential input interferometer.

GEOMETRIC OPTICAL DESIGN

Fundamentally, the system is simple. A schematic view of the optics is shown in figure 4. The source is placed at the focal point of M1; this produces a collimated beam. It passes through the IPOP and hits M2. It is focussed down onto the DH, and then retraces its path back to the focal point of M1.

In practice, there are some subtleties. First, the mirrors are paraboloids used far off axis (see figure 5). Also, the system is not fed right at the focal point of M1 but instead at an angle (to allow separation of the input and output) (see figure 6). This separation, and the focal length of M1, must be large enough to allow dichroic filters to be placed in the output beam to separate the beam into 0-20 and 20-100 icm bands. This is to reduce somewhat the demand on the detectors. The large etendu leads to a big solid angle, so much of the light is not paraxial anyway. These nuances complicate the understanding of the geometric optics. To get a quantitative view of what the light paths are under various conditions, a computer program has been written to do ray tracing.

The program allows a random set of rays of a given maximum radius and angle to be launched from a source, and propagated through a system of mirrors. The mirrors can be spherical, parabolic, flat, dihedral, trihedral, ellipsoidal, or toroidal,



GEOMETRIC OPTICS:
SCHEMATIC VIEW

Figure 4

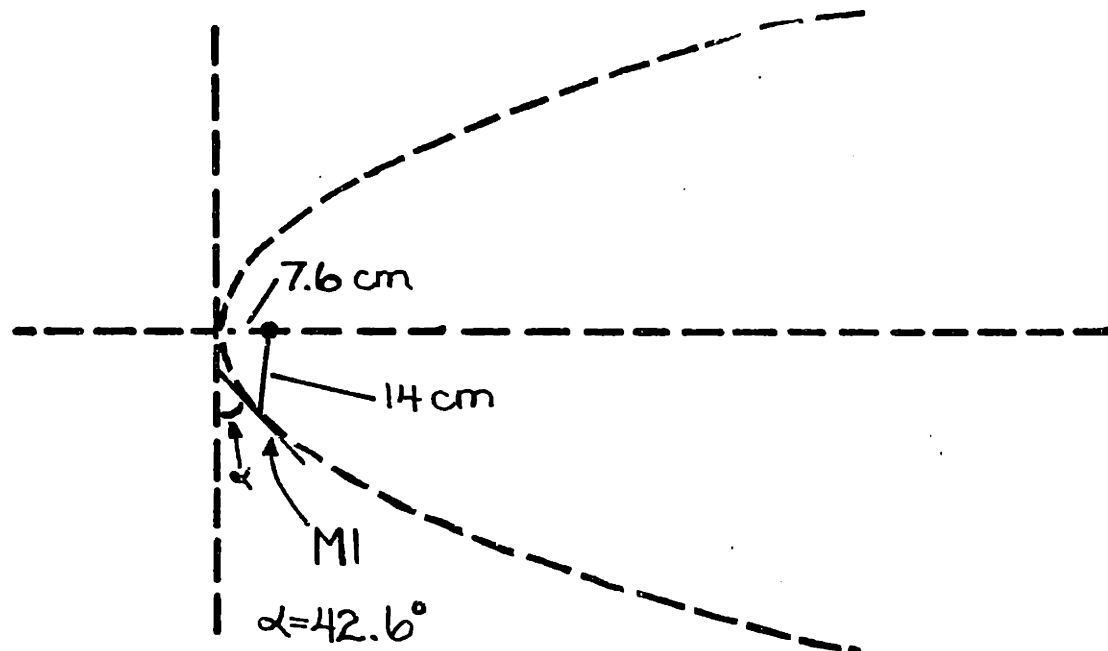


Figure 5

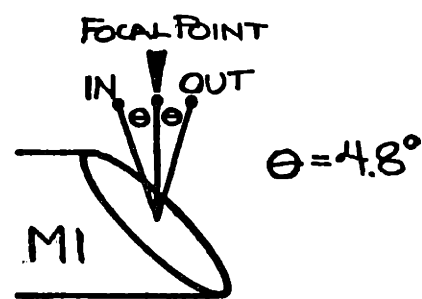
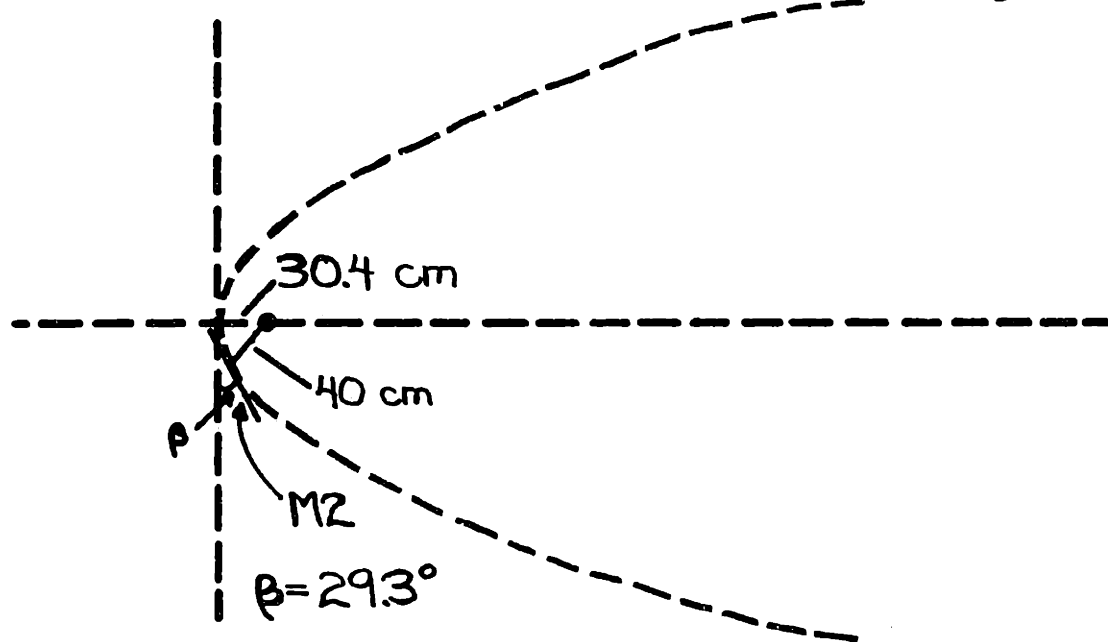


Figure 6

OFF-Axis PARABOLOIDS M1 AND M2

with adjustable position, direction, off axis angle, focal length, etc. Finally an output plane can be situated where desired and a plot of the ray intersections with that surface generated. With the available optics and the design criteria the specific layout was chosen based on calculations by the ray tracing program. Among the refinements from the ray tracing undertaking is the discovery, following a suggestion from John Mather of NASA, that the aberrations in the systems are reduced if M2 has its focus at M1 rather than at the DH. The ray tracing program uses a coordinate system centered in M1, with the normal to the baseplate of the interferometer the Z axis, the direction parallel to the carriage travel the Y axis and the parallel to the BS- IPOP line the X axis. Table 1 shows the design as given to the raytrace program.

TABLE: OPTICAL DESIGN A LA RAYTRACE

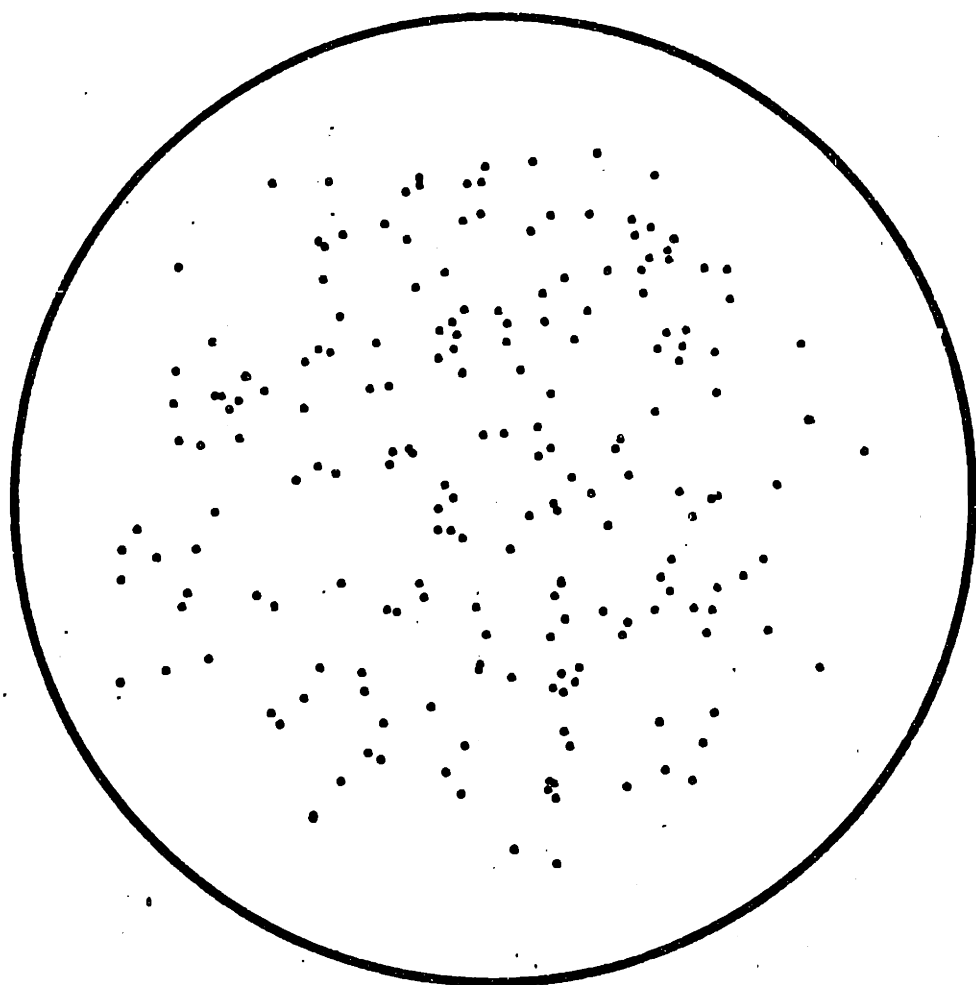
Distances are in centimeters.

| | | X | Y | Z |
|--------------|-------------------|--------|--------|-------|
| M1: | point on surface | 0 | 0 | 0 |
| | normal at point | .5296 | .9504 | 1 |
| | location of focus | .5742 | 1.0304 | 13.97 |
| M2: | point on surface | 19.458 | 34.916 | 0 |
| | normal at point 0 | -1 | 0 | 0 |
| | location of focus | 0 | 0 | 0 |
| DH: | point on axis | 39.916 | 0 | 0 |
| | surface normals | -.4868 | .8735 | 1 |
| | | -.4868 | .8735 | -1 |
| Input horn: | center | 0 | 0 | 14.02 |
| | axis | 0 | 0 | -1 |
| Output horn: | center | 1.148 | 2.061 | 13.82 |
| | axis | .07233 | .14912 | 1 |

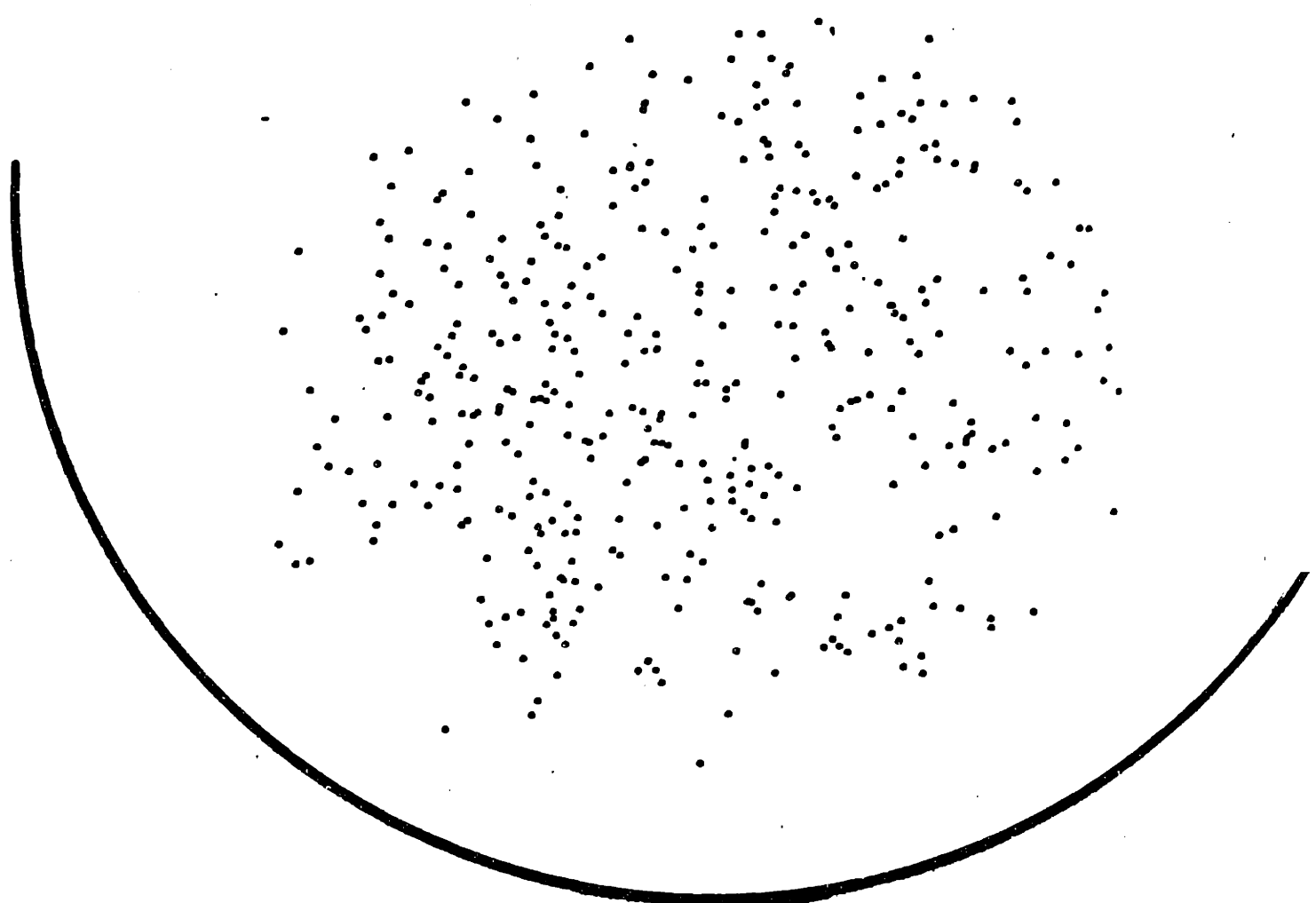
Figures 7 through 12 show the spot patterns on various planes through the interferometer. The actual extent of the surface (mirror or beamsplitter) closest to that plane is also shown. These raytraces are for input conditions for a Lambertian source of 16.2 degrees maximum half angle at the position and of the size of the input Winston cone. As can be seen, the surfaces are designed to be larger (1.5 times in diameter) than the geometric beam to include diffracted light. The optics which do not follow this dictum are the Winston cones. Their acceptance angle and area just match the design etendu, and so limit the instrument geometric throughput.

A major problem with an instrument of this large etendue is to couple efficiently to input and output optical systems. The demand for $A = .5 \text{ cm}^2 \cdot \text{sr}$ leads to an input beam 1.55 cm in diameter and 18 degrees in half angle for the selected focal length of M_1 . We presently use Winston parabolic concentrators to take this beam and convert it to a $\pi/2$ source of 4.5 mm diameter to illuminate the detector. A design using ellipsoidal concentrators has been traced; their focussing properties reduce the predicted scatter in the beam.

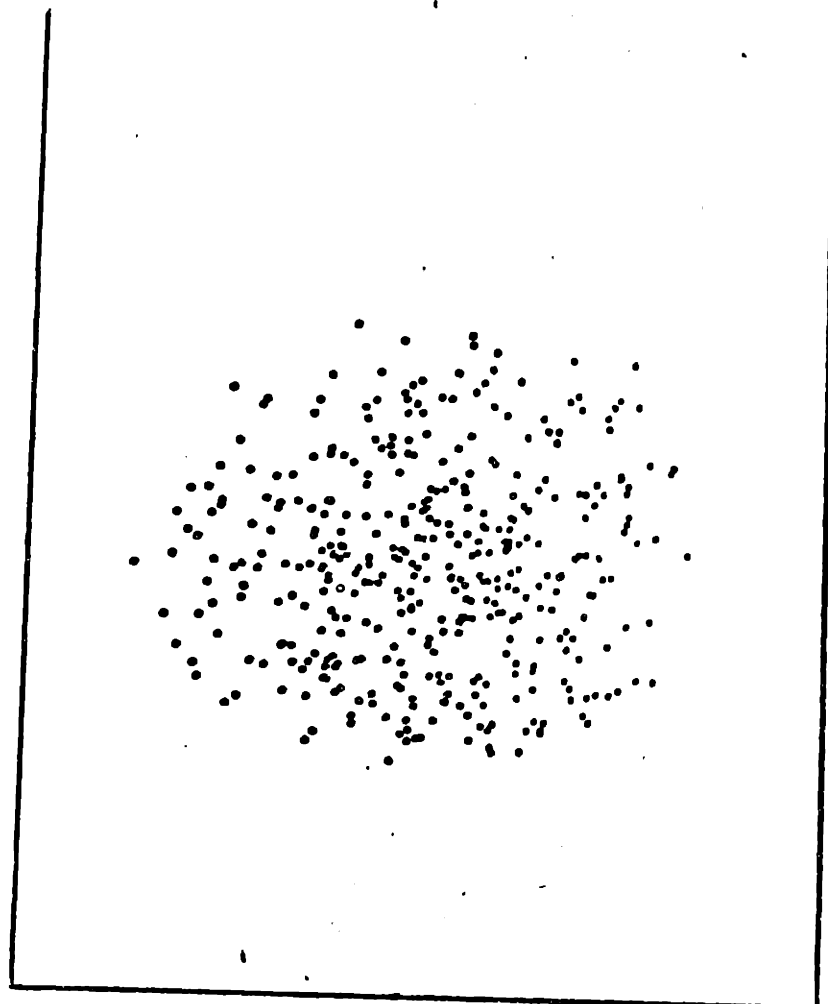
To give a qualitative feel for the functioning of the interferometer, figures 13 and 14 show the interferogram and resulting spectrum from a rapid scan run, using a BB as the source and a silicon bolometer at 4.2 degrees K as the detector.



Raytrace: M1 #1 Figure 7

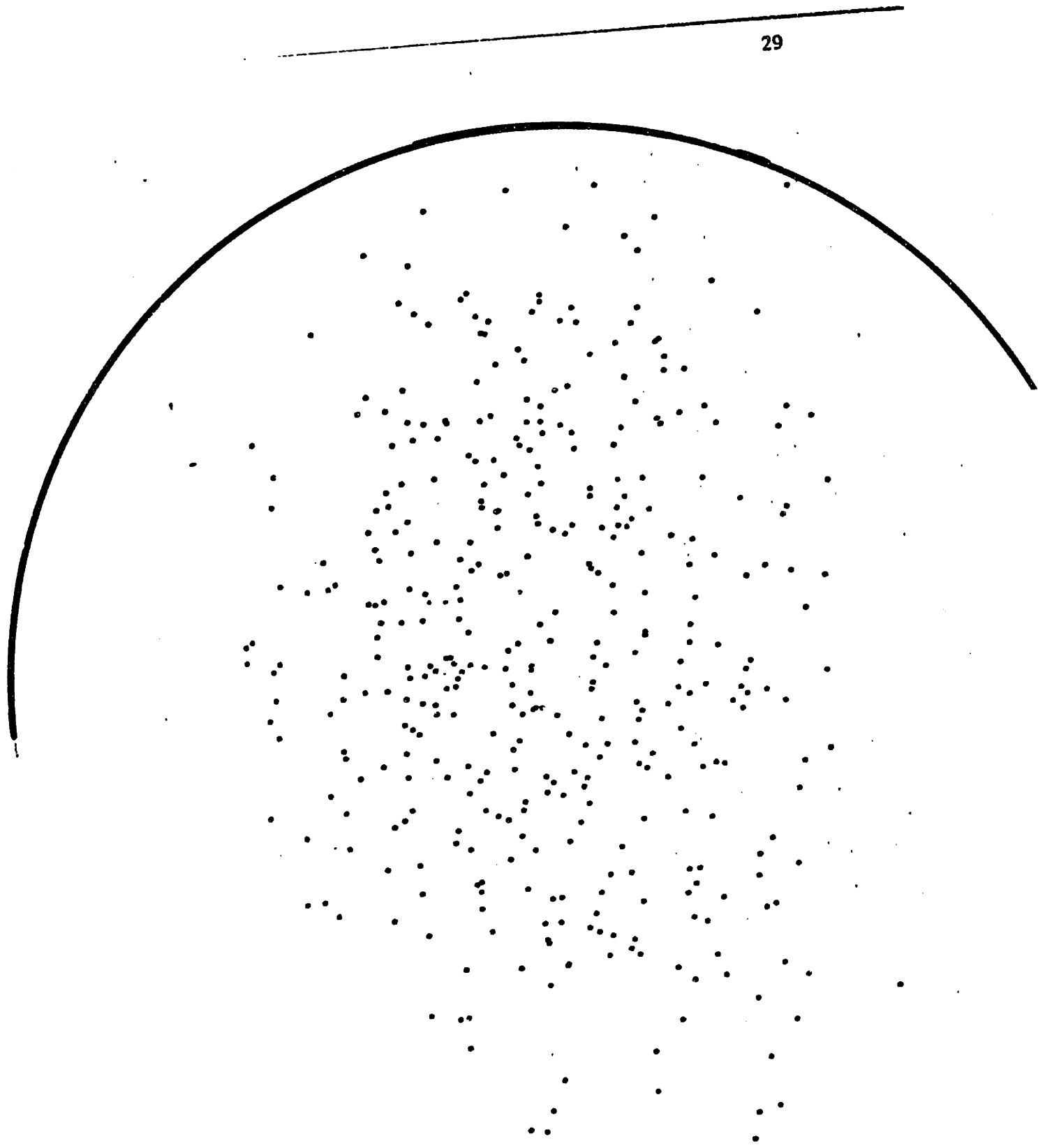


Raytrace: M2 #1 Figure 8

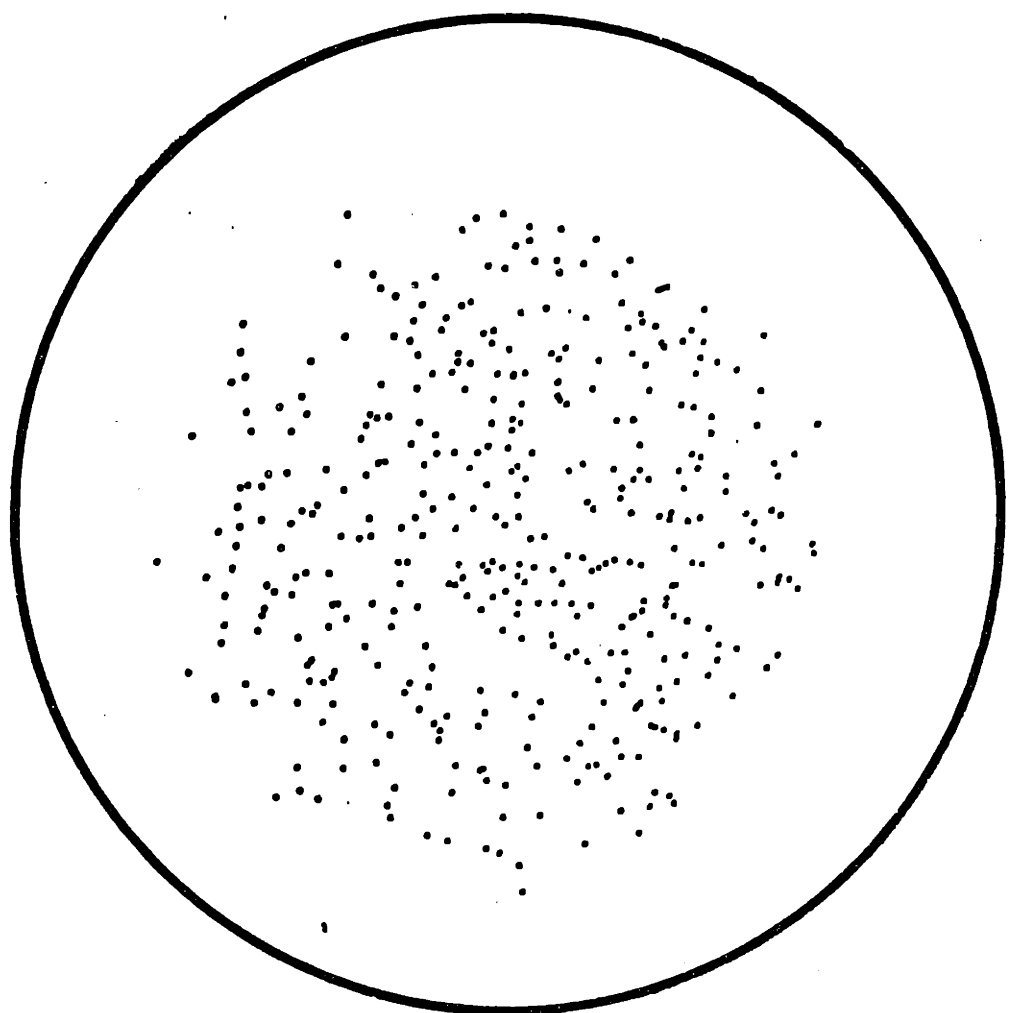


Raytrace: DH Figure 9

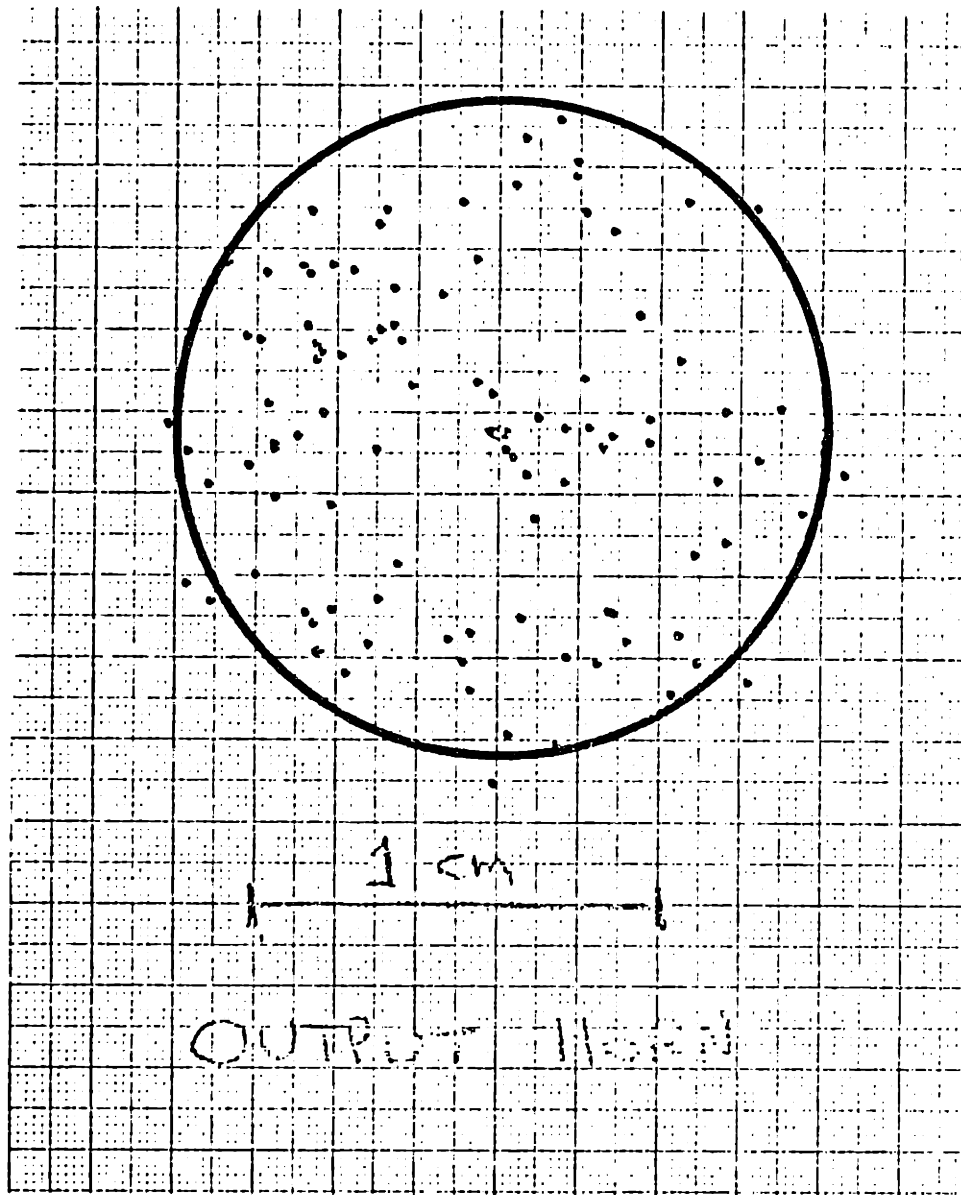
29



Raytrace: M2 #2 Figure 10



Raytrace: M1 #2 Figure 11



Raytrace: Output Figure 12



Figure 13: Sample Interferogram

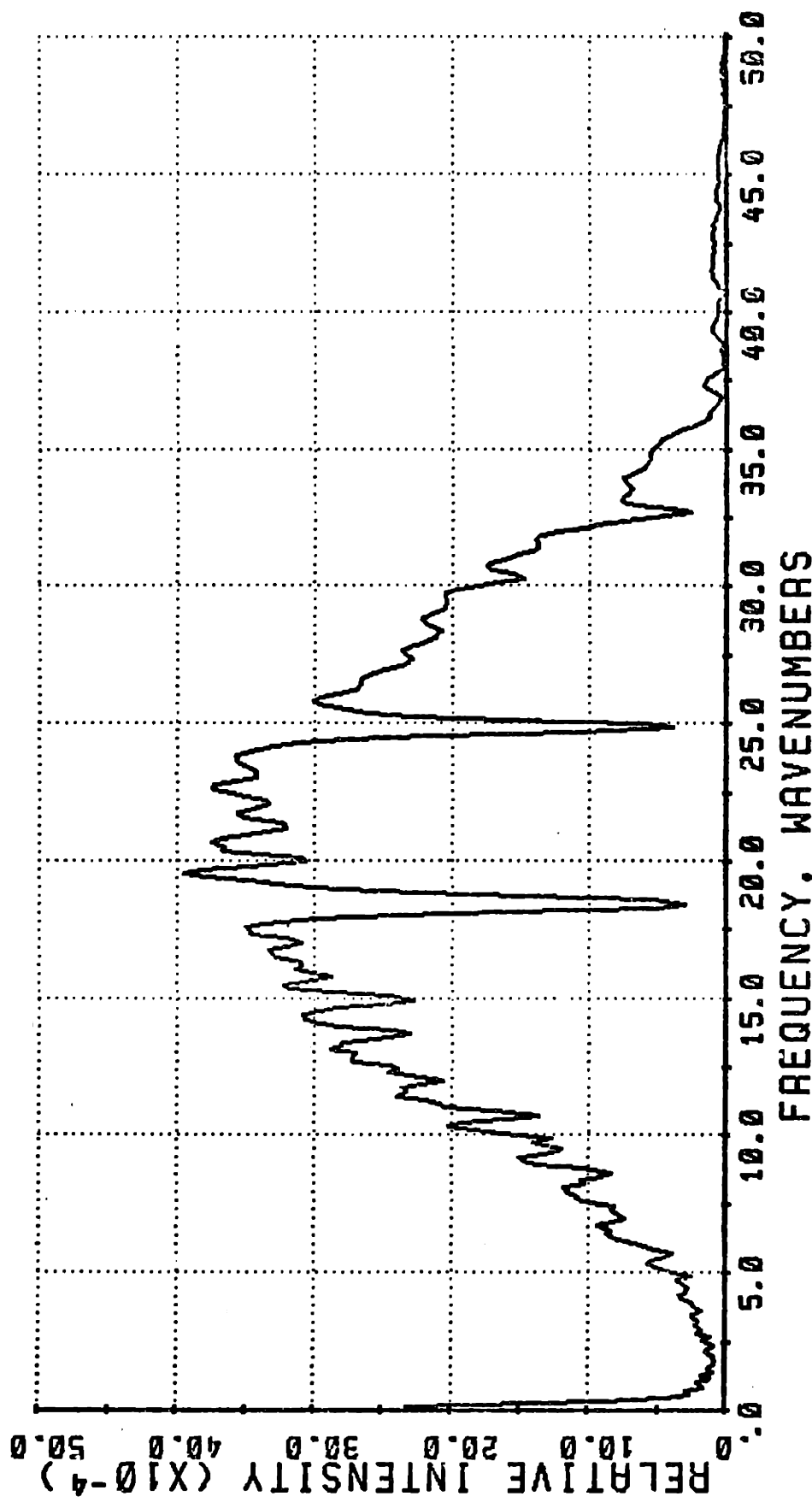


Figure 14

SAMPLE SPECTRUM: 1100 DEGREE K BLACK BODY

SLOW. 621 1024 PTS

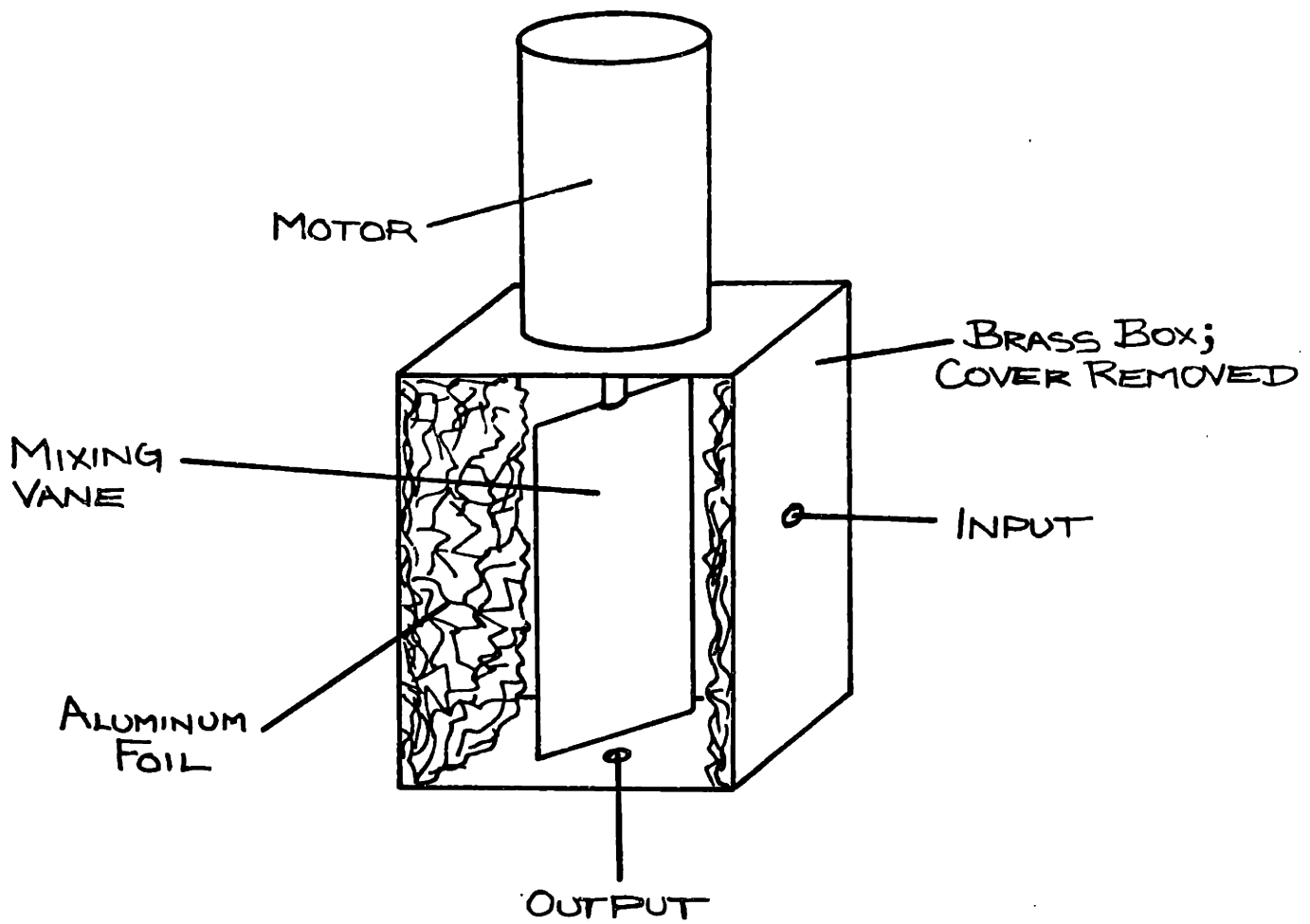
The water absorption lines can be seen superposed on the quadratically growing spectrum at low frequencies (the Rayleigh-Jeans end of the Planck law) and the rolloff at the high end (due to detector filters that limit the bandwidth). The peak intensity is about 1×10^{-11} watts.

3) INSTRUMENT TRANSFER FUNCTION

A) MEASUREMENT OF THE EFFICIENCY

The most clear cut measurement is made with an incoherent source. The detector system (a silicon bolometer) is fed either directly by the BB at 1100 deg K or via the interferometer through the same input-output optics. The measurement was made at both the central maximum and at maximum delay. The effective bandwidth for the measurement is 16 icm centered on about 18 icm; no diffraction effect or polarizer inefficiency is expected in this frequency range, so the overall efficiency measured is primarily a test of the geometric optics. The result is .62 .13, the error being the scatter in measurements.

A measurement at 3 mm was performed. The klystron fed a WC via a mode mixer. The mode mixer is a device designed to make any measurement with the klystron an average over all of the standing wave patterns and both polarizations available. The mixer is illustrated in figure 15. A vane, which rotates at a speed much faster than the chopping or sampling frequency, reflects the klystron radiation against the crumpled aluminum foil that lines the mixer box. It then scatters until it finds the exit hole. This signal was either sent through the interferometer and received at the opposite output with the carriage set at the central maximum, or the two WC from source



MODE MIXER

Figure 15

and detector were placed against each other; the ratio of intensities gives the efficiency. Because standing waves existed between the two cones, the distance between them was varied, the standing wave pattern recorded, and the average value extrapolated to zero separation. The efficiency figure from this measurement is .63 .06, the error obtained from repeated measurements. Because of the change in loading conditions on the klystron for the two arrangements (con-cone vs. cone-interferometer-cone) and the possibility that the standing wave extrapolation is not correct, the error may be much greater.

An estimate of the efficiency can be made by calculation of the expected intensity from a BB source. The source, at a known temperature, leads to a calculable spectral intensity which can be compared with a measurement. The power at the detector is calculated to be

$$P = B(\nu, T)$$

$$\epsilon' = (T(\nu))_{\text{filters}} (\text{chop loss}) (\text{dewar optical system})$$

$$\nu = 1/L$$

L = length of scan

when ϵ' = efficiency external to the interferometer. The voltage at frequency ν in the bandwidth $1/2t_{\text{int}}$ is then

$$V(\nu) = (P(\nu))(S_{\text{detector}})(G_{\text{electrical}})$$

This calculated voltage was compared with the measured voltage at 15 to 20 icm where the interferometer is anticipated to function at its best. The efficiency figure that results is .53 \pm .2, with the large uncertainty arising mostly from the calculation of the losses in the dewar light pipe system.

Measurements of the modulation efficiency here performed for a variety of bandwidths. The modulation here is defined as $2*(1-I_{\delta=0}/I_{\delta=0})$; it is 1 if all the power through the interferometer is modulated, and 0 if none is modulated. The modulation contrast has 1.00 for all bandwidths up to 0-40 icm, and has 83% for a bandwidth of 0-65 icm.

To identify the source of the losses, and to study the functioning of the device in general, two approaches were followed. The experiemntal effort involved mapping the beam intensity at various points in the instrument. The mapping program (BEAMAP) drives a raster scan of a surface of interest by a detector and converts the intensity on the detector (optical or infrared) into a graph where the intensity in each pixel is indicated on a scale from .1 to 10, normalized to the peak. The total intensity and the intensity inside a circle or rectangle of arbitrary position and dimensions can be obtained. With this tool, the amount of power falling inside the collecting area of the optical elements was measured.

To study the geometric paths in the interferometer a .5 micron source was utilized, and intensity maps at the reflective surfaces were made. A photodiode was used as the detector. The .5 micron source was placed, with a diffuser, at the back of a Winston cone. The beammap made at 15 cm from the WC where the M1 lies is shown in figure 16. The key is this: + is 10 .25, the first space is 9.5 .25, 9 equivalent to 9 .25 and so on that 8 is .8 .025, and the periods indicate half values. The amount of light falling inside the size of M1 is .95 of the total light collected.

Next the plane of M2 was mapped after the .5 micron light had been collimated by M1. Up to the half power point the pattern is fairly circular. Because the input beam is 4.8 degrees from the focus of M1 some aberration is seen. The amount of light falling inside the radius of M2 is .998.

In figure 18 the light from M2 at the DH is shown. The aberrations are now in both vertical and horizontal directions. The amount of light falling inside the DH sized as they were at the time is .96, with the carriage centered. Because of the beam profile, the included light would not change much with carriage motion.

Figure 19 shows the return beam from the DH at M2. To make this beam map an aluminized mylar beamsplitter was used to switch some of the return light to the opposite side of the interferometer. The image is now squashed horizontally, presumably as a result of astigmatism in the first M2. There also appears to be a flair in the upper right of the image; however, not much of the intensity is lost. The light falling inside the second M2 is .934 of the total.

At the second M1 we have the pattern shown in figure 20. The second M2 has nicely undone much of the distortion seen in the last figure; the two M2 mirrors, while not well figured, are very similar to each other. The beam is larger than desired, however. .86 of the light collected is inside the diameter of the second M1.

The last map in the series, figure 21, is made at the plane of the output WC. The beam is nicely distributed in intensity, that is the net aberration in the system is small, but the image is larger than expected. Only .688 of the light collected was inside the input area to the WC. A small increase in the size of the cone (from 1.6 to 1.73 cm in diameter) would increase the amount collected to .76, but to collect 90% of the light would require an aperture 2.2 cm in diameter.

Figure 16: Beemap, .5 micron, MI #1

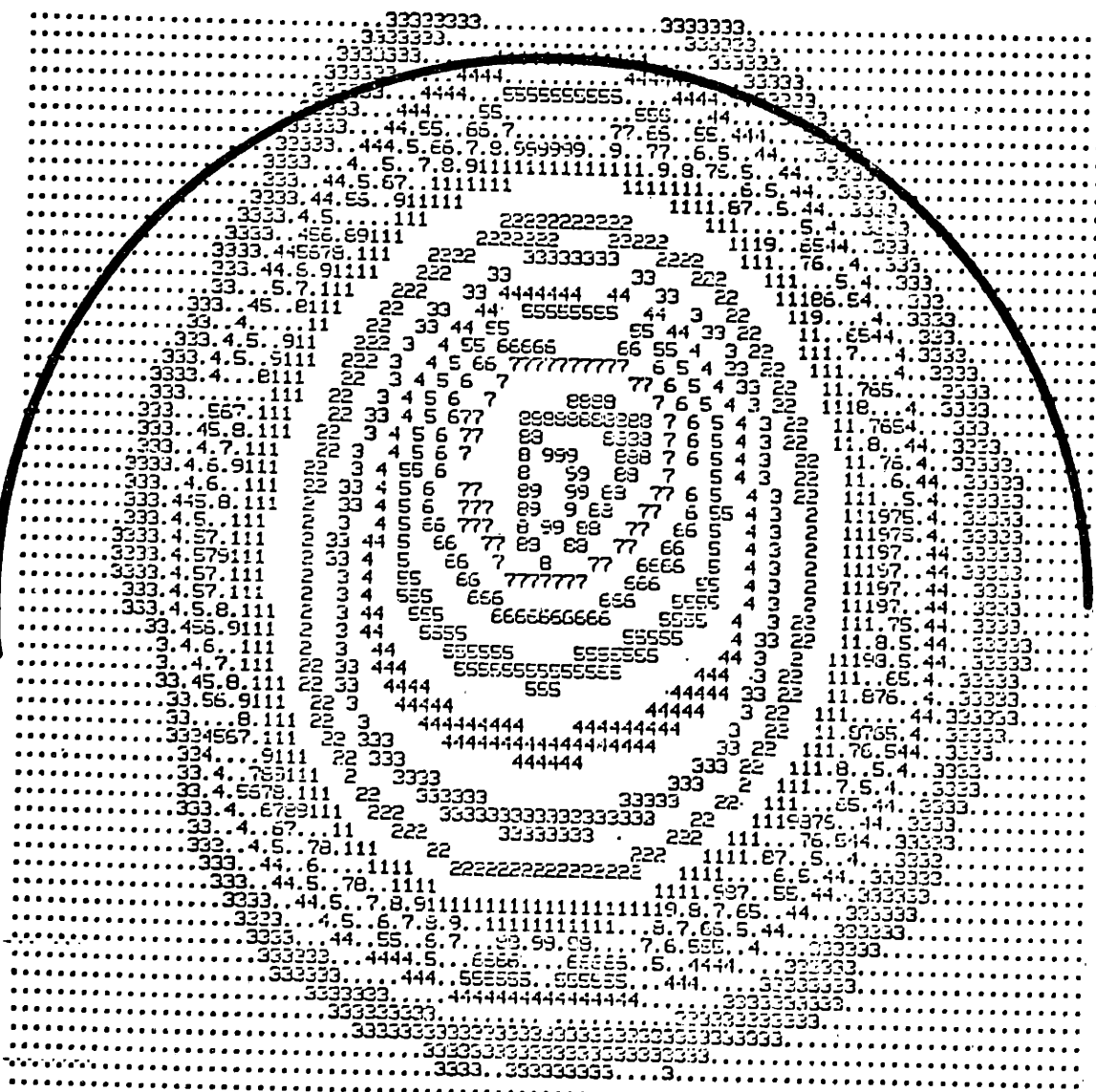


Figure 17: Beemap, .5 micron, M2 #1

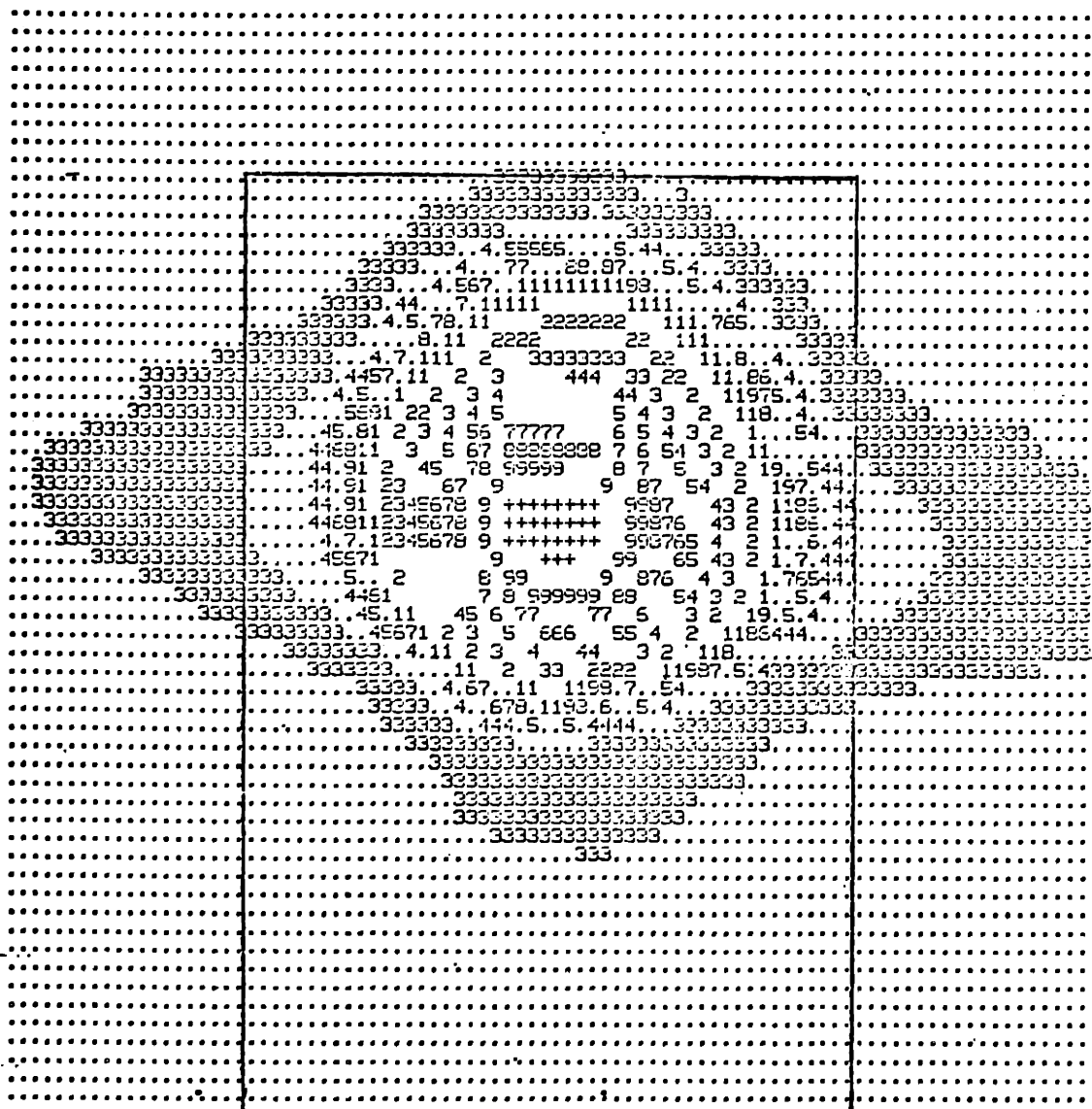


Figure 18: Beampat, .5 micron, DH

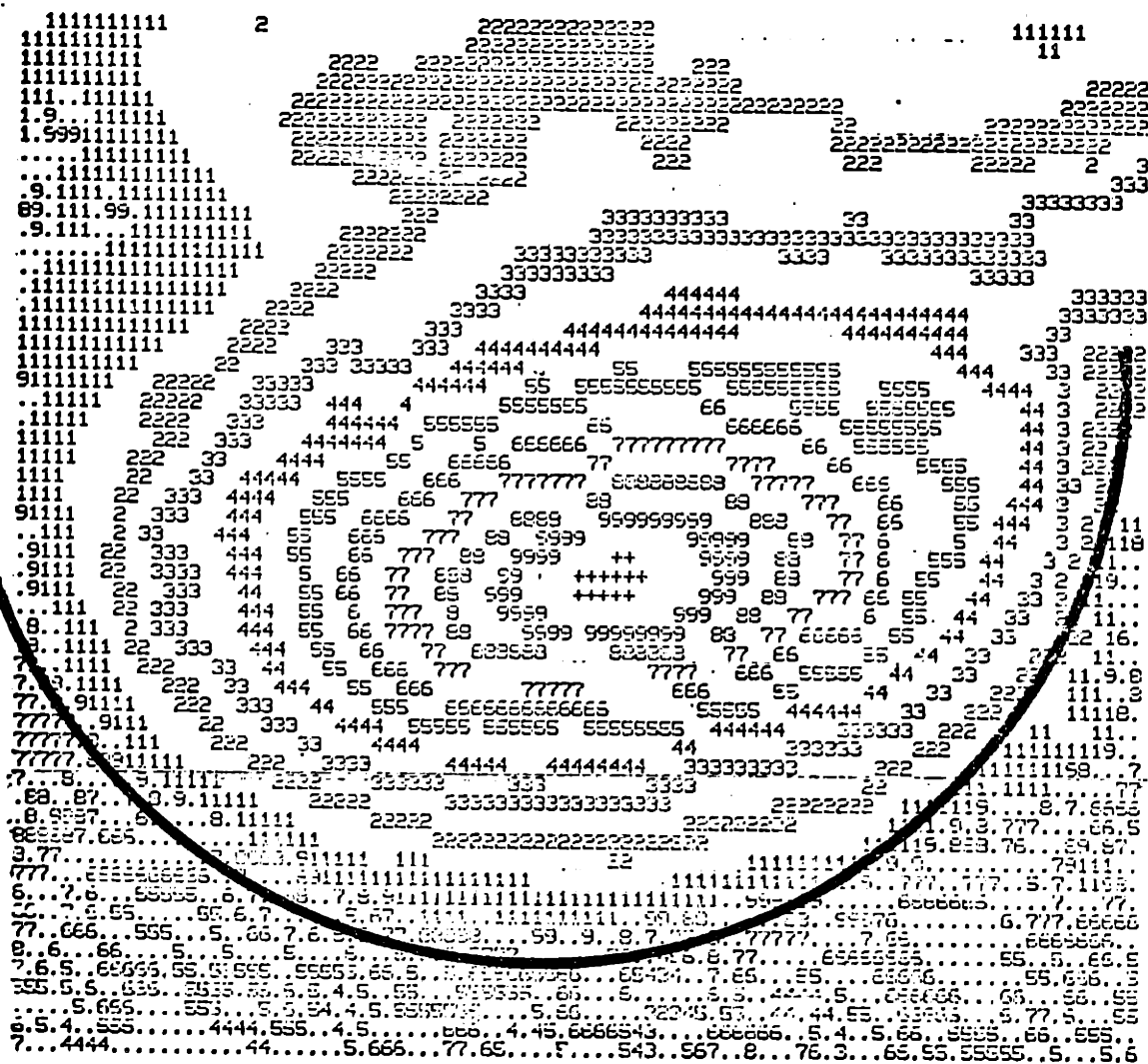


Figure 19: Beampap, .5 micron, M2 #2

Figure 20: Beemap, .5 micron, M1 #2

Figure 21: Beampat, .5 micron, Output

The product of the light captured at each mirror for the entire optical path is .53, which is the computed efficiency for the beamap measurement. The accuracy of this measurement is most sensitive to the map with the largest loss, because there an error in position translates to a large error in light collected (the derivative of the intensity as a function of position is large). The uncertainty in the .53 figure is estimated to be .05.

One explanation which is consistant with the data is that the WC at the input is putting out a larger range of angles than it was designed to. This would not necessarily show up as a greater FWHM at the M1 below it; the gentle rolloff observed outside of the half angle indicates the excess angular output, and it is possible that within the FWHM there may be steeper angles; a graphic example is shown in figure 22. For an image at 15 cm, the ϵ' could be 20.72 degrees for the light to fall within the 18 degree half angle.

To further investigate the serious losses at the first M1 and at the output plane, an optical system consisting of the two M1 mirrors and an input cone was assembled (figure 23). With the .5 micron source the path was traced; in figure 24 the WC output pattern is shown at 15 cm as before, and in figure 25 at 10 cm. Figure 26 shows the pattern at the second M1. The losses were again in the output plane (figure 27). To determine

WINSTON CONE EXTREME ANGLES

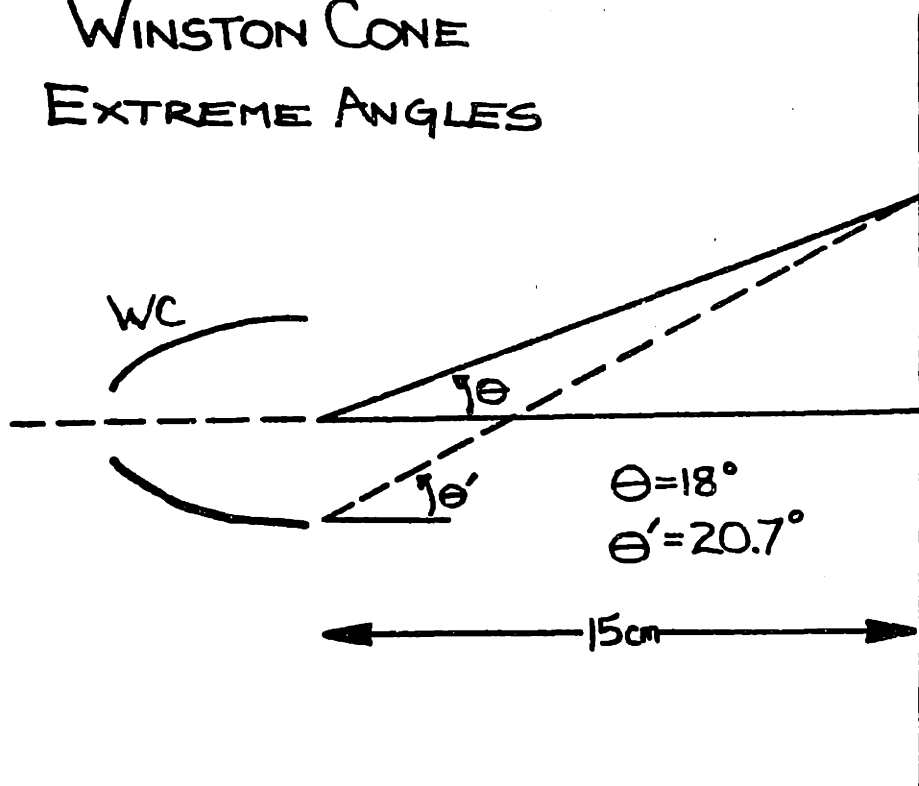


Figure 22

WINSTON CONE

IN



OUT



Figure 23

M1-M1 SYSTEM FOR BEAMAPPING

Figure 24: Beamap, .5 micron, M1 #1 M1-M1

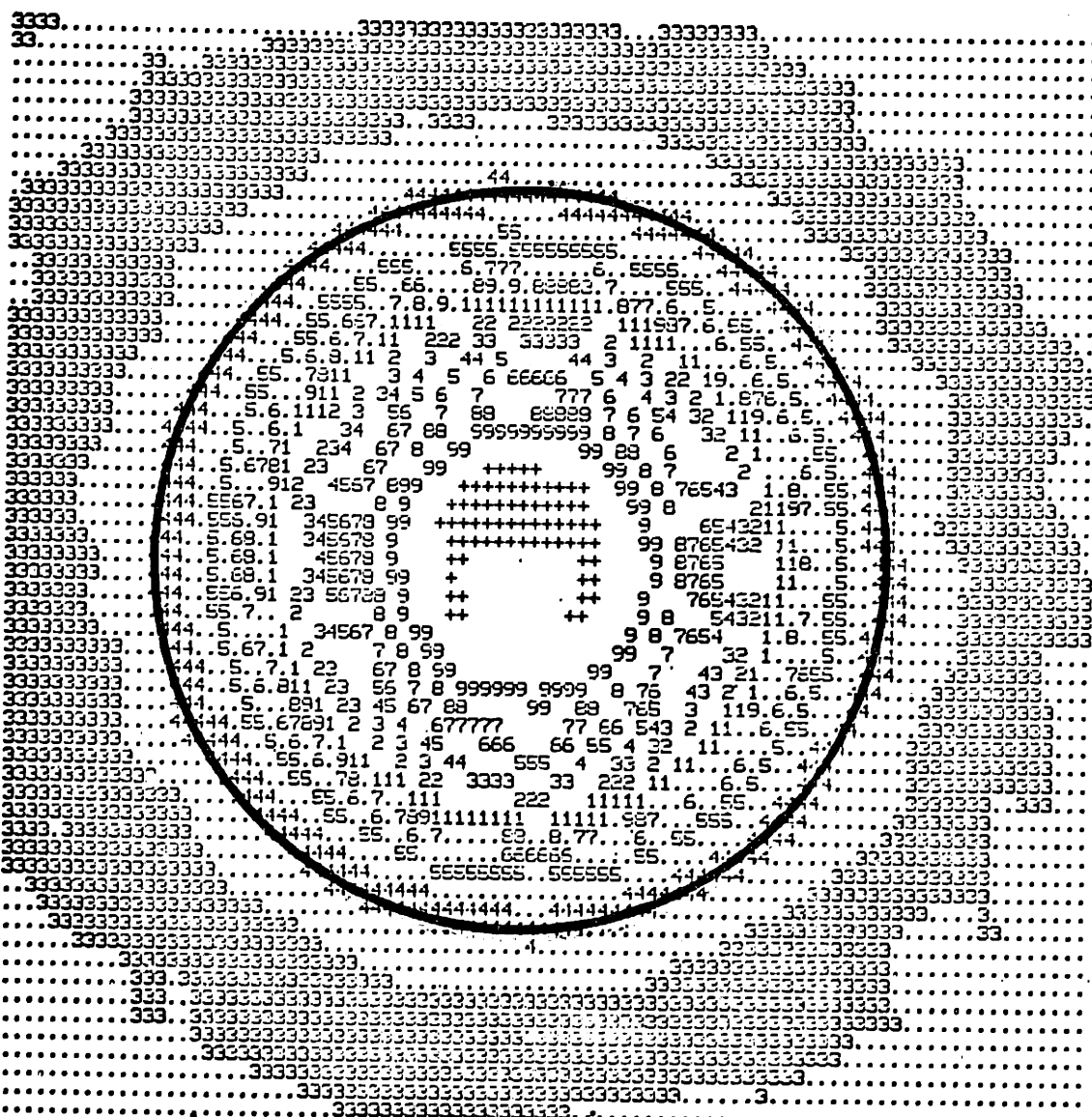


Figure 25: Beampat, .5 micron, 10 cm from WC

Figure 26: Beamap, .5 micron, M1 #2 M1-M1

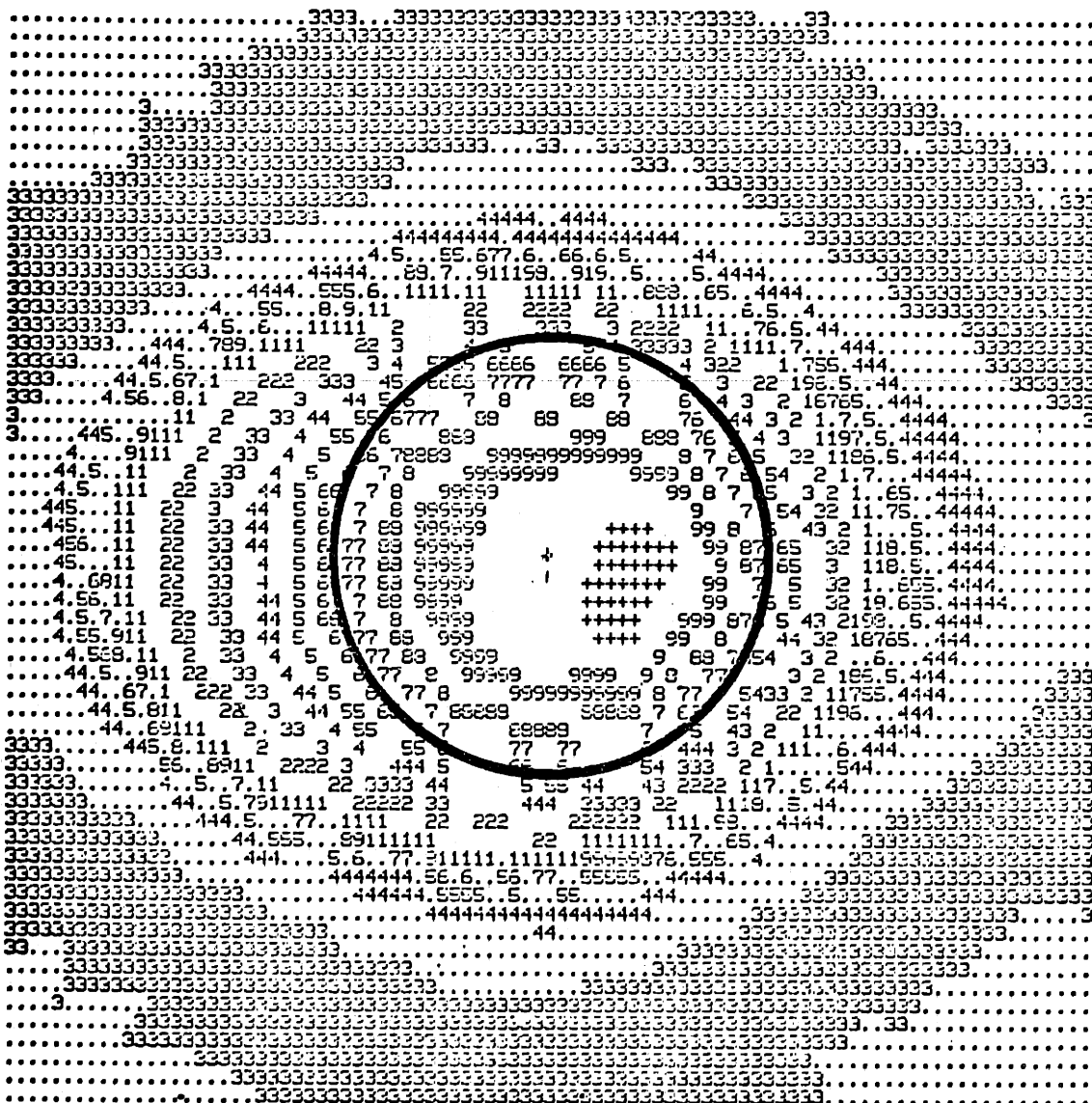


Figure 27: Beemap, .5 micron, Output M1-M1

Figure 28: Beamap, .5 micron, 3 cm up Mi-Mi

Figure 29: Beemap, .5 micron, 1 cm up M1-M1

Figure 30: Beampat, .5 micron, 1 cm down M1-M1

Figure 31: Beampat, .5 micron, 2 cm down M1-M1

if the losses might be due to lack of focus, output planes 3 cm and 1 cm above and 1 and 2 cm below the focus were mapped (figures 28 to 31). The maximum light was collected at the expected focus, with the included light being .69.

Another beam mapping effort was made at long wavelengths using the 3 mm klystron as the source. This sheds more light (or should it be microwaves?) on the diffraction regime. The klystron was fed into the mode mixer and thence into the small end of the input WC. A pyroelectric detector was used. The first beamap (figure 32) is at 15 cm from the WC. The FWHM for this map is 18.4 degrees, 15 degrees greater than for the .5 micron measurement. The included light is less also: .81 falls inside the radius of M1. The reduction in light collected is due to diffractive spreading of the beam, and is the point in the optical system where most of the low frequency energy is lost.

The next figure (33) shows the intensity pattern at the position of M2 after the 3 mm radiation has been collimated by M1. This map is similar to the .5 micron case: .995 of the incident light falls on M2, and the distribution is similarly aberrated. The signal/noise is poorer, leading to the jitter in values at low intensity.

The light at the plane of the DH is shown in figure 34. Again the pattern is like the 1/2 micron case. .976 of the light

Figure 32: Beemap, 3 mm, M1 #1

Figure 33: Beemap, 3 mm, M2 #1

Figure 34: Beemap, 3 mm, DH

Figure 35: Beemap, 3 mm, M2 #2

Figure 36: Beamap, 3mm, M1 #2

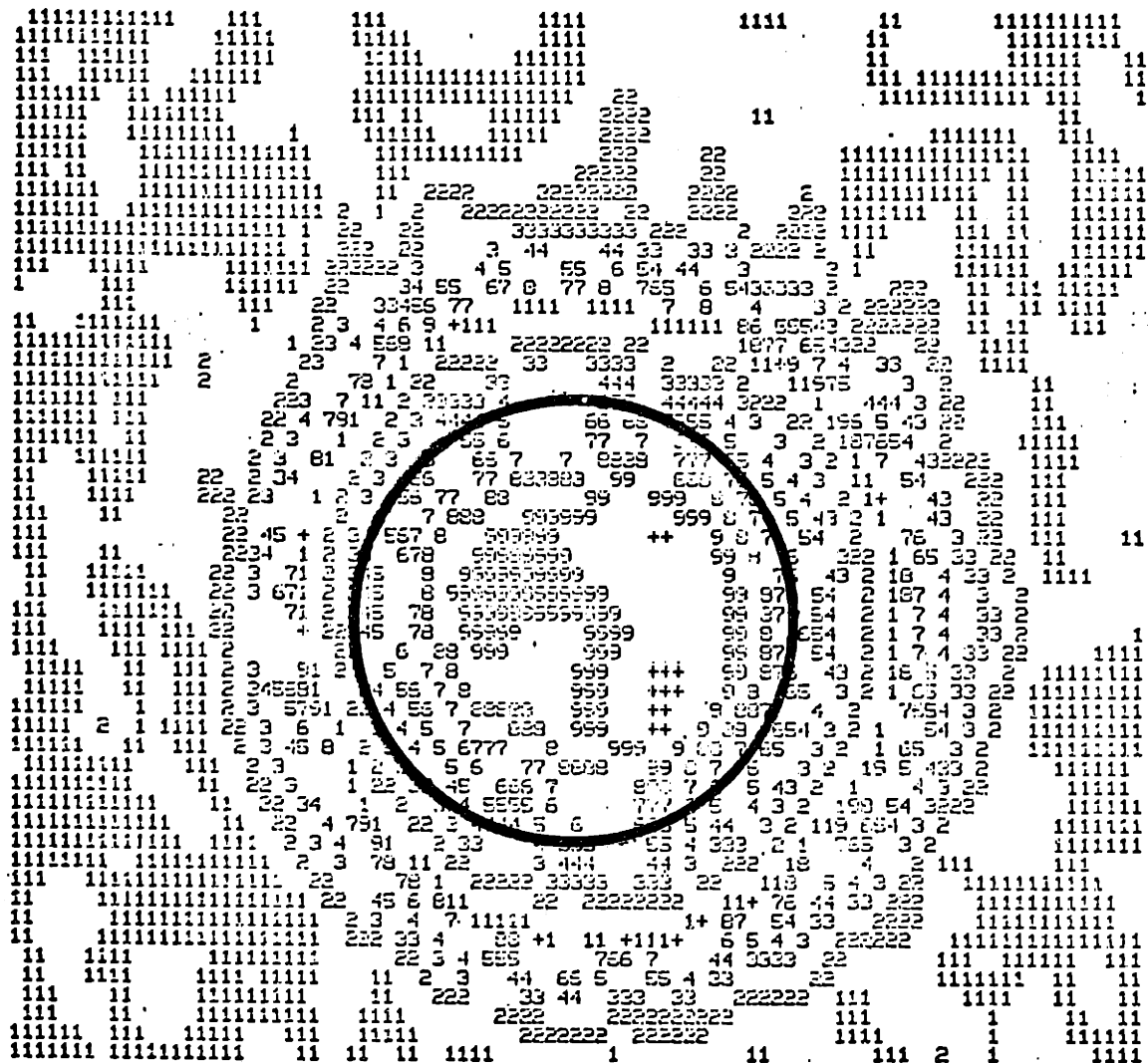


Figure 37: Beampattern, 3 mm, Output

falls inside the outline of the DH.

In figure 35 we have the light at the second M2. In comparing it with the .5 micron case, it is noted that the flare is absent; this suggests that some scattering due to surface roughness on the scale of a few microns is scattering the 1/2 micron light, a problem which will not affect the instrument in the far infrared. Otherwise, the two maps are very similar. .984 of the collected light falls inside M2.

At the second M1 (figure 36) the lack of decimal points between the second decade integers disguises the beam, but the light falling inside the mirror is .93 of the light collected. This is better than for the corresponding 1/2 micron map, possibly because of the surface roughness argument.

The last figure in the series, figure 37, is at the output WC plane. The pattern is again similar to the 1/2 micron map, and large losses are seen; .70 of the light collected is inside the diameter of the output cone.

Because there was a possibility that two different effects-- diffraction at 3 mm and scatter at .5 microns-- were causing the losses at the output plane, a black body with its peak at about 10 microns was tried as a source. At the first M1 (figure 38), .95 of the light falls into the area of M1. Note the much more square beam intensity as a function of angle than was

Figure 38: Beamap, 10 micron, M1 #1 M1-M1

Figure 39: Beemap, 10 micron, ml #2 M1-M1

Figure 40: Beemap, 10 micron, output M1-M1

Figure 41: Beampat, 10 micron, Output; with aperture

observed for the 3 mm or .5 micron source.

This is also true for the second M1 plane (figure 39); here .971 of the light falls inside the optical element. At the last surface, the WC output plane, the losses are comparable to those with other sources (figure 40), .67.

To determine if the problem lay in the slightly excessive 1/2 angle (18.9 degrees, vs. 18 calculated), an aperture was placed below the WC which limited the half angle to 16 degrees. The beamap at the output plane (figure 41) shows that .72 of the light now falls inside of the WC. This is an improvement, but it appears that the problem is in excess angle toward the center of the WC output.

The incoherent source measurement gives an efficiency of 62%; this is the most direct and credible measurement. The beamaps indicate the points of greatest loss: both M1 mirrors, and especially the output plane. The WC, which does not behave as geometric optics says it should, is probably the source of the problem.

B) HIGH FREQUENCY RESPONSE

FACTORS THAT LIMIT THE HIGH FREQUENCY RESPONSE

There are a number of effects which can degrade the high frequency response. These include imperfections and misalignments in the polarizer, depolarization by M2, and various rotations, phase shifts, and absorptions. They will be discussed in turn.

The polarizers are parallel wires on a flat frame. At higher frequencies, where the wavelengths are comparable to the wire diameter and spacing, the polarizer becomes less effective. Using the waveguide analysis of inductive and capacitive strips in free space, a computer program has been written to predict the response of the polarizers used. In fact, the polarizers are made of cylindrical wires; the calculation should be redone with this twist. The figure (42) shows four properties of the polarizers: the reflection and transmission parallel (inductive) and perpendicular (capacitive) to the wires. What is plotted here are the amplitudes squared; in fact the R's and T's are complex, with both the phase and the amplitude functions of To relate these properties to the expected response of the entire instrument, the matrix analysis of the instrument was redone allowing for imperfect $R(V)$ and $T(V)$ of the polarizer. To make the algebra workable, the $R_{cap} = 0$ and $T_{ind} = 0$ (no leakage; just

loss in T_{cap} and R_{ind}); furthermore, R and T are taken as real.

Again, a more complete analysis should be done. With these assumptions, the polarizer matrices are

IPOP =

$$\begin{pmatrix} 0 & 0 & T & 0 \\ 0 & -R & 0 & 0 \\ T & 0 & 0 & 0 \\ 0 & 0 & 0 & -R \end{pmatrix}$$

and

BS =

$$\begin{pmatrix} -R & -R & T & T \\ R & -R & T & T \\ T & T & -R & R \\ T & T & R & -R \end{pmatrix}$$

The resulting output vector is, assuming T and R real,

$E_{out} =$

$$\begin{pmatrix} -IR^2T^2\sin\delta E_{+y} - RT^3\cos\delta E_{-x} \\ -IR^2T^2\sin\delta E_{+x} + R^3T\cos\delta E_{-y} \\ -RT^3\cos\delta E_{+x} + IR^2T^2\sin\delta E_{-y} \\ -RT^3\cos\delta E_{+y} + IR^2T^2\sin\delta E_{-x} \end{pmatrix}$$

and the output intensities become

$$I_{+out} = (R^2T^6E_{-x}^2 + R^6T^2E_{-y}^2)\cos^2\delta + R^4T^4I_{+in}\sin^2\delta$$

and

$$I_{-out} = (R^2T^6E_{+x}^2 + R^6T^2E_{+y}^2)\cos^2\delta + R^4T^4I_{-in}\sin^2\delta$$

so

$$I_{diff} = R^2T^6(E_{-x}^2 - E_{+x}^2) + R^6T^2(E_{-y}^2 - E_{+y}^2)\cos^2\delta + R^4T^4(I_{+} - I_{-})\sin^2\delta$$

Note the high powers at which T and R appear, and that there is a polarization sensitivity insofar as T is not equal to R.

Another way in which the BS polarizer can limit the high frequency response is in the lack of physical flatness. Because the optical delay in the device is only a function of the optical delay from the BS to the DH and back, it is only those components which must be analyzed as causes of lack of interference. If there is an error of 4x (a factor of two for the path to the DH and back, and a factor of two because if the polarizer is closer to one DH, it is further from the other). A reasonable criterion for flatness is $\lambda_{\min}/10$. For 100 icm, this leads to a requirement of flatness in the BS of 2.5 microns and for the DH of 5 microns across the beam diameter. The DH, being made of first surface aluminized glass mirrors, are easily flat to $\lambda_{\min}/50$. They must be accurately at 90 degrees, however.

The BS and DH must be aligned correctly for optimum contrast. If the BS is rotated about the axis normal to the base of the interferometer, the error in phase at the outside edge of a 5 cm diameter beam is $20 \theta_2$ cm; if errors are to be less than $/10$ at 100 icm, must be less than 10 minutes. A rotation of a DH about the same axis has half this affect. Operationally, the BS can be rotated to eliminate a small error in DH position.

If the lack of flatness is a smooth curve, it can be crudely modeled as a BS misalignment of angle θ there is the angle between the average plane of the BS and a tangent to the average angle in the BS curve. Then, for both misalignment and simple curvature, the delay becomes a function of position on the BS; δ becomes $\frac{1}{2} + 4\theta x$ where θ is the error angle and x is the position from the center of the BS. The result is a frequency dependent efficiency in the interferometer which goes as

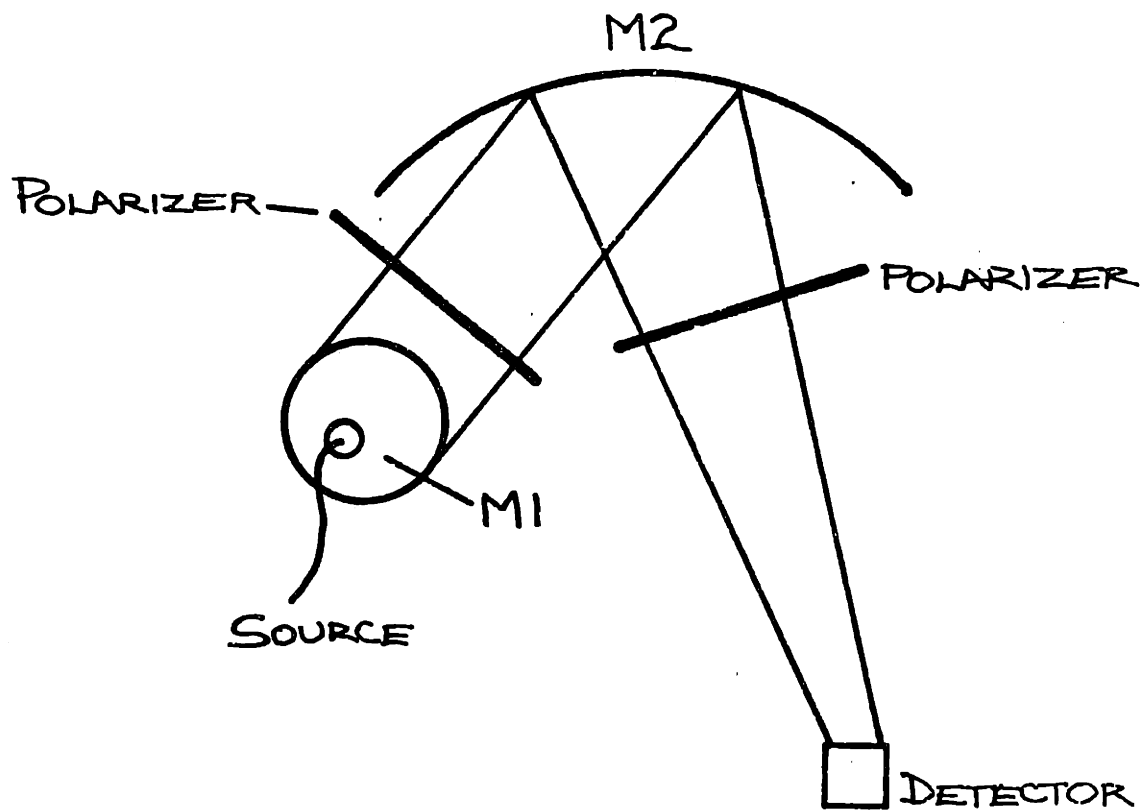
$$2J_1(x)/x$$

where

$$x = \frac{\lambda R \theta}{2}, R \text{ the radius of the beam at the BS}$$

While discussing conditions on interference, the possibility that the beam from the IPOP is depolarized upon reflection from M2 should be mentioned. This could occur if there are surface ripples on M2 that are on the scale of the wavelengths of interest in depth and size. A simple test for this would be to insert M2 in a beam between crossed polarizers; the increase in signal from the unperturbed path would be a measure of the depolarization (see figure 43). This has not been tried.

Once again we turn to the matrix analysis for some conclusions as to the sensitivities of the instrument response to alignment errors which affect the phases, but not the geometric paths, in the interferometer.



A TEST FOR DEPOLARIZATION
By M2

Figure 43

1) Assymetric phase shift and loss: If a propagator modeling a loss on one side of the interferometer outside of the region of interference (BS and DH) is inserted in the path,

$$T = \begin{pmatrix} A & 0 & 0 & 0 \\ 0 & A & 0 & 0 \\ 0 & 0 & 1 & 0 \\ 0 & 0 & 0 & 1 \end{pmatrix}$$

where A can be complex, every component of the output electric field is multiplied A. The only affect on the interferogram is that the intensity is down by a factor of A^2 . This would be the case if IPOL were displaced from the symmetry line, or if M2 were absorptive and displaced.

2) Input polarizer rotated about the normal to its face: If the rotation matrix is applied to IPOL for small angles, one obtains:

$$IPOL = \begin{pmatrix} 0 & -\theta & 1 & \theta \\ -\theta & 1 & \theta & 0 \\ 1 & \theta & 0 & -\theta \\ \theta & 0 & -\theta & 1 \end{pmatrix}$$

to first order. This results in an output vector

$$E_{out} = \begin{pmatrix} -I\sin\delta E_{+y} + (\cos\delta - 12\theta\sin\delta)E_{-x} \\ I\sin\delta E_{+x} + (\cos\delta - 12\theta\sin\delta)E_{-y} \\ (\cos\delta + 12\theta\sin\delta)E_{+x} + I\sin\delta E_{-y} \\ (\cos\delta + 12\theta\sin\delta)E_{+y} - I\sin\delta E_{-x} \end{pmatrix}$$

and output intensities

$$I_{+out} = \frac{1}{2}(I_+ + I_-) + \frac{1}{2}(I_- - I_+) \cos 2\delta \\ + 2\theta(E_{-x}E_{+y} - E_{-y}E_{+x})(1 - \cos 2\delta)$$

$$I_{-out} = \frac{1}{2}(I_+ + I_-) - \frac{1}{2}(I_- - I_+) \cos 2\delta \\ - 2\theta(E_{-x}E_{+y} - E_{-y}E_{+x})(1 - \cos 2\delta)$$

$$I_{common mode} = I_+ + I_-$$

$$I_{differential} = (I_- - I_+) \cos 2\delta \\ + 4\theta(E_{-x}E_{+y} - E_{-y}E_{+x})(1 - \cos 2\delta)$$

For the term in θ to have any influence time averaged, $-x$ and $+y$ or $+x$ and $-y$ must be correlated! This will not be so with the BB sources, but it is conceivable that with multiple bounces through the interferometer that sources on one side of one polarization could appear on the other side with rotated polarization.

3) Rotation of the BS around the normal to its face; With the same rotation as above, a deviation from 45 degrees of θ for the BS results in a matrix for the BS of

$$BS = \begin{pmatrix} 1+\theta & -1 & 1-\theta & 1 \\ -1 & 1-\theta & 1 & 1+\theta \\ 1-\theta & 1 & +\theta & -1 \\ 1 & 1+\theta & -1 & 1-\theta \end{pmatrix}$$

To first order, this has no affect on the output.

4) Misalignment of the DH: If one, or both, DH are rotated about their directorix, the matrices to first order are

a) one DH:

DH=

$$\begin{pmatrix} 1 & 2\theta & 0 & 0 \\ 2\theta & -1 & 0 & 0 \\ 0 & 0 & 1 & 0 \\ 0 & 0 & 0 & -1 \end{pmatrix}$$

b) two DH:

DH=

$$\begin{pmatrix} 1 & 2\theta & 0 & 0 \\ 2\theta & -1 & 0 & 0 \\ 0 & 0 & 1 & 2\theta \\ 0 & 0 & -2\theta & -1 \end{pmatrix}$$

There is no effect on the output to first order for either of these errors. If one DH has a complex but not polarization sensitive absorption, one can write

DH=

$$\begin{pmatrix} A & 0 & 0 & 0 \\ 0 & -A & 0 & 0 \\ 0 & 0 & 1 & 0 \\ 0 & 0 & 0 & -1 \end{pmatrix}$$

This results in an output electric field of

$$E_{out} = \begin{pmatrix} (-Re^{i\delta} + e^{-i\delta})E_{+y} + (Re^{i\delta} + e^{-i\delta})E_{-x} \\ (-Re^{i\delta} + e^{-i\delta})E_{+x} - (Re^{i\delta} + e^{-i\delta})E_{-y} \\ (Re^{i\delta} + e^{-i\delta})E_{+x} + (Re^{i\delta} - e^{-i\delta})E_{-y} \\ -(Re^{i\delta} + e^{-i\delta})E_{+y} + (Re^{i\delta} - e^{-i\delta})E_{-x} \end{pmatrix}$$

and output intensities of

$$I_{+out} = [(1+AA^*)(I_+ + I_-)]/4 + (|A|^2/2)\cos(2\delta+\theta)(I_- - I_+)$$

$$I_{-out} = [(1+AA^*)(I_+ + I_-)]/4 - (|A|^2/2)\cos(2\delta+\theta)(I_- - I_+)$$

$$I_{\text{common mode}} = \frac{1}{2}(1+AA^*)(I_+ + I_-)$$

$$I_{\text{differential}} = |A|\cos(2\delta+\theta)(I_- - I_+)$$

Note that while a phase and amplitude shift results, no frequency dependent terms are present.

MEASUREMENTS OF THE HIGH FREQUENCY CHARACTERISTICS

Here will be discussed measurements of the wire grid polarizers, the result of misaligning the beamsplitter, and finally the high frequency response of the instrument.

The transmission of two versus one polarizer has been measured at normal incidence. The ratio, which is the measured quantity, is

$$I_{\text{out}}(2\text{pol})/I_{\text{out}}(1\text{pol}) = T_{\text{ind}}^4 + T_{\text{cap}}^4) / (T_{\text{ind}}^2 + T_{\text{cap}}^2)$$

if the assumption of $T(\lambda)$ and $R(\lambda)$ real is made. The measured properties of the polarizer are similar to those predicted with the simple intensity model (see figure 44). Ideally, accurate independent measurements of all four reflection amplitudes and transmission amplitudes of the polarizer should be made. This would reveal the extent of absorption in the polarizer, and allow (with a more thorough matrix analysis) a prediction of the high frequency response. A crude attempt to relate the measured properties of the polarizer to the expected response of the interferometer can be made: if the reflection from the polarizer is 1 - transmission, then the fourth power of the transmission in intensity enters into the expression for the output.

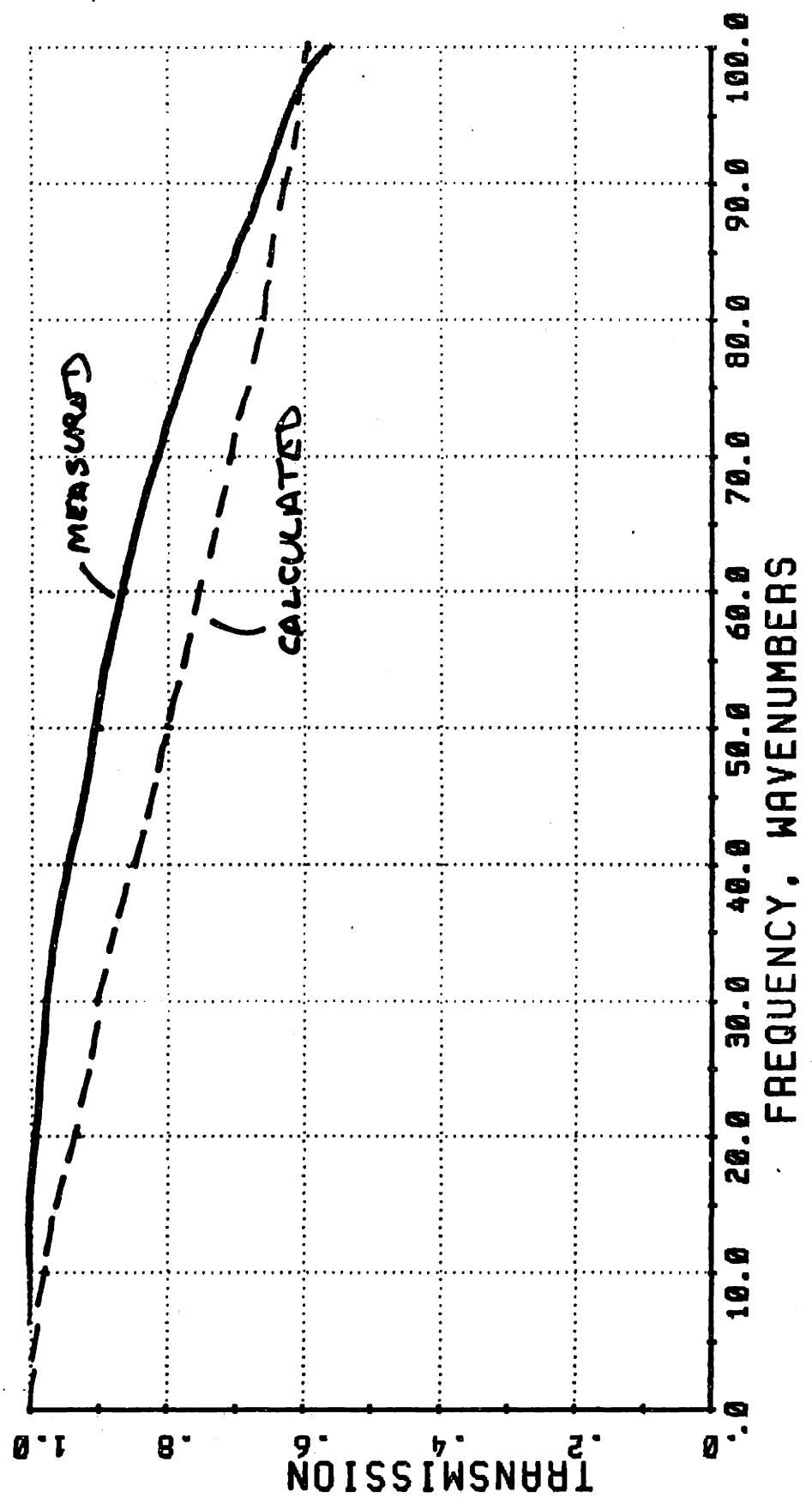


Figure 44

TRANSMISSION OF POLARIZERS

RATIO OF 2 TO 1 POL., NORMAL INCIDENCE

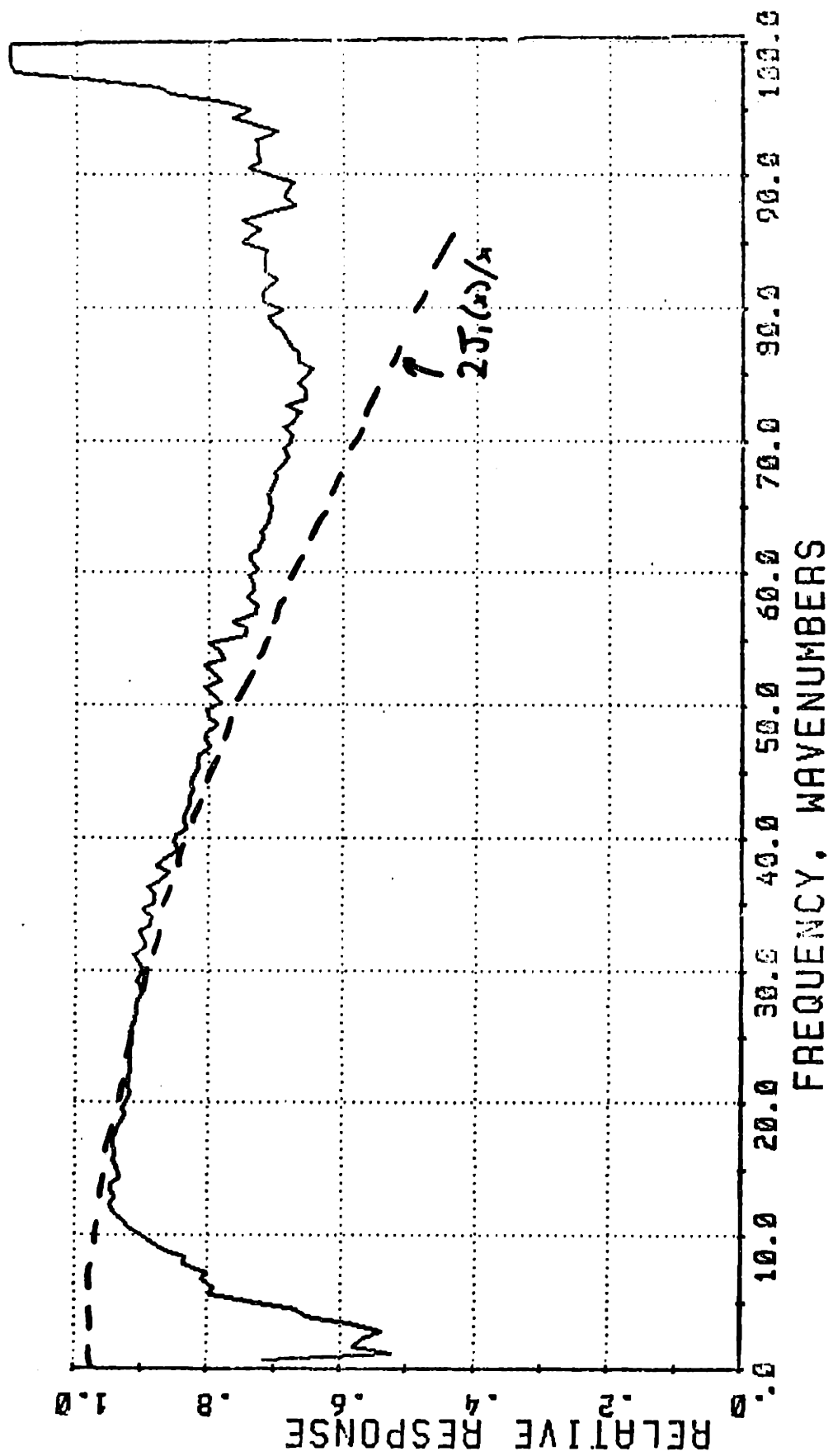
Initially the interferometer was constructed with polarizers made of Mylar backed gold strips, 50 micron spacing, 20 micron wide strips, manufactured by the Buckbee-Mears Company. The anomalously poor high frequency response of the instrument led to a measurement of the BM polarizers, showing that their transmission was degraded at frequencies well below the frequency expected for the 50 micron spacing. These polarizers are made by electrodepositing gold on a nickel form, gluing the Mylar backing to the gold, and etching away the nickel backing. A sample of the backing did not show the absorption seen in the polarizers, so the problem must lie in the gold deposit. This led to the manufacture of the free standing grids now in use.

The flatness of the BS was measured by translating it on a stage while viewing its surface with a microscope. The microscope has a depth of field of about 2 microns and a fine focus knob calibrated in microns. An upper limit of 15 microns can be put on the flatness from edge to edge (18 cm); the beam diameter at the BS is roughly 7 cm, so the criterion of $\lambda/10$ for 100 micrometers is just about met. The nature of the lack of flatness is a smooth curve, so some of the error can be eliminated by adjusting the critical angle of the BS. If the measured flatness of the BS is translated into an angular error of $15\mu/9\text{cm} = 1.7 \times 10^{-4}$ radians and the simple analysis likening lack of flatness to misadjustment is applied, the predicted response of

the instrument at 100 cm is limited to .91; this is not a significant contribution to the high frequency rolloff.

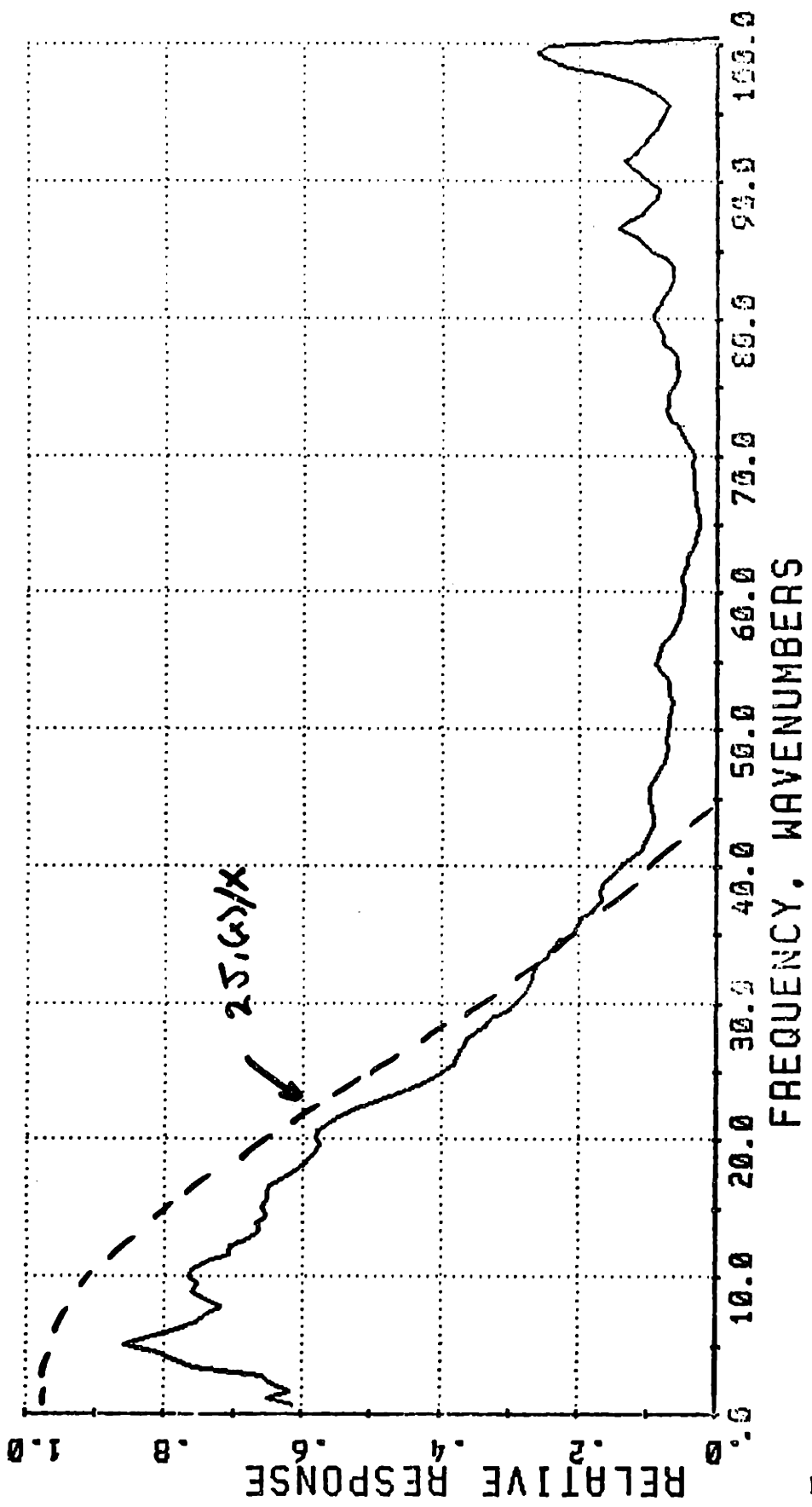
One misadjustment that was investigated is a rotation around the z axis of the BS polarizer. The results of the earlier analysis, for the ray trace calculated beam radius at the BS of 2 cm, is plotted in figure 45^a, along with experimental results for 2 angles of deviation from optimum contrast: 4×10^{-4} and 1.3×10^{-3} radians. The agreement is good, confirming both the alignment criterion and the raytrace diameter calculation.

None of the misalignments analyzed by the matrix method have been investigated systematically. The BS is not in fact at 45 degrees to the entering polarizations, because of the compound angle resulting from the 30 degree entrance angle; this makes the actual angle of the BS 49 degrees. This makes the calculated error on the order of .5%, and hence not verifiable. It is also known that if the D4 are degrees away from 90 degrees the contrast suffers.



BEAMSPLITTER MISALIGNMENT: 1.37 MINUTES

Figure 45a



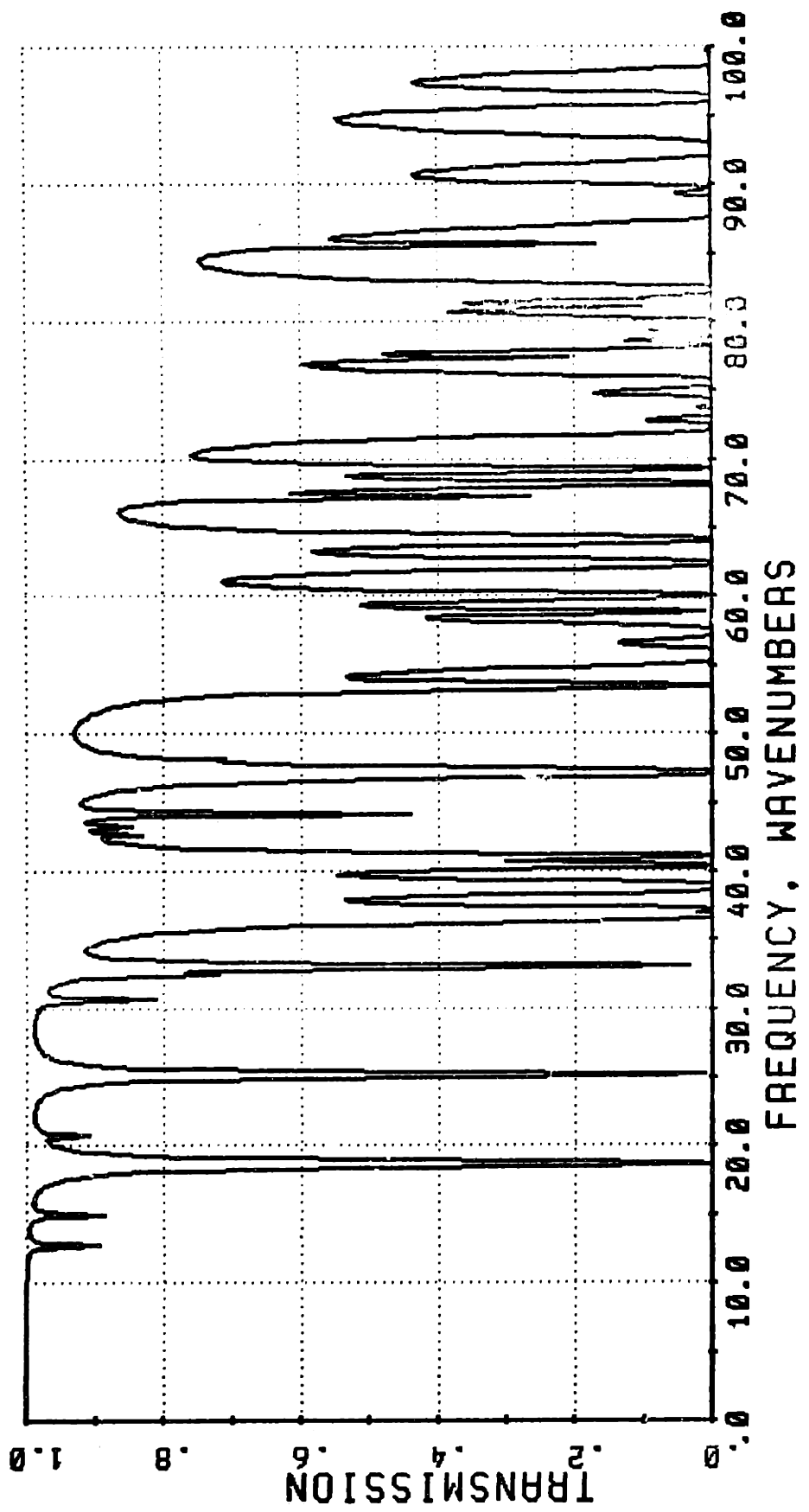
BEAM SPLITTER MISALIGNMENT: 6. 24 MINUTES

Figure 45b

OVERALL HIGH FREQUENCY RESPONSE

There are difficulties external to the properties of the interferometer itself in making an absolute measurement of the HF response. One is the strong absorption in the infrared of H₂O. A program has been written to calculate the transmission of the atmosphere from 1-100 1cm given the column density of water and data on the position and strength of the water lines. It uses a Lorentz line shape and calculates for a .1 icm resolution and a .1 icm line width. Figure 46 shows the transmission for 50% humidity, 20 degrees C, and a 2 meter path, and so is typical of conditions for the interferometer. If one can reduce the column density of water by a factor of 20, measurements up to 100 icm become reasonable. (see figure 47). The fashion in which this is presently done is to place inside the Plexiglas interferometer enclosure and externally refillable container of liquid nitrogen. The dry boiloff gas creates a positive pressure, and effectively though not uniformly reduces the humidity in the box.

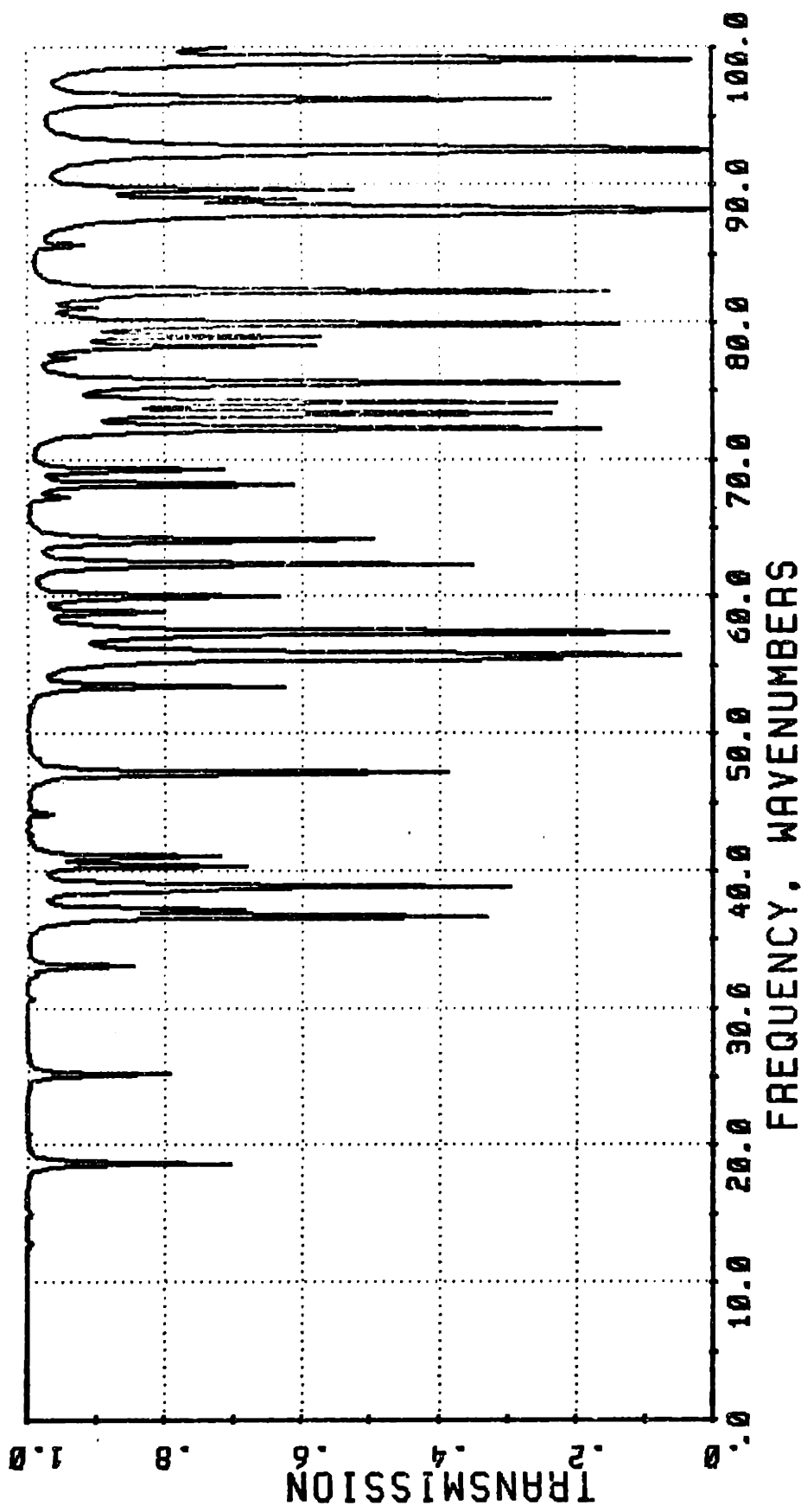
Another problem lies with the detector system. The fundamental assumption in the HF measurement is that the source intensity as a function of wavelength is known (a BB to the desired accuracy of measurement) and also that the detector response as a function of wavelength is known. The first assumption is not a bad one; especially as the size of the radiation becomes small compared with the size of the cavity, a good



TRANSMISSION OF WET AIR: 50% HUMIDITY

2 METER PATH, 20 DEGREES C

Figure 46



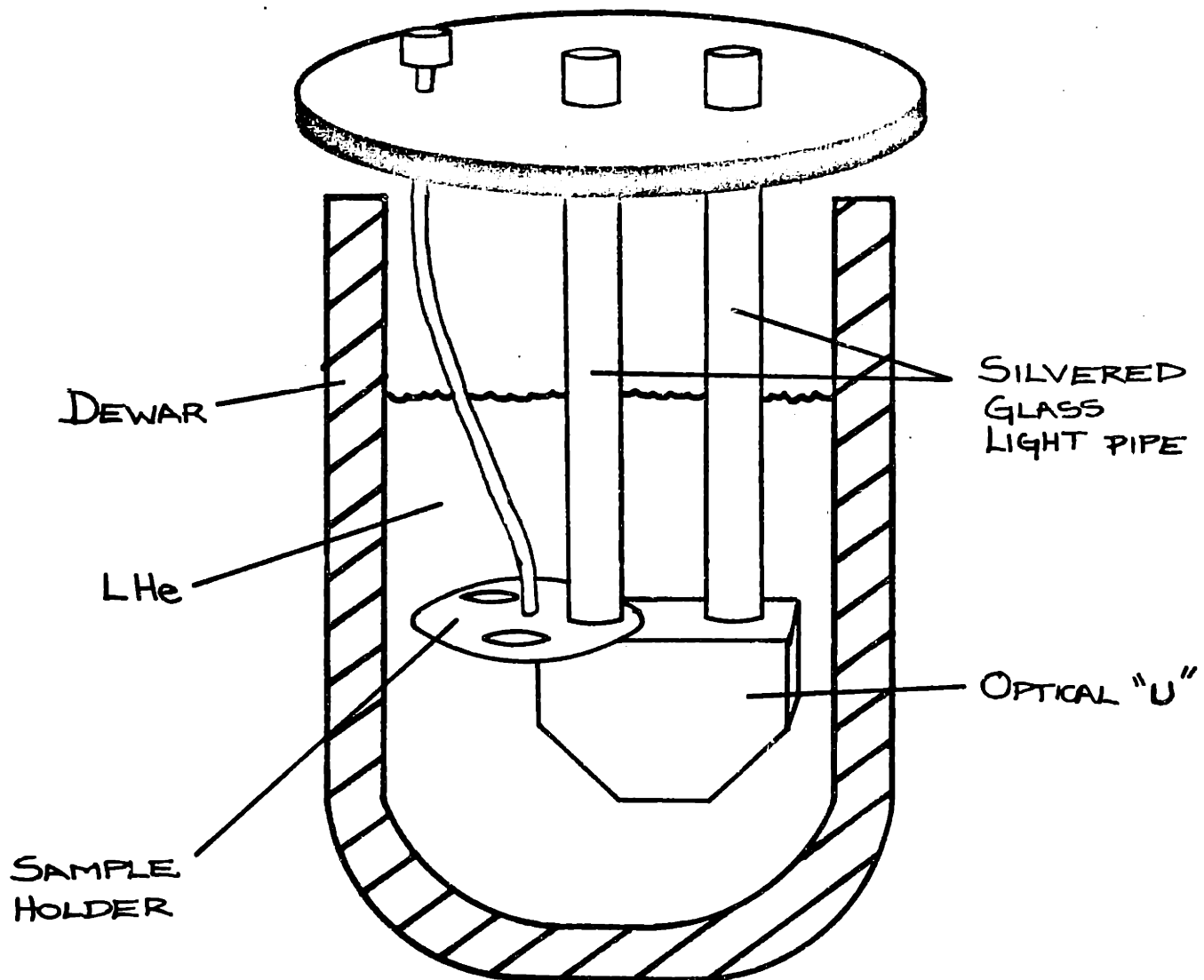
TRANSMISSION OF WET AIR: 2.5% HUMIDITY

2 METER PATH, 20 DEGREES C

Figure 47

BB is not hard to make. The detector, on the other hand, must be filtered to prevent the immense background power from both contributing noise (from statistical fluctuations; "background limiting") and heating the detector away from the desired operating point. The dewar has two filters: a piece of black polyethelyne at about 100 degrees K to stop the bulk of the radiation, and a piece of glass filled Teflon (Fluorogold) at 4.2 degrees K to stop the response above about 100 icm. Because these filter materials have different characteristics when cold, a cold measurement of their passband was made. An accessory dewar which can be inserted in the input light path has been made (see illustration 48). It allows three positions for filter measurements at 4.2 degrees K. With this device, the passband of Fluorogold similar to the filter in the detector dewar was measured, and that characteristic used to correct the raw high frequency curve. Because both of the Fluorogold filters were quite thin and possibly inhomogenous, a measurement of the piece that was actually used as the detector filter should be made.

In correcting the high frequency response, measurements at 300 degrees of the black polyethelyne were used; ideally the response of the piece in question at 100 degrees would be determined. It is not expected that a cold measurement would differ greatly from the 300 degree results.



APPARATUS FOR COLD
TRANSMISSION MEASUREMENTS

Figure 48

The various filters and windows also contribute channel spectra. If the index of a medium is n , the thickness t , and the frequency of incident light ν , then the transmission of a filter is given by

$$T = \left(\frac{4n}{1+n} \right)^2 \left(1 + R'^2 - 2R' \cos 2\beta \right)^2$$

where

$$\beta = 2\pi\nu nt$$

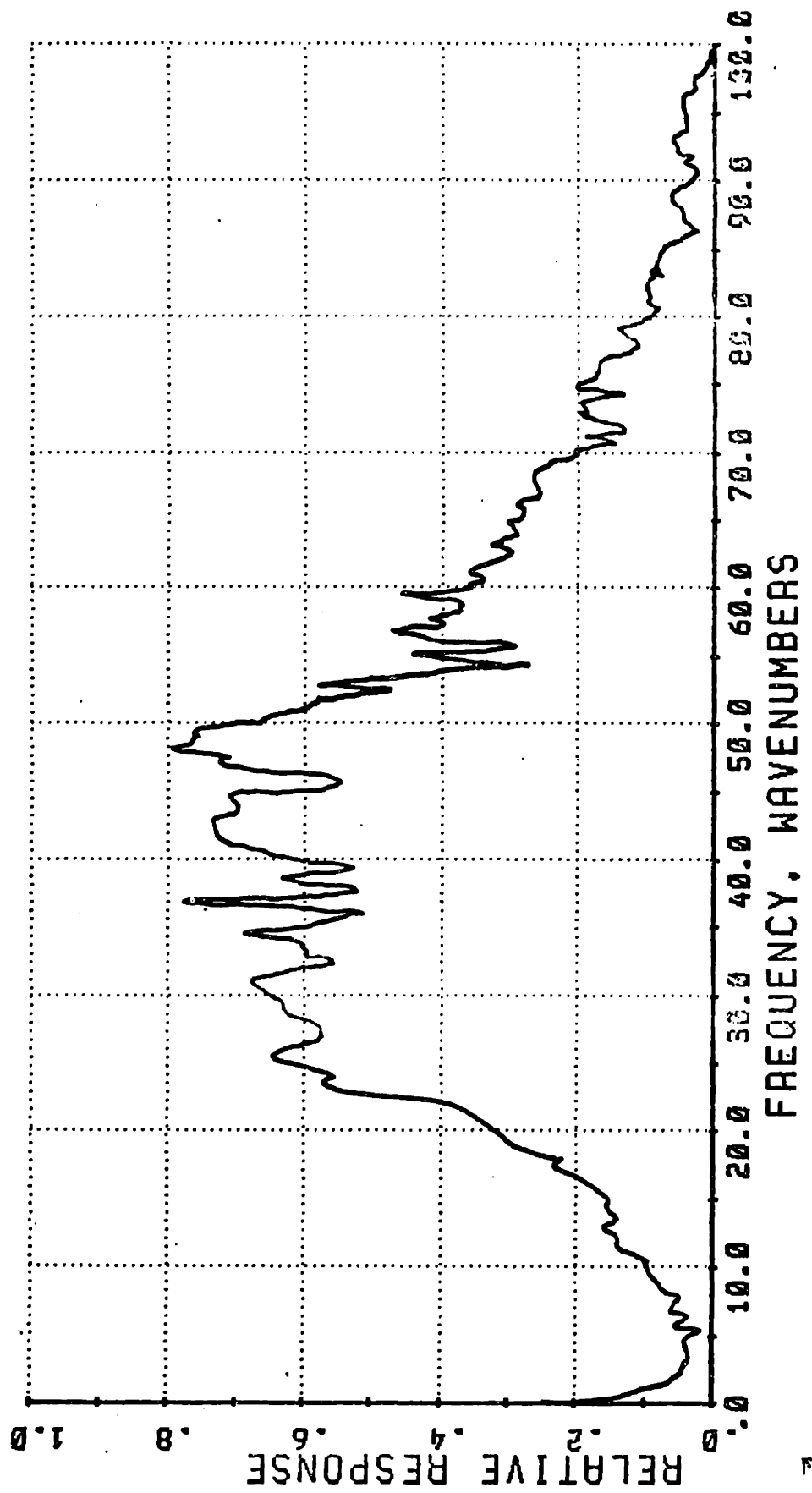
and

$$R' = (1-n)/(1+n)$$

for normal incidence. There is also an exponential damping of the sinusoidal modulation due to losses in the filter and the solid angle of the beam. Using the known index, one can fit for minimum ripple to try to eliminate the channel spectra. Some of the more obtrusive wiggles have been removed in this way.

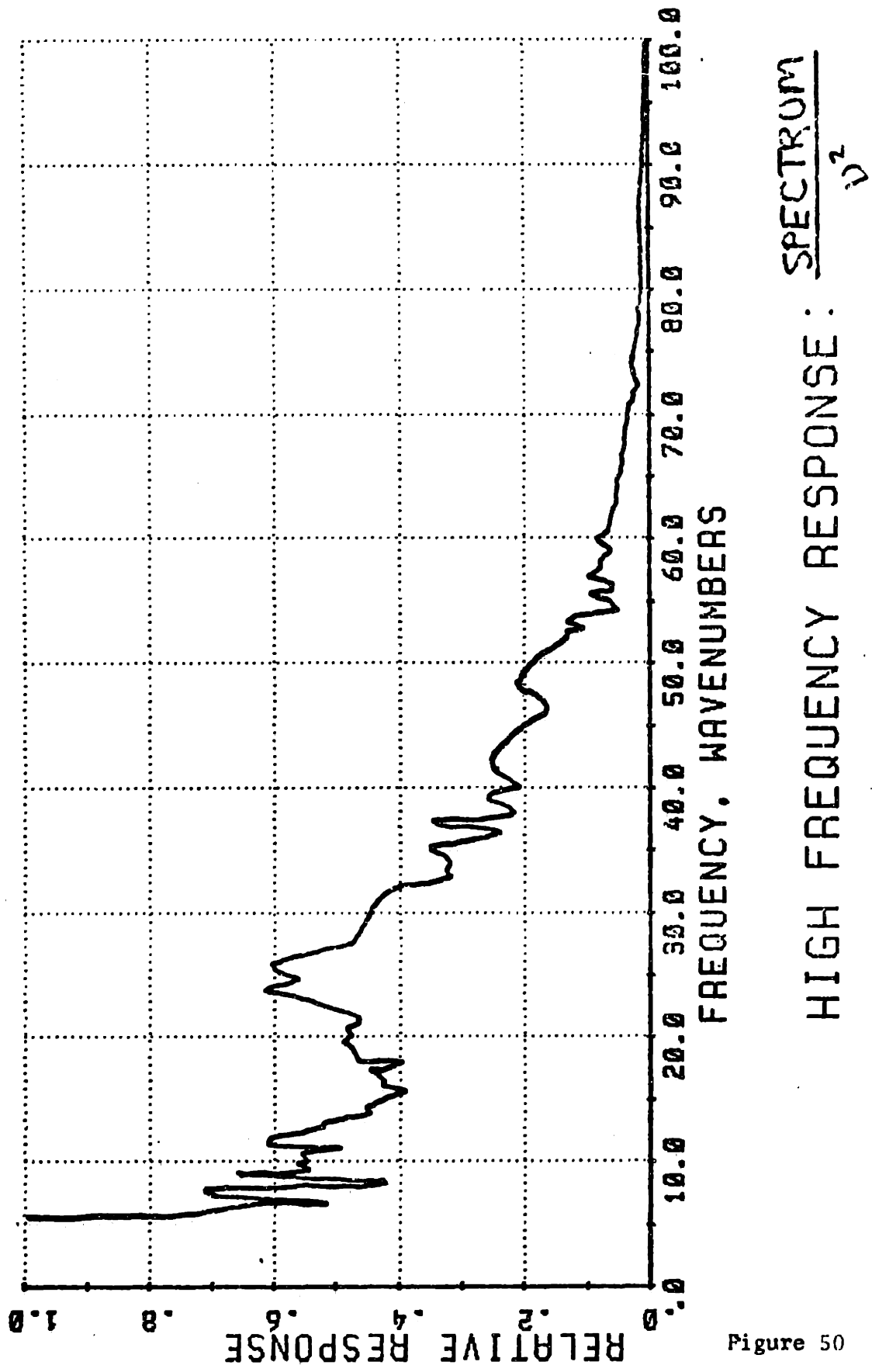
The figures 49 through 53 show the progression from raw spectrum through corrected HF response. Figure 49 is the spectrum as collected, figure 50 is the spectrum divided by ν^2 which corrects for the BB Rayleigh-Jeans spectrum, and figure 51 has been corrected for the cold Fluorogold filter. Figure 53 shows the spectrum corrected for some channel spectra and for the black poly filter, and also for the electrical filters.

The measured HF response and the expected response (due to the polarizer rolloff) are plotted together in figure 53. The filter removal involves the assumption mentioned earlier that the filters in the dewar are the same as those measured. The error in average thickness of the Fluorogold filter could be 10% (1 mil



HIGH FREQUENCY RESPONSE : RAW SPECTRUM

Figure 49



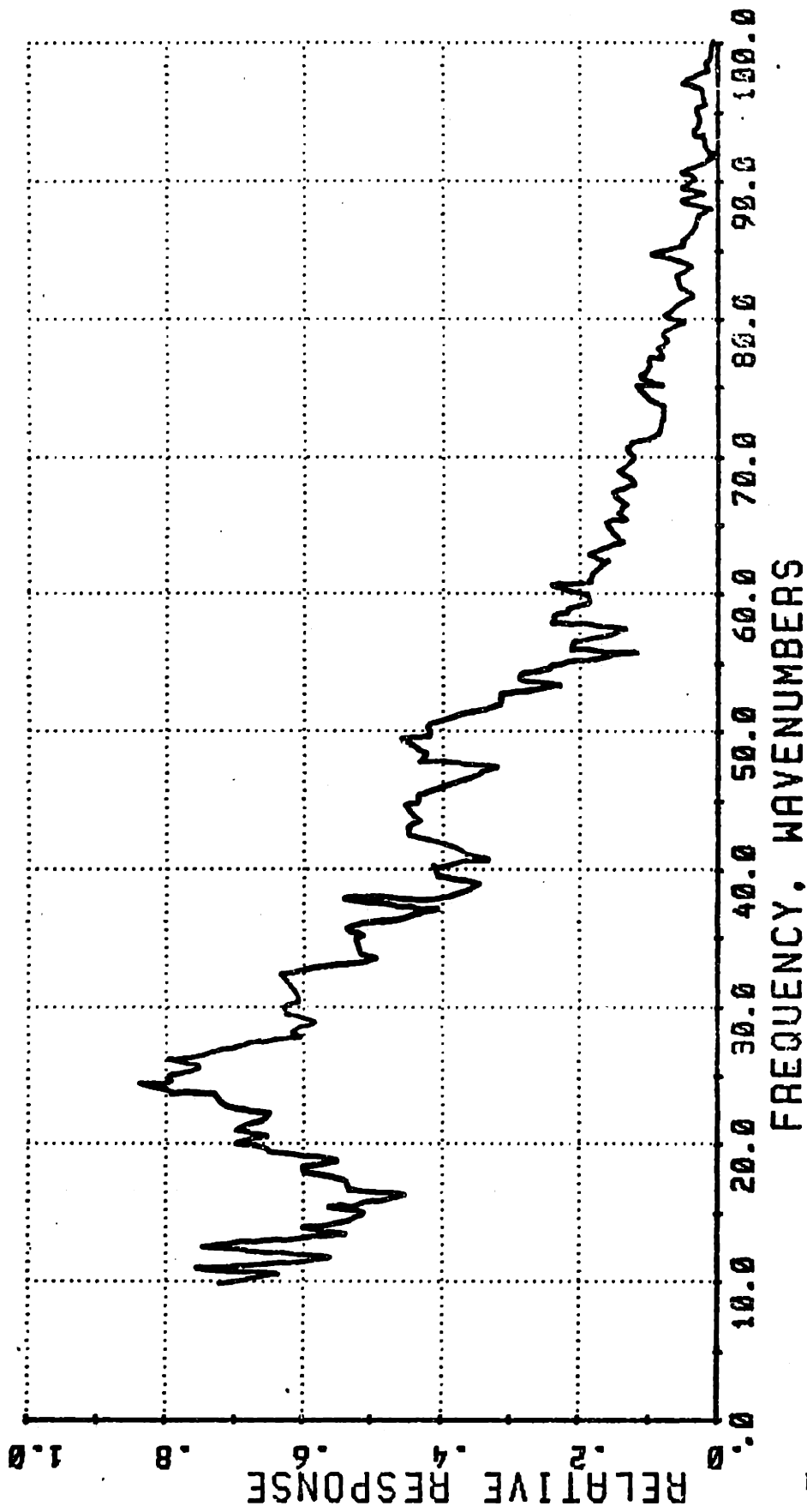
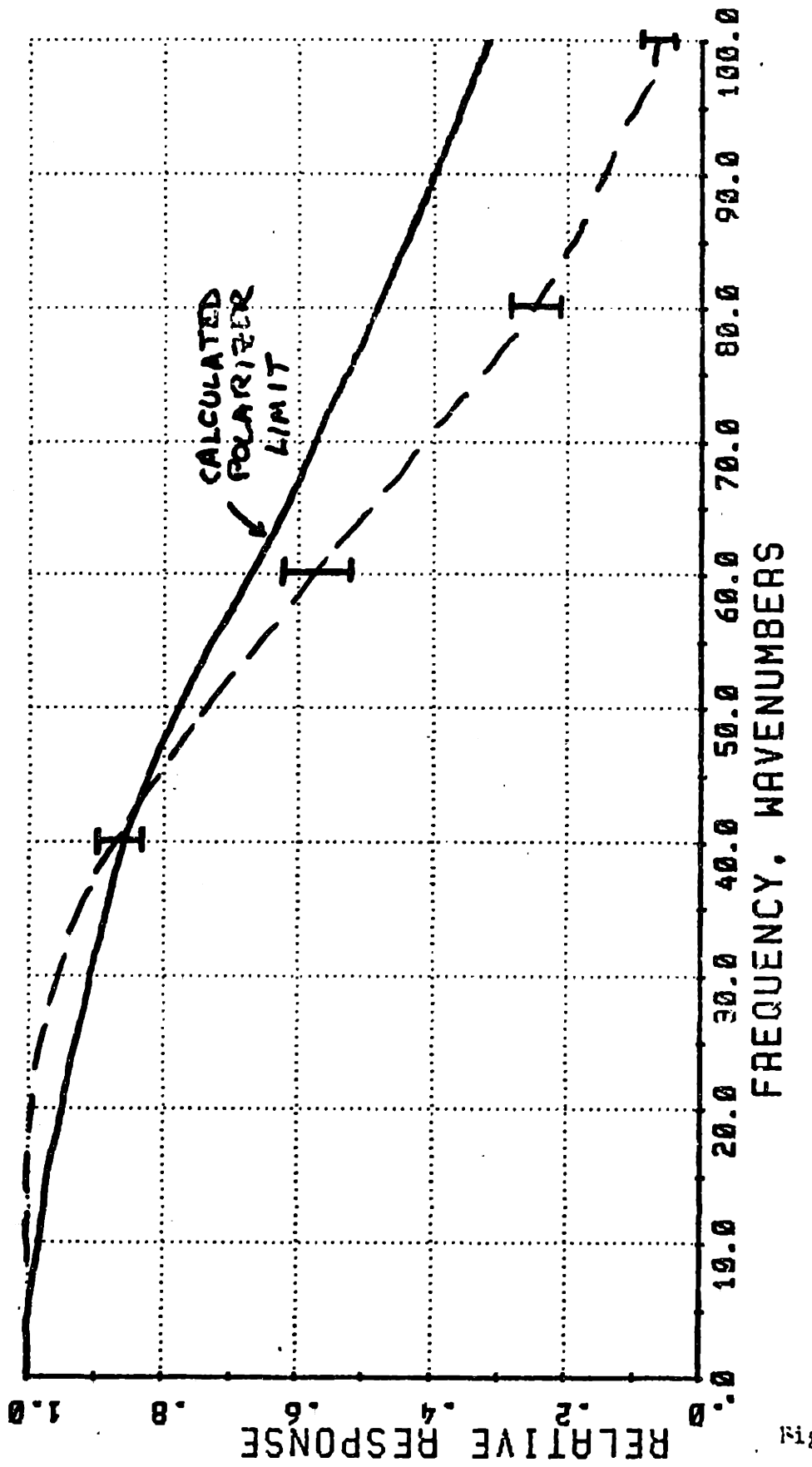


Figure 51

HIGH FREQUENCY RESPONSE:

CORRECTED FOR FLUOROCOLD



HIGH FREQUENCY RESPONSE

Figure 53

out of 10); this leads to the error bars shown on the measured response. The errors may be greater if the Fluorogold is inhomogenous at these thicknesses. The predicted response is based on the computer generated curves for the polarizers. The assumptions are that there are no losses (i.e. $T=1-R$) and that the functional dependence is correct. No measurements of the reflection from the polarizers have been made, and the data on transmission suggests that the model is not quite right. More complete measurements of the polarizers would be necessary to say whether or not the HF response is understood completely. Depolarization on M2 also remains as a candidate for causing rolloff.

C) LOW FREQUENCY RESPONSE

FACTORS AFFECTING THE LOW FREQUENCY RESPONSE

In the design of the optics, the mirrors were chosen to be sufficiently oversized to include the second dark ring of the diffraction pattern due to a 10 icm wavelength. The diffraction is given by

$$I = (2J_1(x)/x)^2$$

where

$$x = \pi D/rf$$

where

r = radius of the aperture

f = f number of the beam

with $x = 7$ for the second dark ring; hence $r_{\text{diff}} = .223 \lambda f$.

The diameter of the geometric spot is determined by the $A\Omega$ and the f number, giving $r_{\text{geo}} = .45 x$ f number. So the mirrors are $(.45+.223)/.45 = 1.5$ times bigger than the geometric beam.

The amount of energy falling inside the mirrors is given by

$$1 - J_0^2(x) - J_1^2(x)$$

This is the expected loss per aperture-mirror pair; it is plotted vs. frequency in figure 54. Probably the most severely restrictive pair is the WC-M1 radiator and receiver. This suggests that the LF response should go roughly as the function above evaluated for this pair. Attempts to calculate explicitly

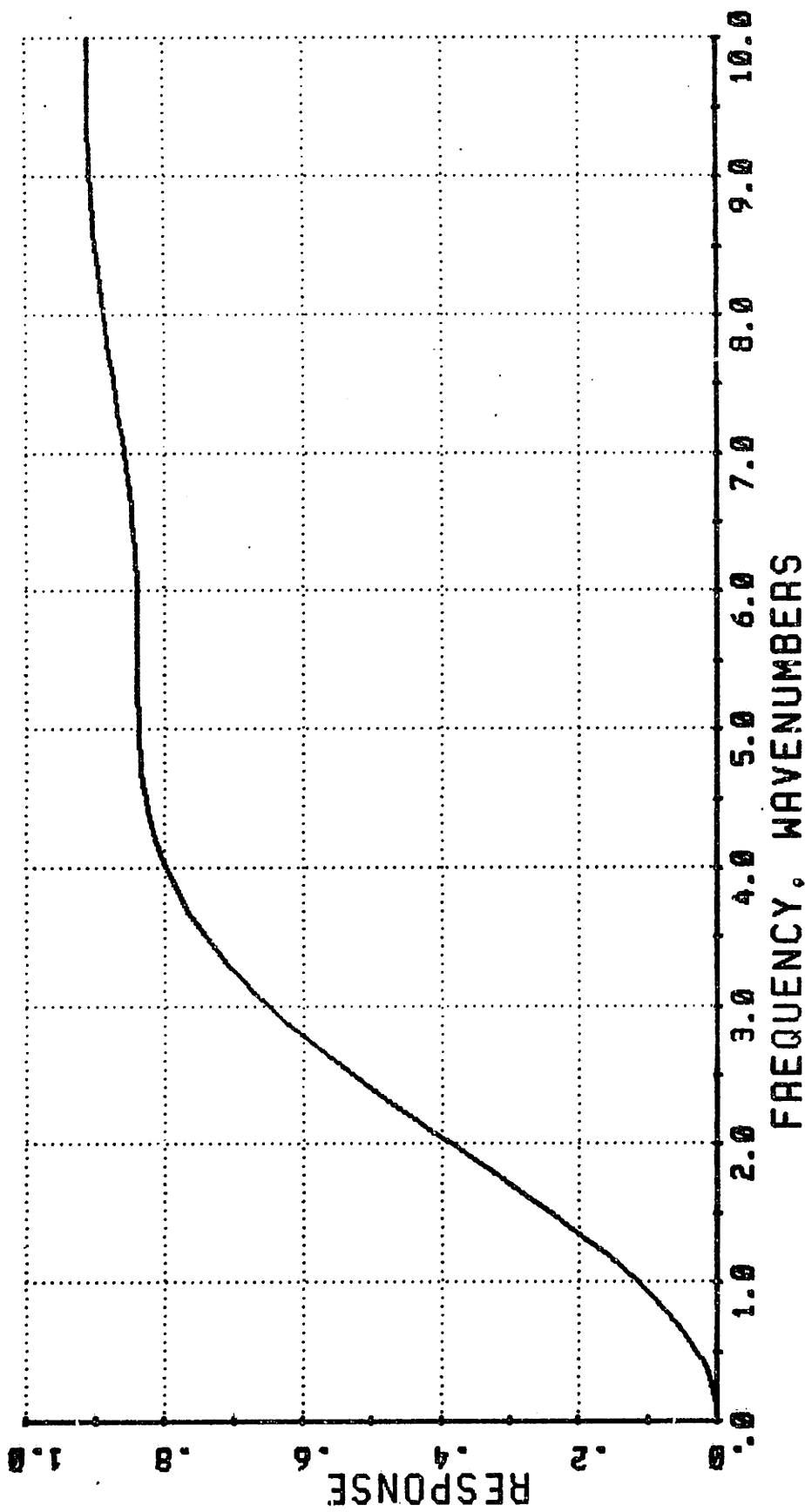


Figure 54

X=7 AT 10 ICM

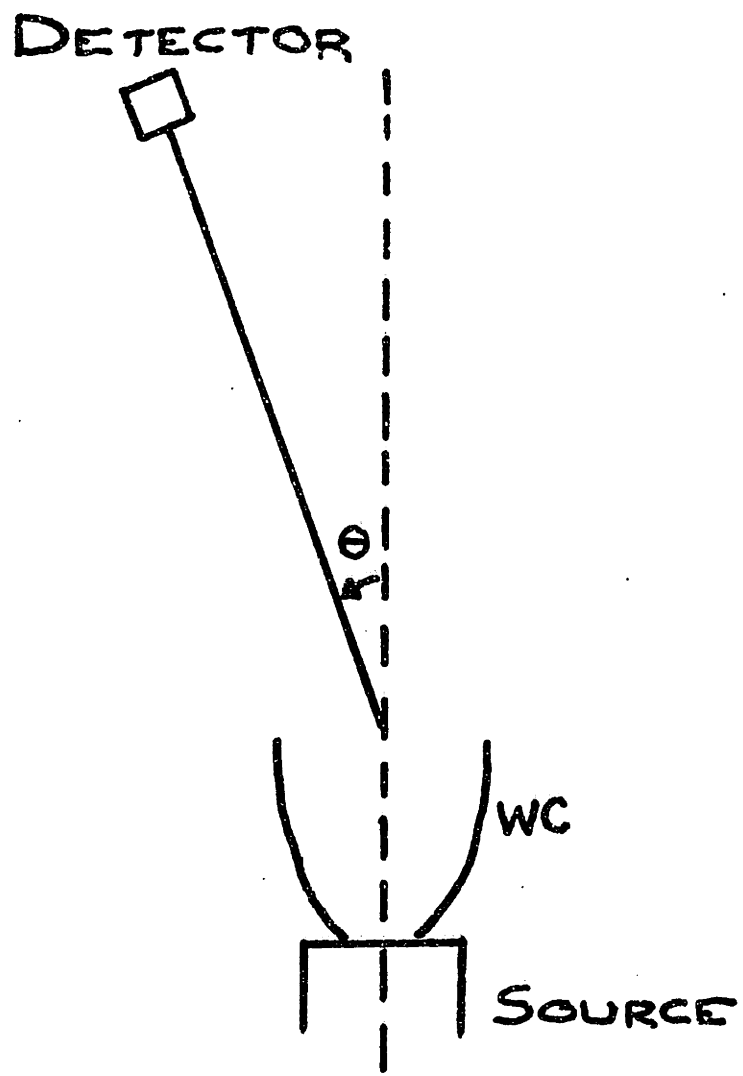
DIFFRACTION LOSSES: $1 - J_0 * J_2 - J_1 * J_2$

the WC diffraction pattern have been made; the models have been convolutions in one and two dimensions of diffraction patterns from circular apertures. However, none of the models gave results that predicted the experimental results (see next section). The importance of the input-output conditions makes this a good candidate for further study.

MEASUREMENTS OF THE LOW FREQUENCY CHARACTERISTICS

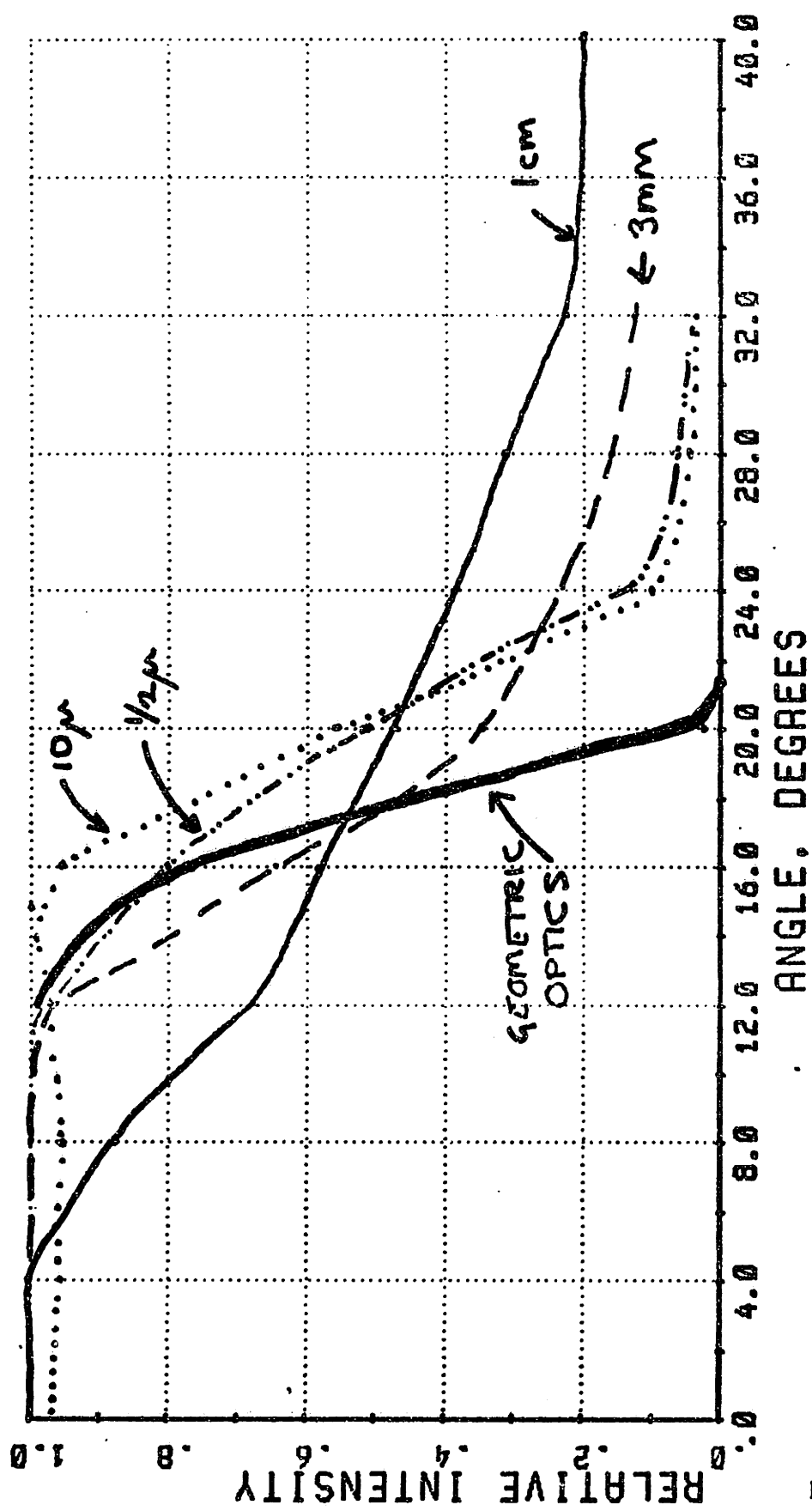
MEASUREMENT OF THE WC OUTPUT PATTERN

The beamaps at 3mm showed significantly greater losses at the first M1 than the shorter wavelength maps; this indicates diffractive spreading of the output beam. This observation led to measurements of the angular output of the WC. The experimental setup (see figure 55) consisted of a source driving the WC and a detector which could map the output as a function of angle at a constant distance from the cone. Measurements for 1 cm radiation (using a klystron and crystal detector), 3 mm radiation (klystron and pyroelectric detector) 10μ (BB and pyroelectric) and $1/2\mu$ (BB and photodiode) were made. They are shown in figure 56. There are some notable points: for long wavelengths the pattern is broader, indicating diffraction, but at all wavelengths the amount of power at large angles is in excess of the theoretical geometric calculation. There is some fear that the input conditions ($a\pi/2$ Lambertian source) were not fulfilled for the long wavelength sources; the mode mixer output (shown in figure 57) has an excess of energy at large angles. The fact that even in the geometric limit the WC is not performing as expected leads one to conclude that some of the difficulty in predicting the diffractive spreading is due to imperfections in the WC.



WINSTON CONE
ANGULAR OUTPUT

Figure 55



WINSTON CONE ANGULAR OUTPUT

Figure 56

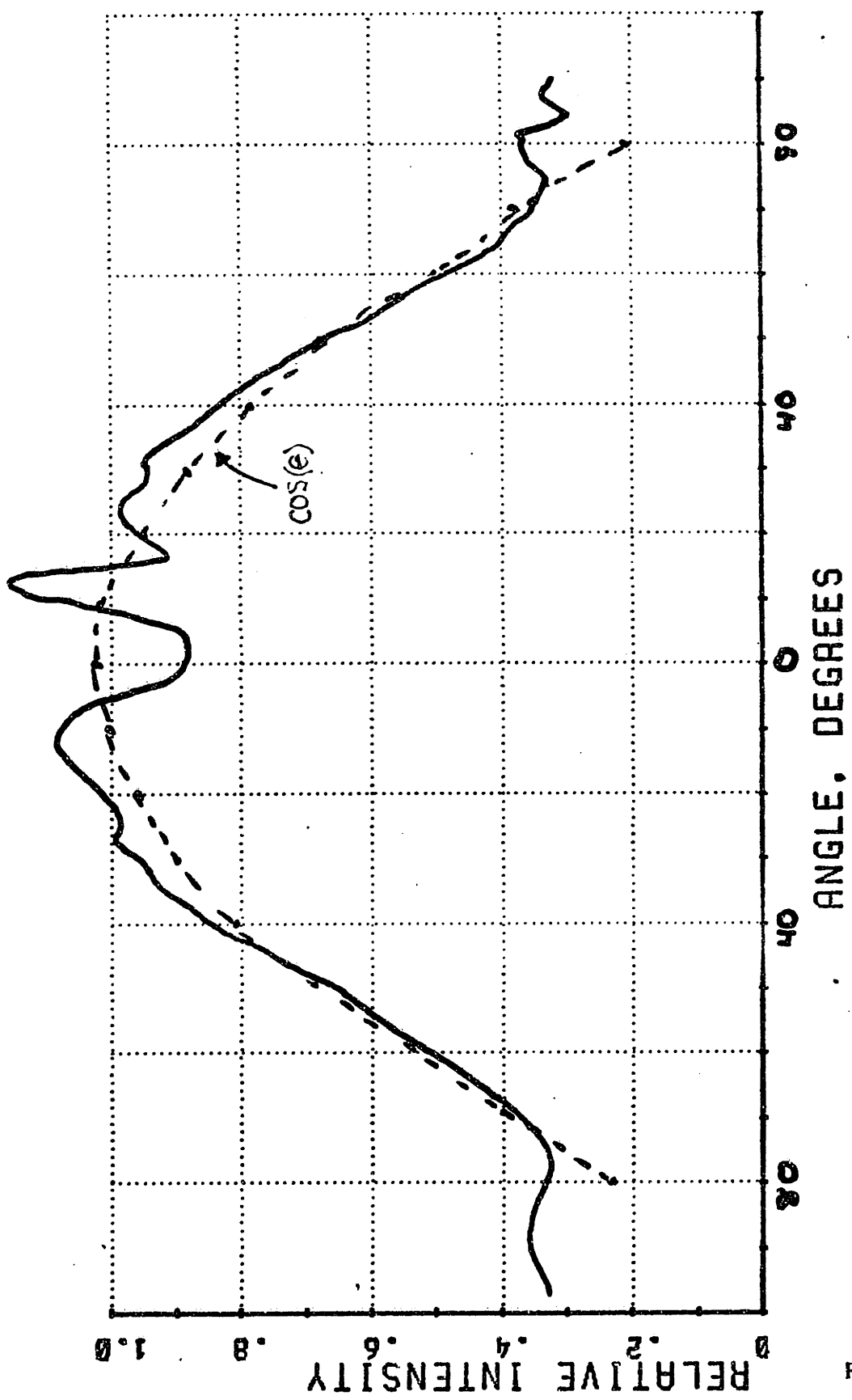
MODE MIXER ANGULAR OUTPUT

Figure 57

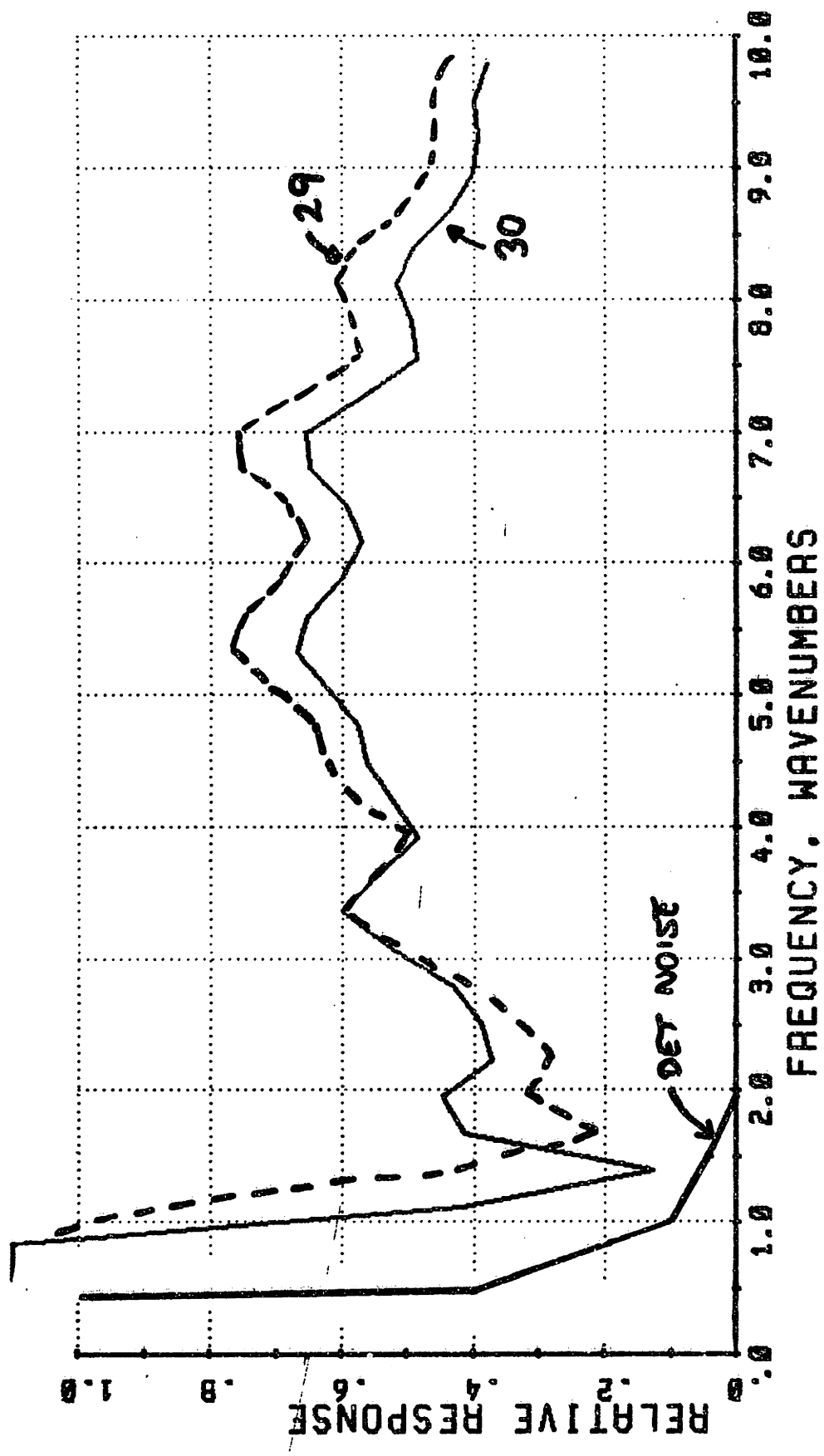


Figure 58

1.75 CM DELAY TOTAL, RAPID SCAN .07 SEC

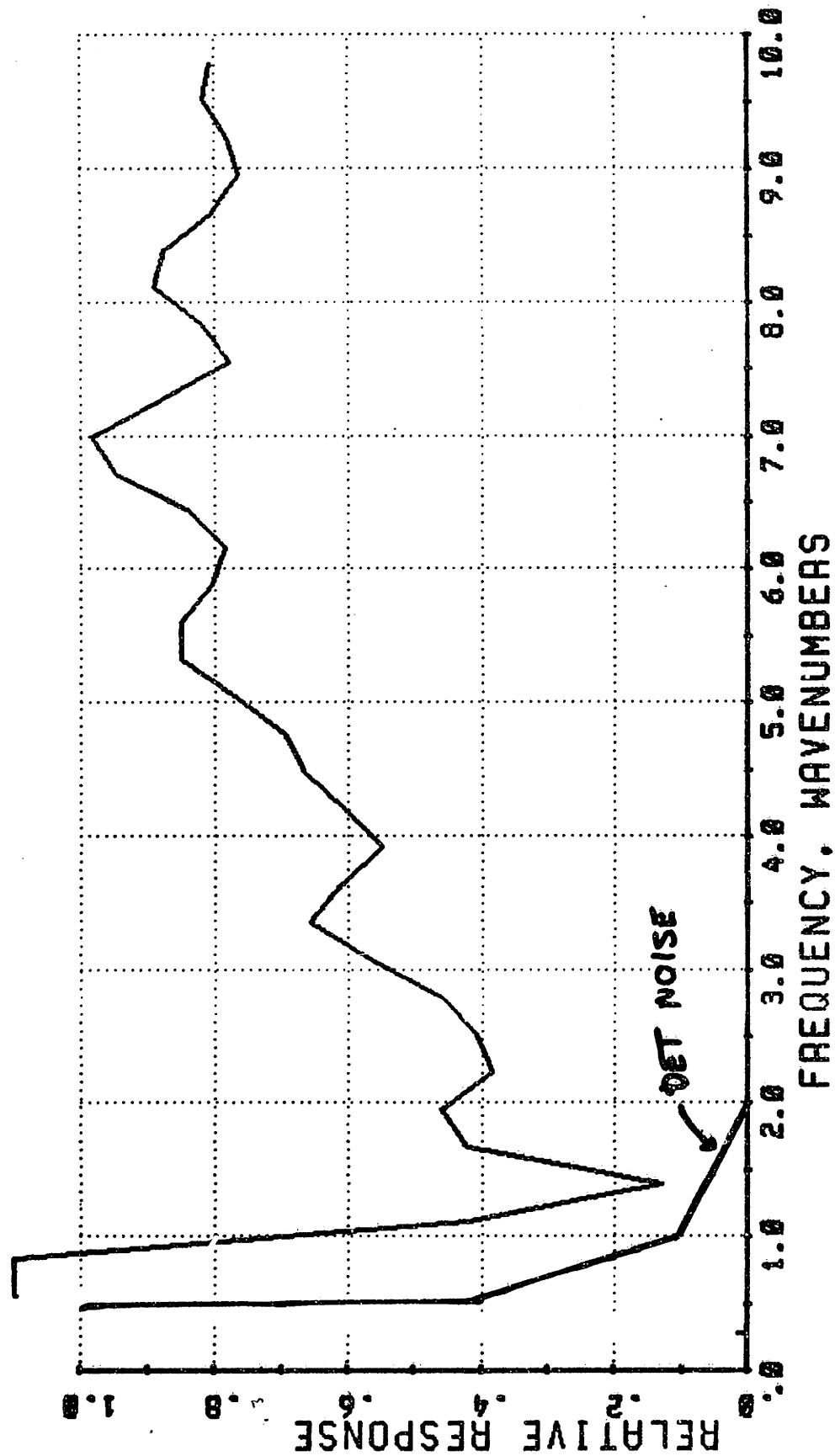


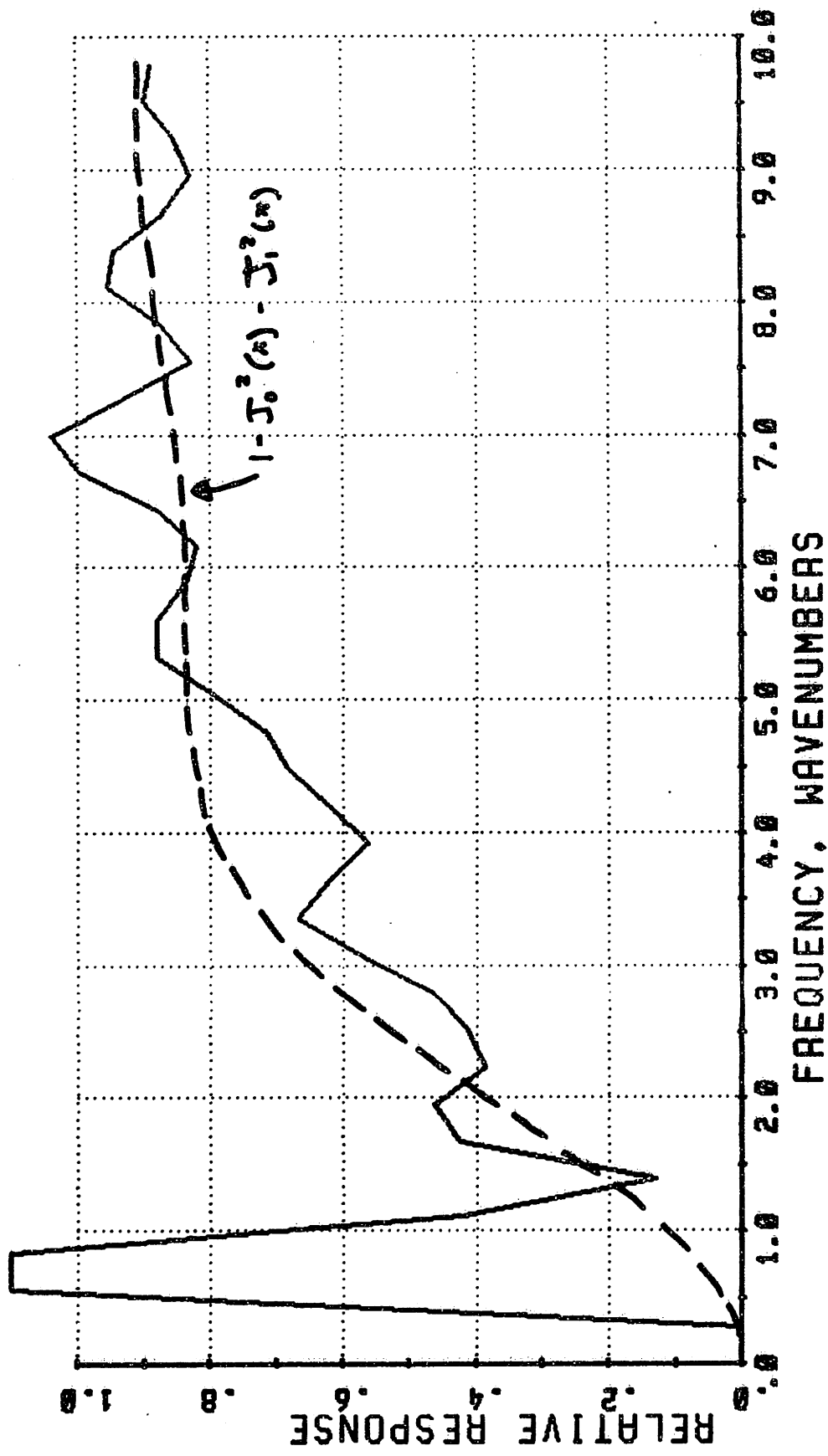
Figure 59

5*.01 SEC .07NORM

INT. 30. CORRECTED FOR ELECTRICAL LP FILTERS

INT. 30. CORRECTED FOR ELEC. AND OPTICAL LP
Figure 60

5*.01LP. .125POLY. .095FL



THE MEASURED LF RESPONSE

The measurement was performed in the rapid scan mode to raise the audio frequency being transformed above the point where $1/f$ noise in the atmosphere is prohibitively large (about .1 hertz). Optical filters were used to limit the BW to 0-15 icm also to reduce the influence of humidity fluctuations. Two sample raw spectra divided by $\sqrt{\lambda}$ are shown in figure 58. Note that the detail above 1.5 icm in the spectra is not noise, but channel spectra, amplitude modulation of the beam, and instrument rolloff. Note also the H_2O lines at 18 and 25 icm. Also plotted is the detector noise divided by $\sqrt{\lambda}$; below about 1.5 icm this noise dominated.

The next figure (59) shows steps in the recovery of the LF response. At the top is the raw spectrum, divided by $\sqrt{\lambda}$, plotted to 10 icm. The resolution for this spectrum is .57 icm. Next the filters have been divided out, and some of the channel spectra removed. The detector noise spectrum is also shown. The next figure (61) shows the LF response and the diffraction losses that are predicted for the WC-M1 pair. The agreement is marginally satisfactory for the BB measurement; the BB peak is at 6 icm, and must be measureable to 1 icm. Since channel spectra and diffraction lamps can be divided out, they are permissible, but

must not be so attenuative as to reduce the signal to noise ratio excessively.

D) FREQUENCY DISTORTIONS

Since the COBE measurement will be looking for deviations on the level of .1% from a known spectrum, the interferometer must introduce very little distortion which causes a shift in power from one frequency to another.

A source for frequency distortion is in amplitude modulation of the output intensity by changing geometry inside the interferometer. As the delay is changed, the path length and hence the focus by M2 on the DH changes. This modulated signal is proportional to the total power through the interferometer. The design gives a minimum spot size at the output for 0 delay; on either side of the central maximum, the spot size grows and the power that gets into the output cone drops. This causes a roughly parabolic amplitude change in the interferogram which shows up as a very low frequency (the first few points of the transform) power in the spectrum. This can be observed in figure 14. In general, the value of the first point is given reasonably well by

$$S(n=1)(\text{watts}/\text{icm}) = 4.9 \times 10^{-3} x^2 P(\text{watts})$$

where x is the real mirror movement in cm and P is the peak value in watts of the interferogram, the latter representing the total power through the interferometer. There is also a contribution to the second point of the transform from amplitude modulation.

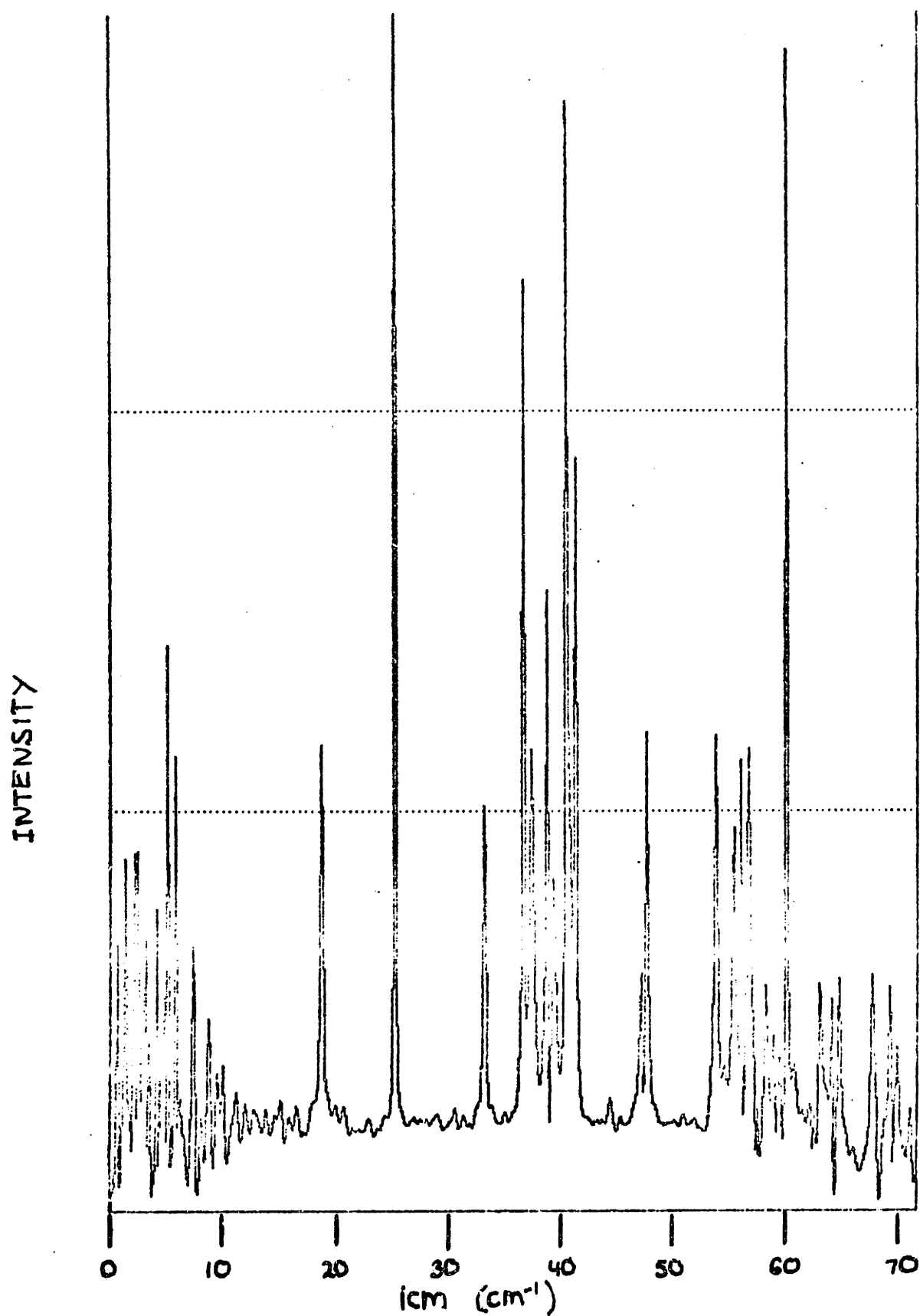


Figure 63: Water Absorption Lines

Its functional dependence is similar to that of the first point but at a level of about .05 of the first point. This would be caused by assymetry in the defocussing due to carriage motion.

An upper limit on the accuracy of the position transducer can be obtained by identifying water vapor absorption lines in the spectra. A linear error would show up as a constant fractional frequency error. In figure 63 the division of a purged spectrum by an unpurged spectrum causes the H₂O absorption lines to appear as peaks. 10 of these lines were identified and their positions compared with their known wavelengths; the result is that there is a linear error of 2×10^{-4} . Some of this may be graphical measurement error, however, so this is an upper limit. If the spectrum is examined for 'ghosts' (due to periodicities in the grating) the upper limit is about 1%; no ghosts are visible, but the baseline noise would obscure any small wings.

Two sources of harmonic distortion are reflections from exterraneus objects and multiple reflections through the instrument. If some of the beam intended for a DH misses the DH, reflects from a stationary object (say the surrounding dewar) and pick up the necessary phase change from multiple bounces, and returns to the BS, it is as though for some of the signal that only one mirror is moving. This makes the change in delay for a displacement of the carriage half of that expected, and

introduces power in the spectrum at half the real frequency.

This will go as the $(\text{reflection})^2$ for the correctly polarized reflection.

Multiple passes through the interferometer can introduce harmonic distortion because the delay for the beams goes as $n \times n$ the number of passes, making power appear at harmonics of the real frequency. The first term is the third harmonic; a signal traverses the interferometer, is reflected at the output back through to the input, and then back to the output, experiencing the differential delay three times. If the reflection is polarization dependent and if it is assumed that the coherence length of the electric field is greater than the 2 meter path through the interferometer, the problem can be easily treated with the matrix analysis. The result is, for a reflectivity R at the input and output,

$$I_+ = R^4 [(\sin^6 \delta + 6\cos^2 \delta \sin^4 \delta + 9\cos^4 \delta \sin^2 \delta) I_{+,n} + (\cos^6 \delta + 6\cos^4 \delta \sin^2 \delta + 9\sin^4 \delta \cos^2 \delta) I_{-,n}]$$

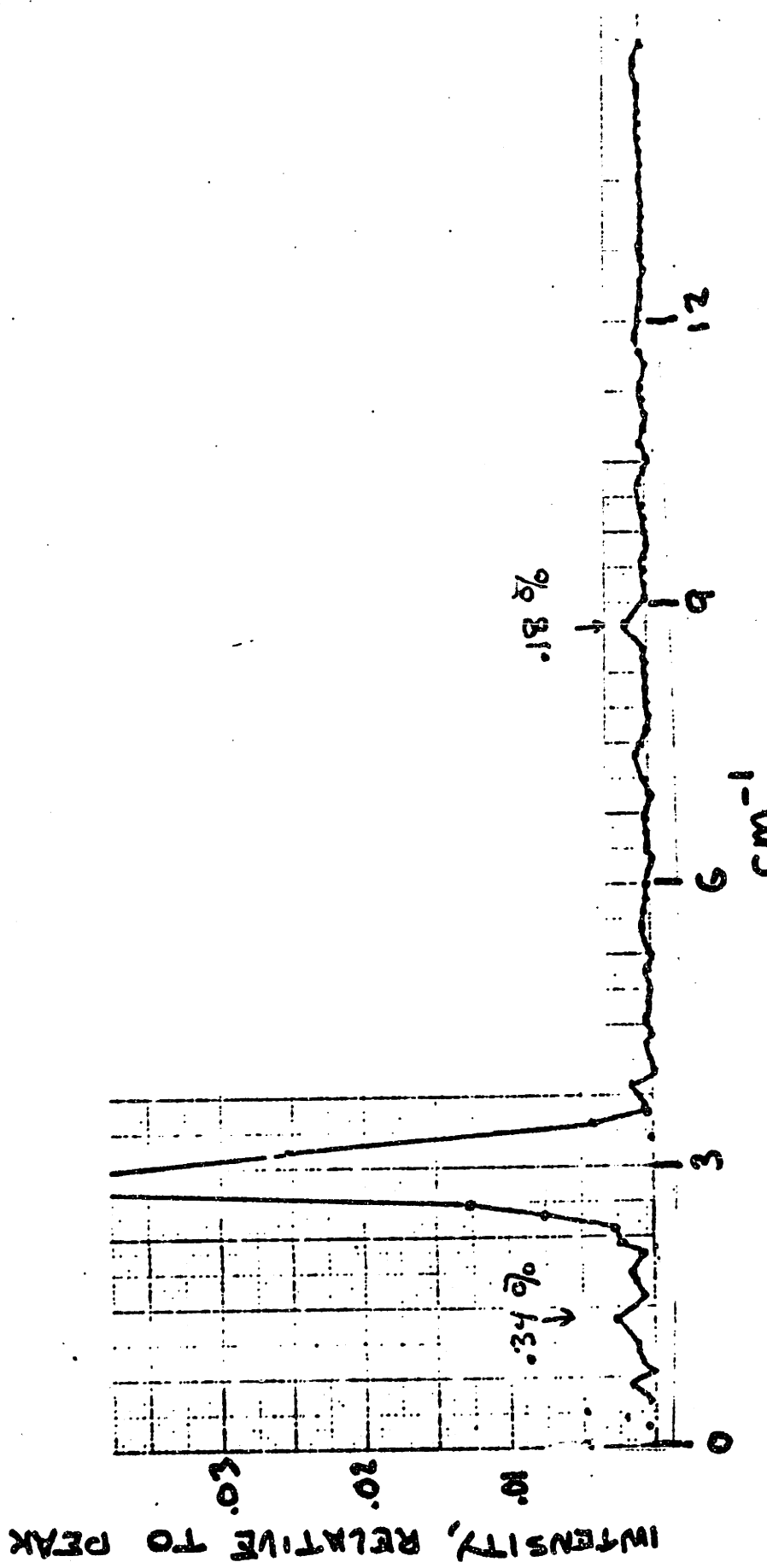
$$I_- = R^4 [(\cos^6 \delta + 6\cos^4 \delta \sin^2 \delta + 9\cos^2 \delta \sin^4 \delta) I_{+,n} + (\sin^6 \delta + 6\cos^2 \delta \sin^4 \delta + 9\cos^4 \delta \sin^2 \delta) I_{-,n}]$$

The intensity of the harmonic goes as R^4 so that moderate reflections are tolerable; an R of .18 gives an harmonic about three orders of magnitude down from the spectral peak.

No evidence for harmonics due to multiple reflections or subharmonics can be found in the BB spectra; any low level

distortions are lost in the channel spectra and noise. The 3mm coherent source spectrum shows both of these features, a result of the long coherence length of the radiation (on the order of 5000 km).

In figure 64 1/2 ν signal is visible at a level of .34% of the peak, and third harmonic is present at .18% of the peak. The latter indicates a WC reflectivity of .2 .



Harmonics and subharmonics in Klystron Spectrum

Figure 64

E) RESOLUTION

As soon as the beam at the BS has a divergence, there are rays that travel different distances from the BS to the DR and back. The design $\Delta\Omega$ and focal length for M2 gives an angle of .1 radian max; the difference in path for this most extreme ray from an axial ray is $l - \cos \theta = (1/200)\theta$. If this distance is comparable to the wavelength, the contrast will suffer. The effect of aberrations in M2 is the same as an increased solid angle and will similarly effect the resolution. For 100 icm, the maximum allowable path length is on the order of .5 icm, so the resolution can only be about 2 icm. For 20 icm, .1 icm resolution is possible, as per the design. The unapodized resolution measured is as calculated (see figure 65) for the 3mm source. For a total path length difference, of 6.98 cm, the FWHM is $l/L = .14$ icm. The klystron is the only source for which the sampling errors or harmonic distortion could be measured, due to its line-like nature. The fact that the FWHM is as calculated indicates that the sampling errors which widen a spectral peak are substantially absent.

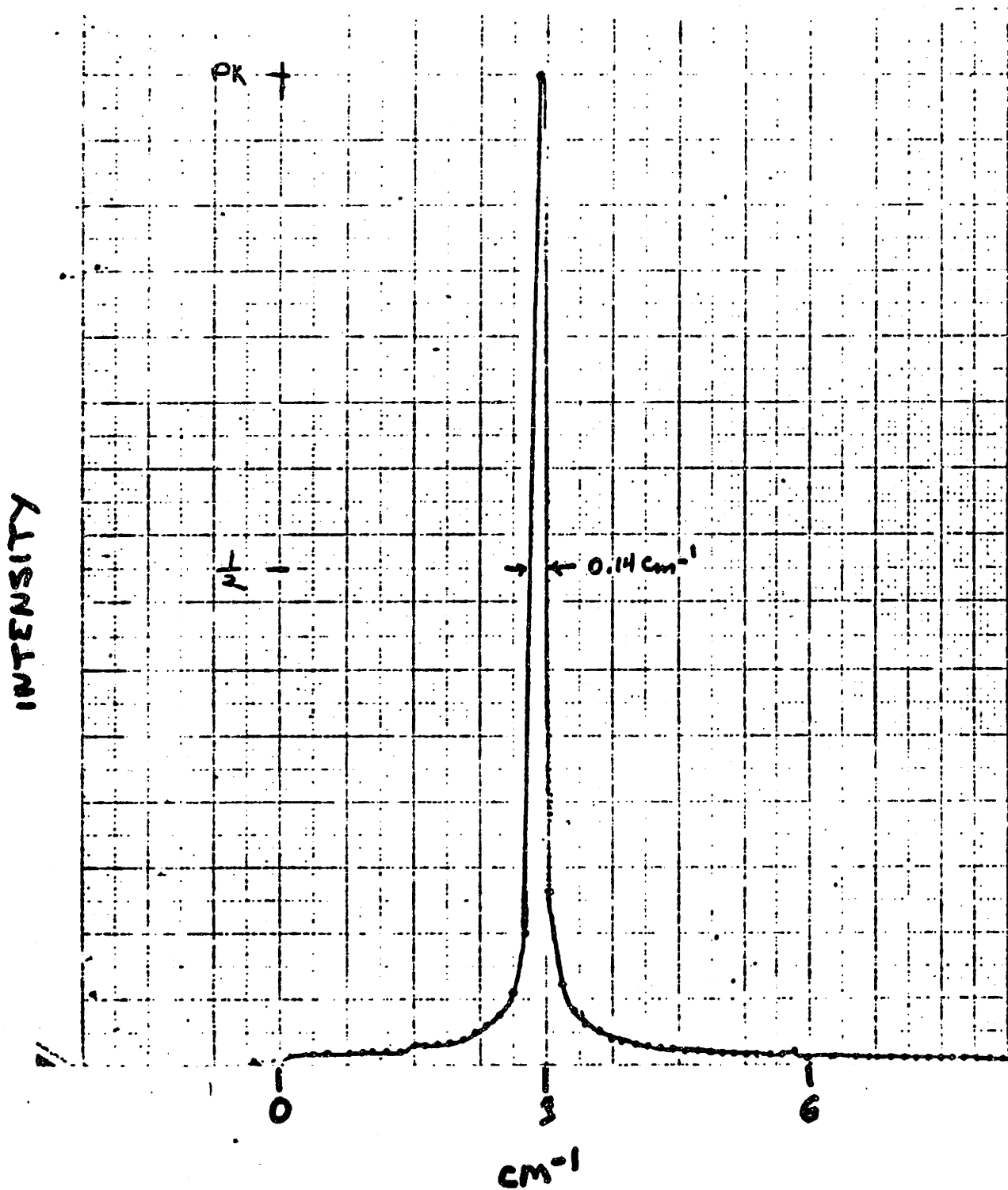


Figure 65: Resolution of Klystron Output

APPENDIX: COMPUTER MODELS OF SAMPLING

SAMPLING ERRORS

To study missampling a computer program (CRR) has been written. It samples or missamples in a variety of ways a sine wave, and then fourier transforms this 'interferogram' to frequency space where it is displayed as a power spectrum. Figure 66 shows the properly sampled spectrum. The input sine wave is 50 icm, and the sampling periodicity is 200 samples/cm, as it is for all of the figures shown. 256 cycles of the wave have been sampled. The total effective scan length is 5 icm, so the resolution is $1/5 = .2$ icm, which is the distance between two points in the spectrum.

One of the most likely errors is random jitter around the intended sampling point. The computer models this as a random evenly weighted deviation of a given maximum percentage of the sampling length. Figures 67a through 67e show the results for various frequencies of sine wave and error amplitudes (the latter given as the fraction of the sampling length). If the sine wavelength is long compared with the scale of the noise, a low level white noise is seen. If the period of the sine wave approaches the size of the noise (80 icm illustration) the white

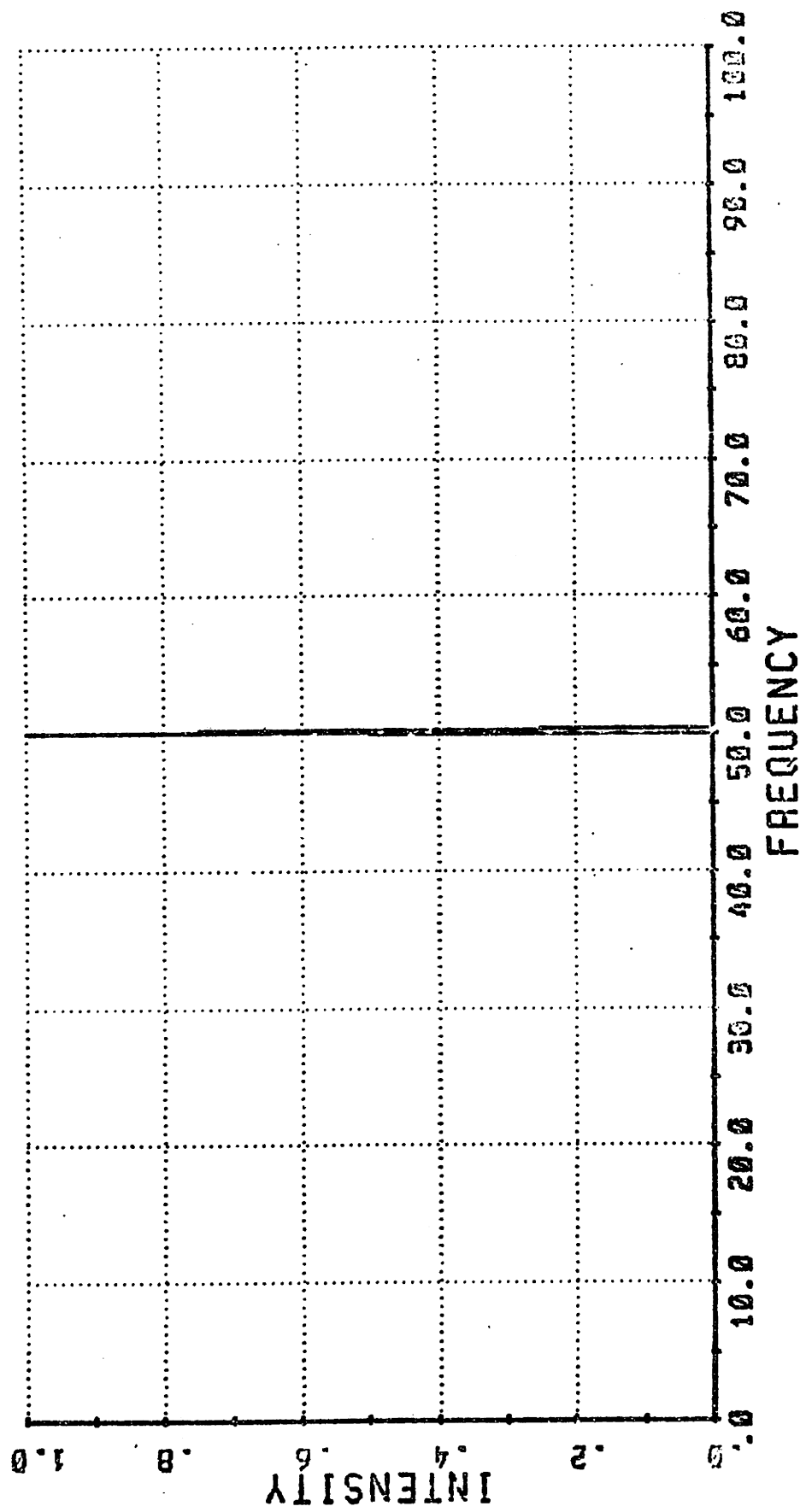


Figure 66

SIGNAL AMPL = .1

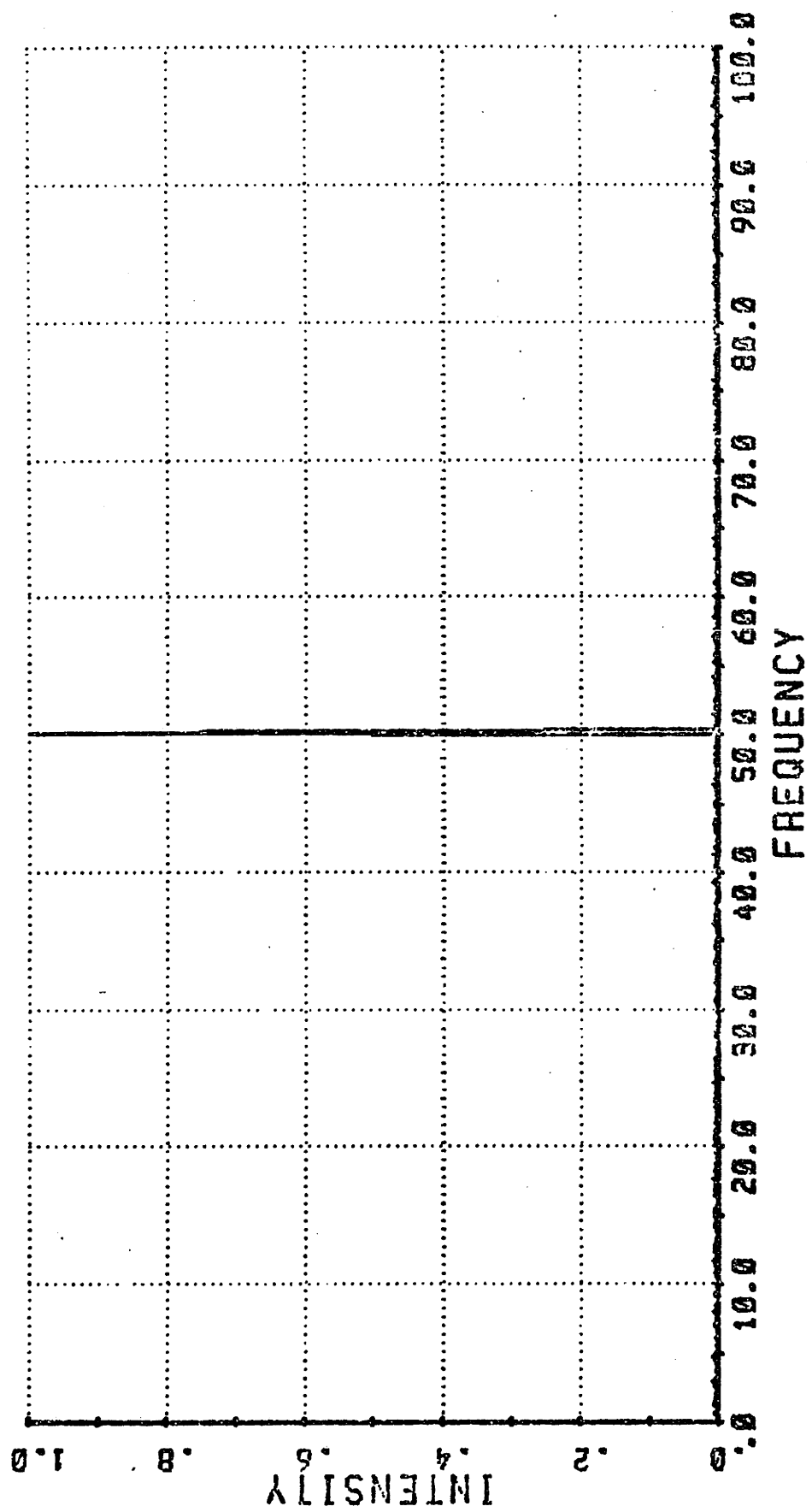
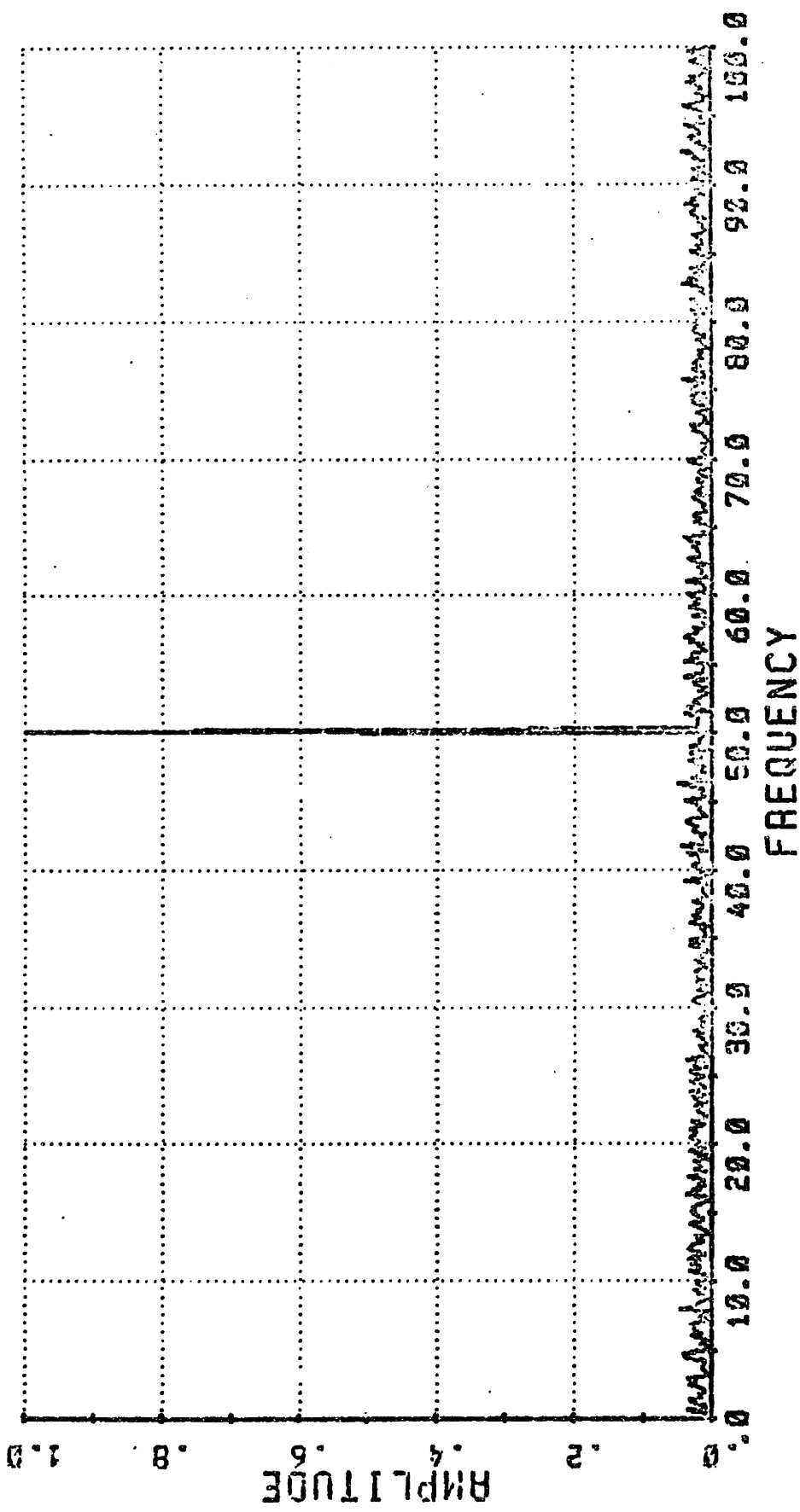


Figure 67a

RANDOM ERROR: AMPLITUDE = .1

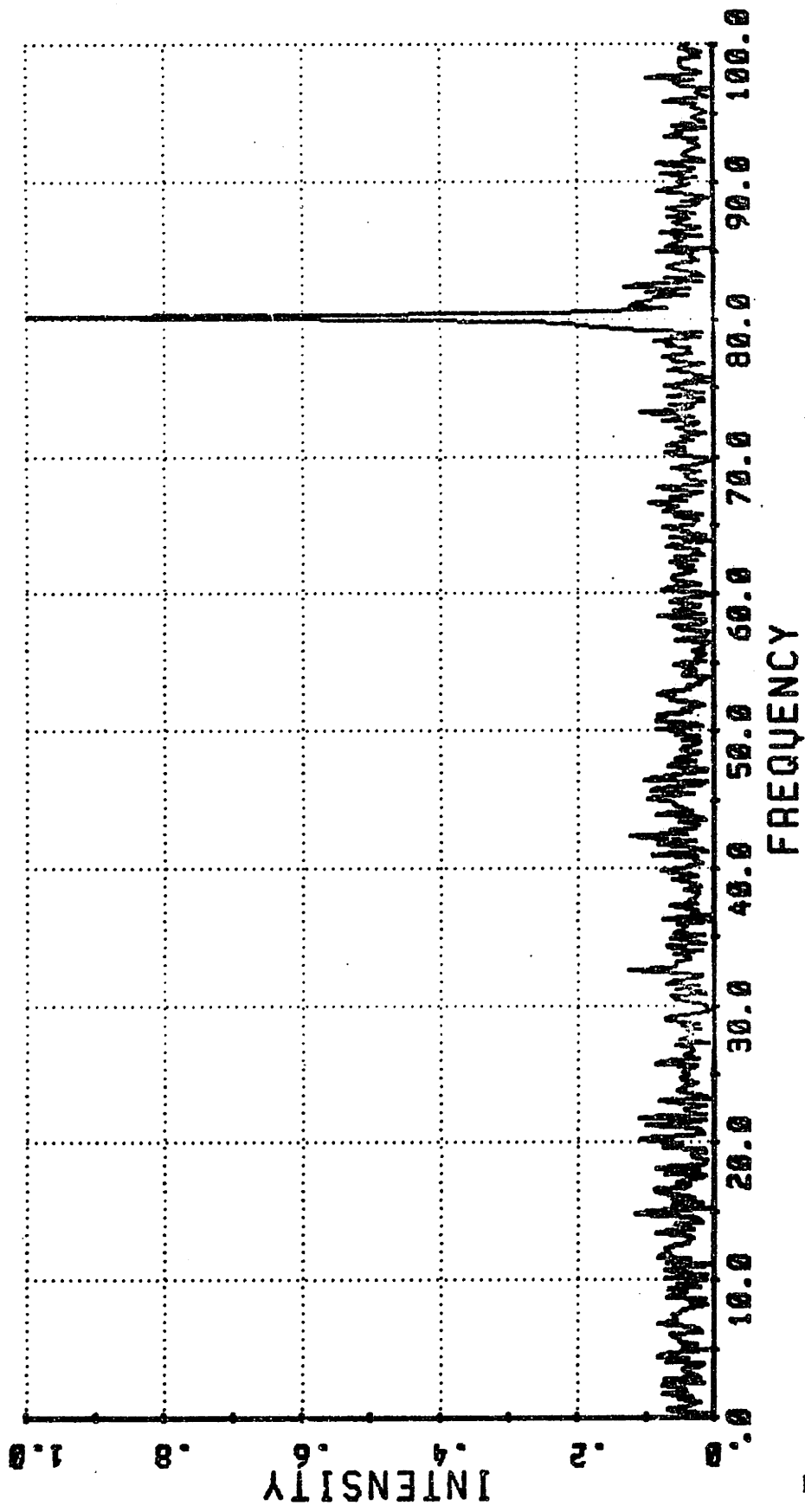
SIGNAL AMPL. = 1.



RANDOM ERROR: AMPLITUDE = .5

SIGNAL AMPL. = 1.

Figure 67b



RANDOM ERROR: AMPLITUDE = .5

SIG FREQ = 80

Figure 67c

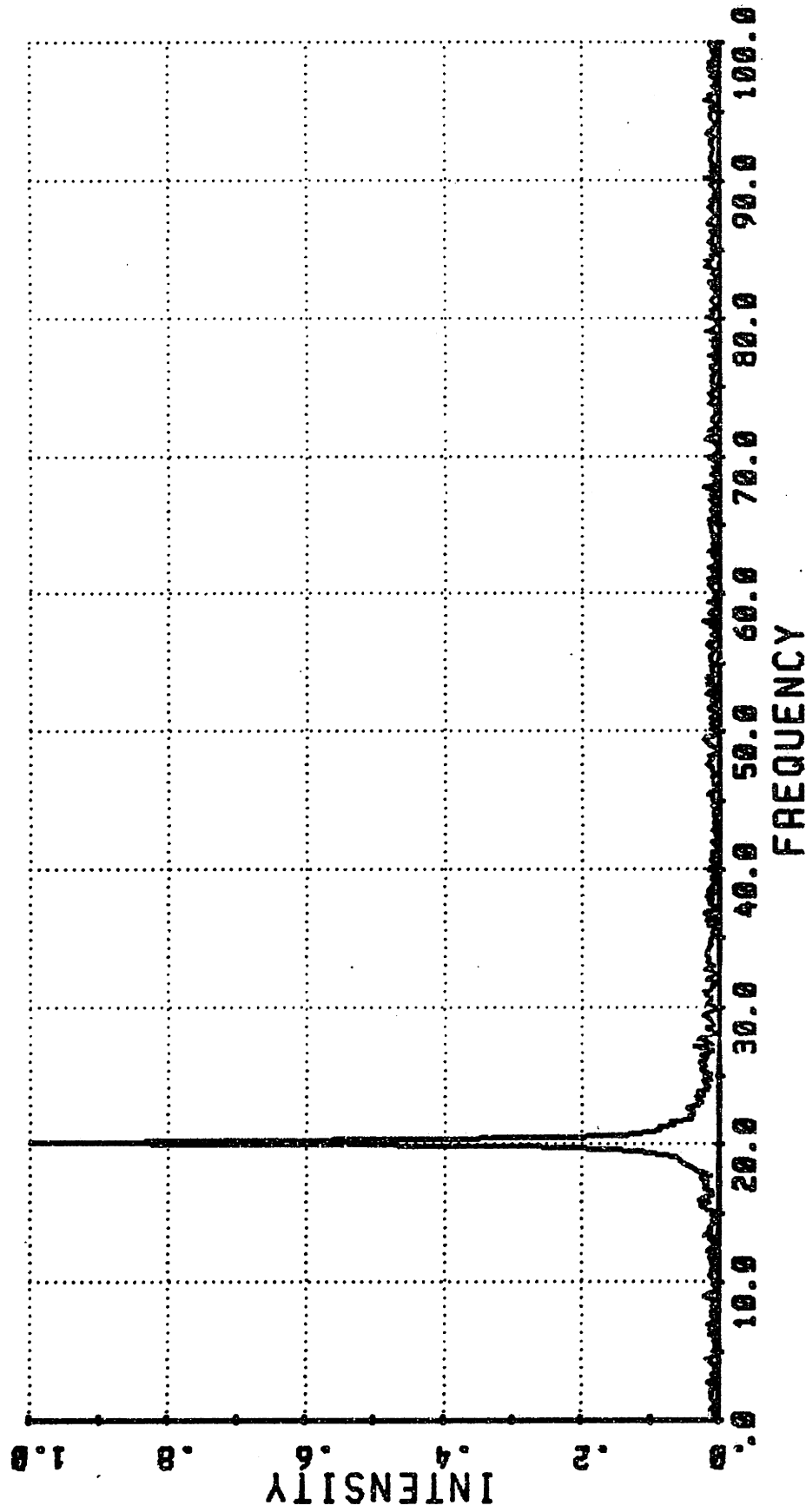


Figure 67d

RANDOM ERROR: AMPLITUDE = .5

SIG FREQ = 20

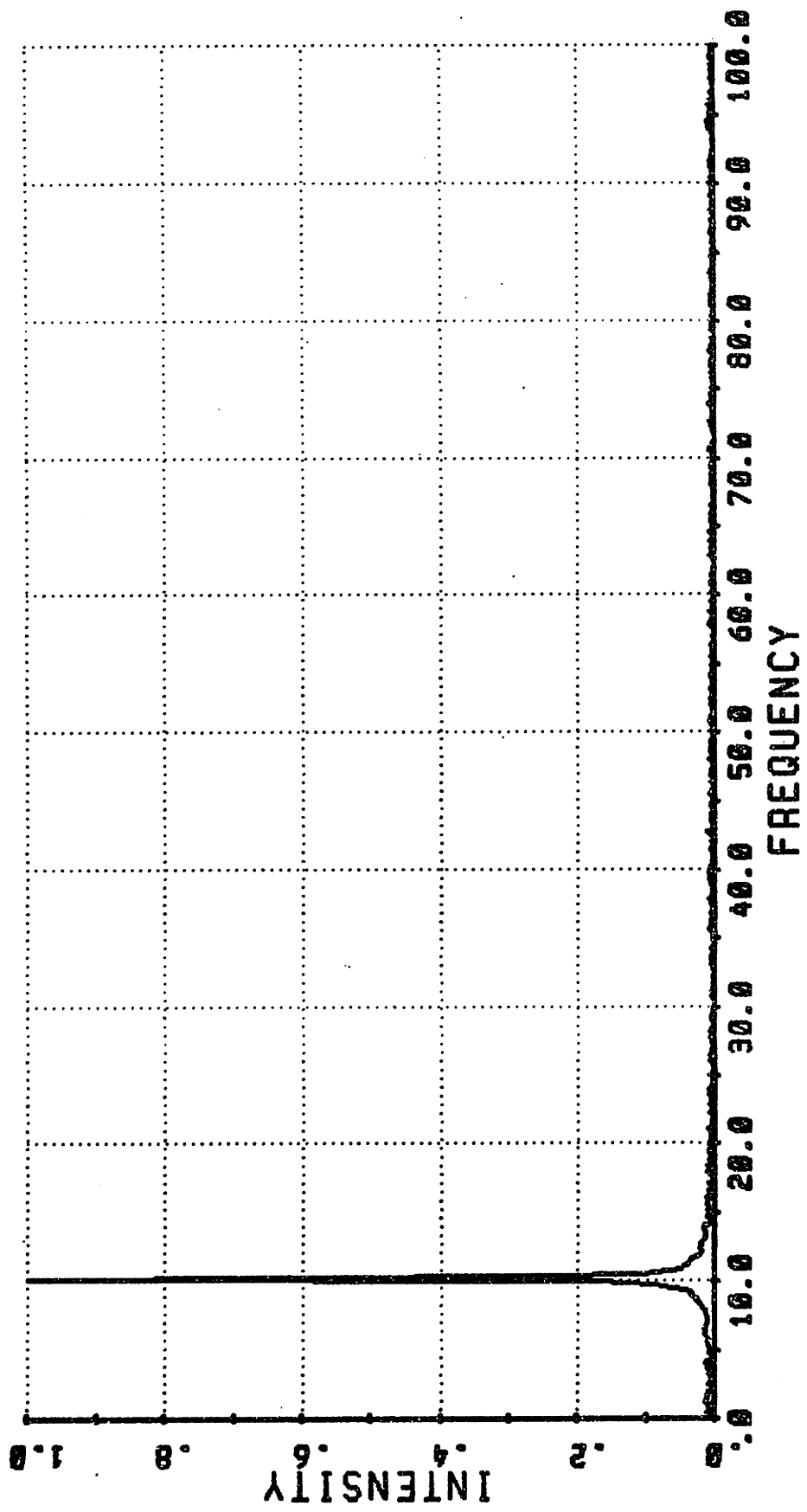


Figure 67e

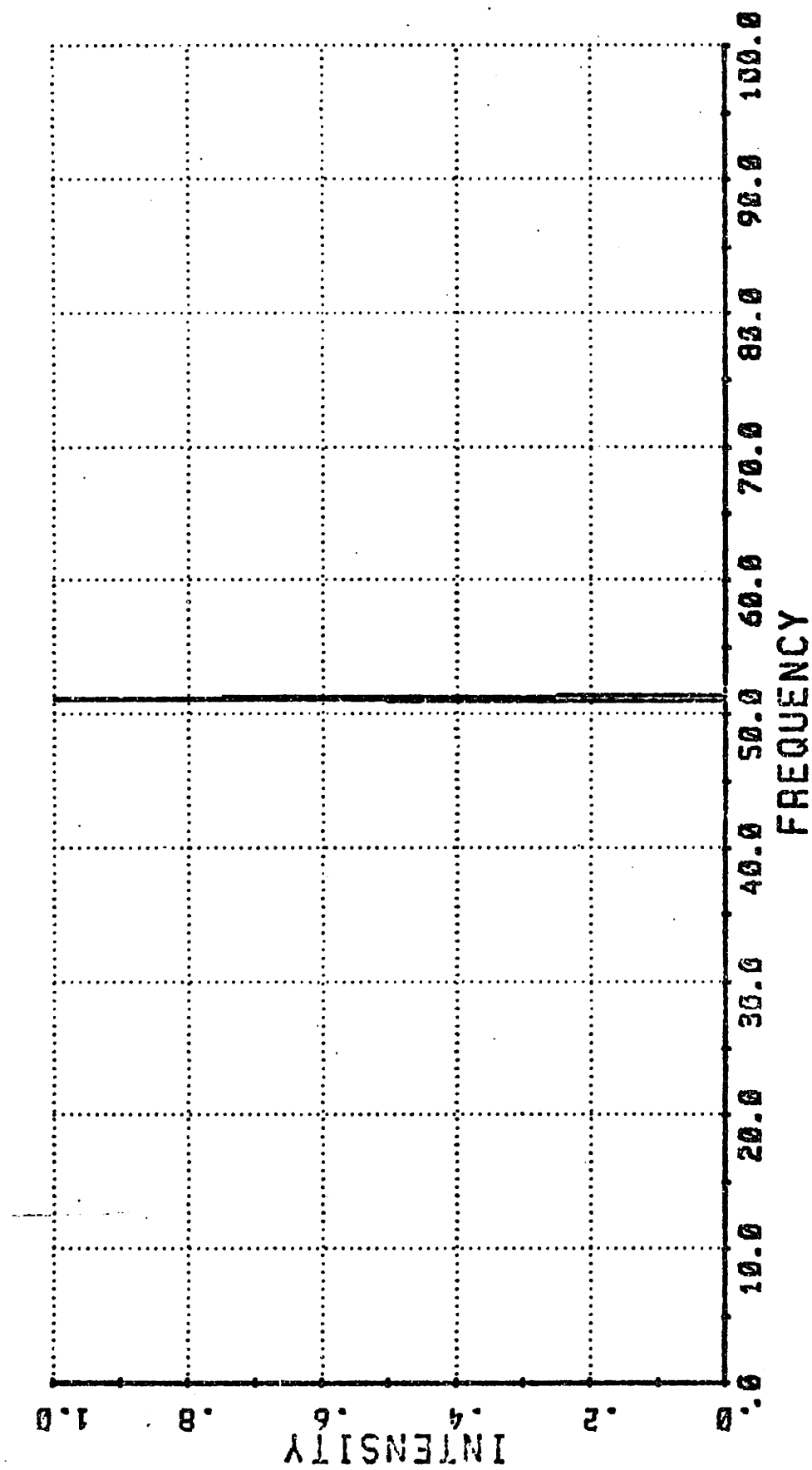
baseline becomes larger.

Figures 68a through 68d illustrate various power law errors in sampling. The simplest error is a linear miscallibration: if the sampling periodicity is different by a constant from the intended periodicity, all frequencies are shifted by a constant. The amplitude given in the figures is the fractional error in the total scan length as it is for all the power law errors. Thus, for an amplitude of .02, the shift of the 50 icm signal is (.02)(50) = 1 icm.

If the error is parabolic, i.e. growing as the square of the distance along the scan, the results shown in figures 68b and 68c are observed. The average frequency is shifted by .5 of the amplitude of the error and power from a given frequency is smeared over a continuous range from f_0 to $f_0 + \Delta f_0$ where $\Delta f_0 = (\text{err amp})x f_0$.

A cubic error is shown in figure 68d. This causes a similar shift upwards in frequency, but is no longer symmetric about the center frequency.

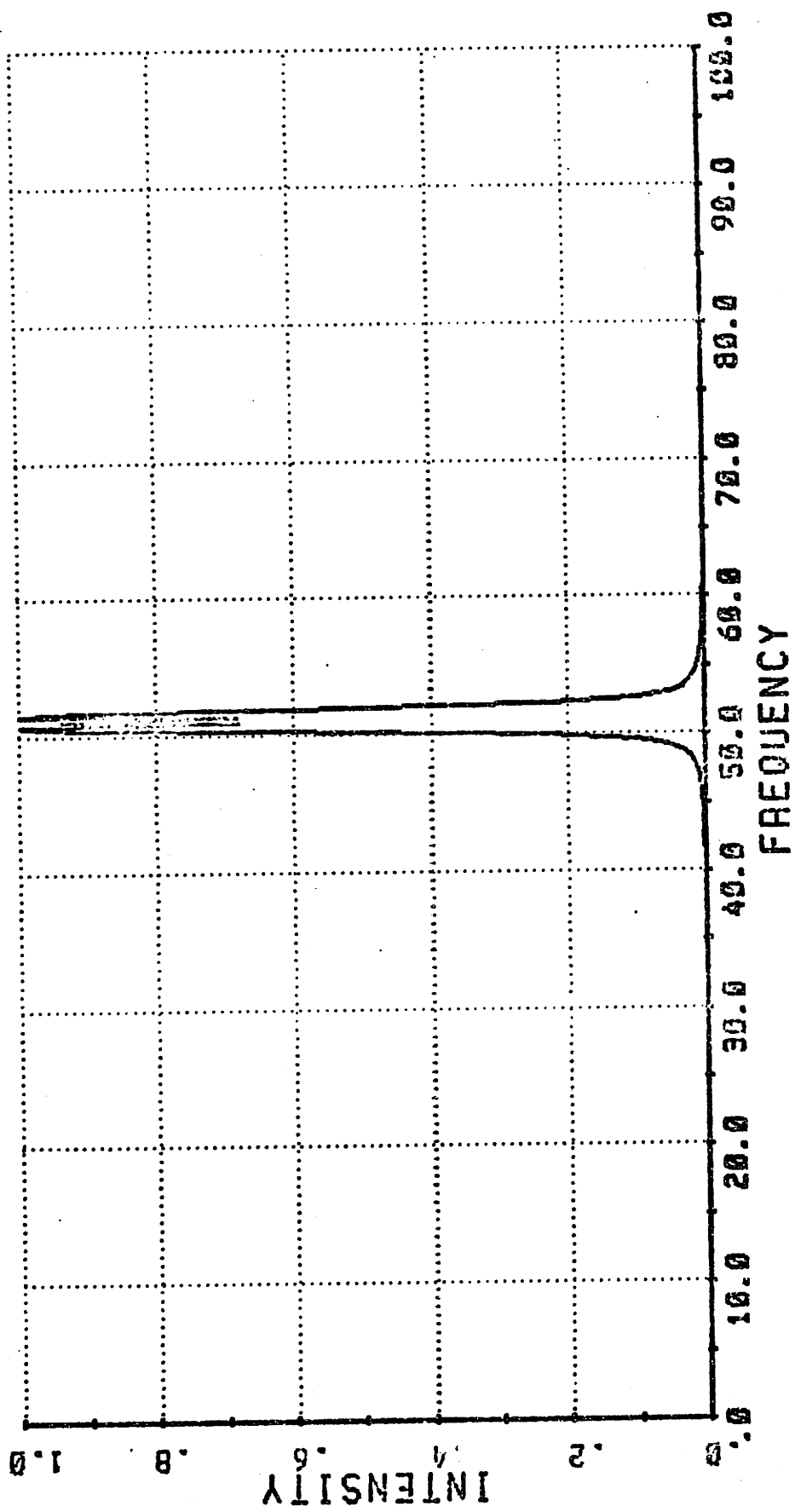
Another class of errors shown in figures 69a through 69b is periodic deviations of the sampling point from the intended position. This is just a frequency modulation of the sampling rate, and results in the familiar Bessel function series causing sidelobes around the center frequency. The amplitudes referred to in the periodic errors are the fraction of the sampling length.



LINEAR ERROR: AMPLITUDE = .02

SIGNAL AMPL = 1.

Figure 68a



QUADRATIC ERROR; AMPLITUDE = .04

SIGNAL AMPL. = 1.

Figure 68b

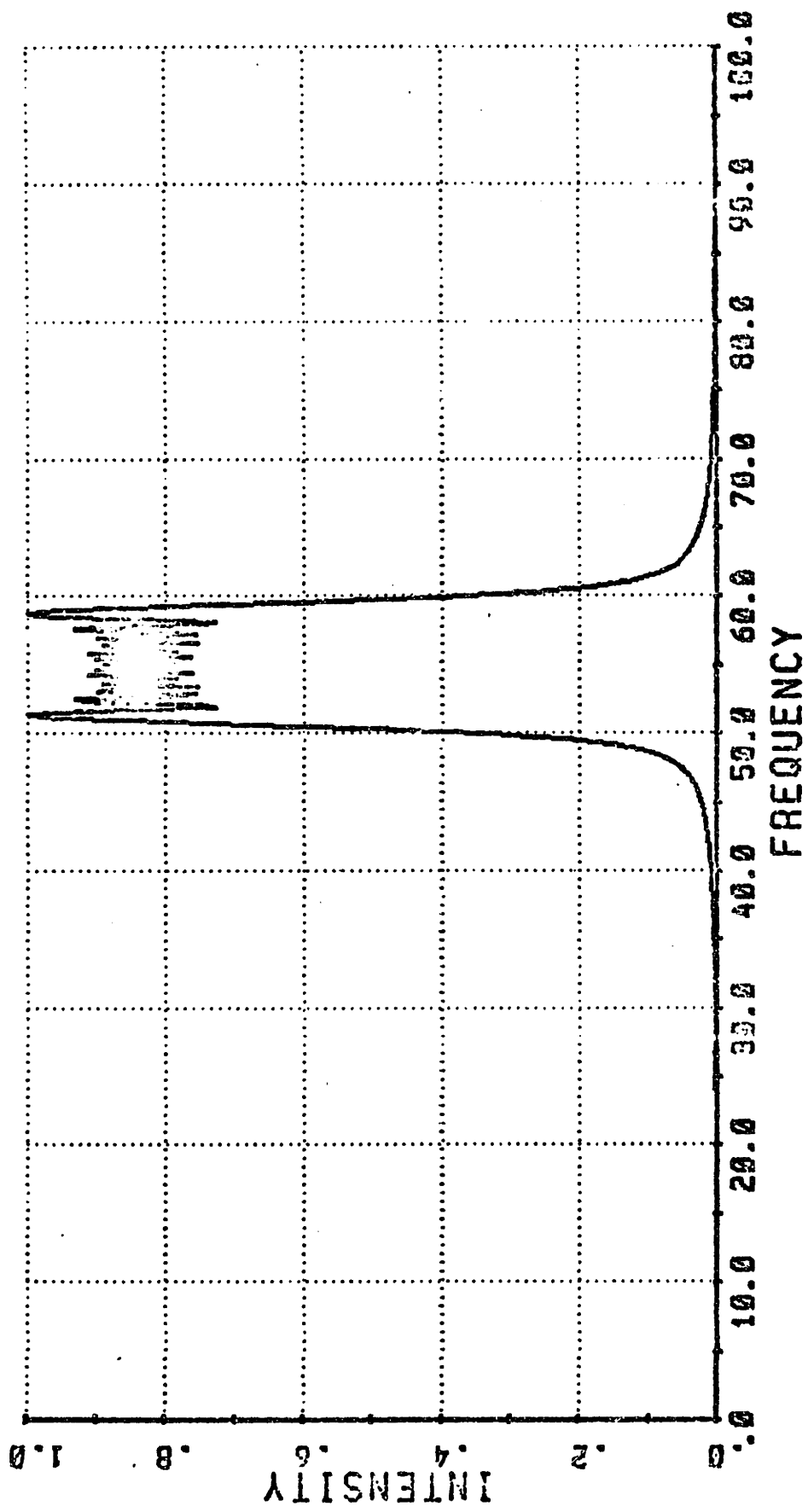
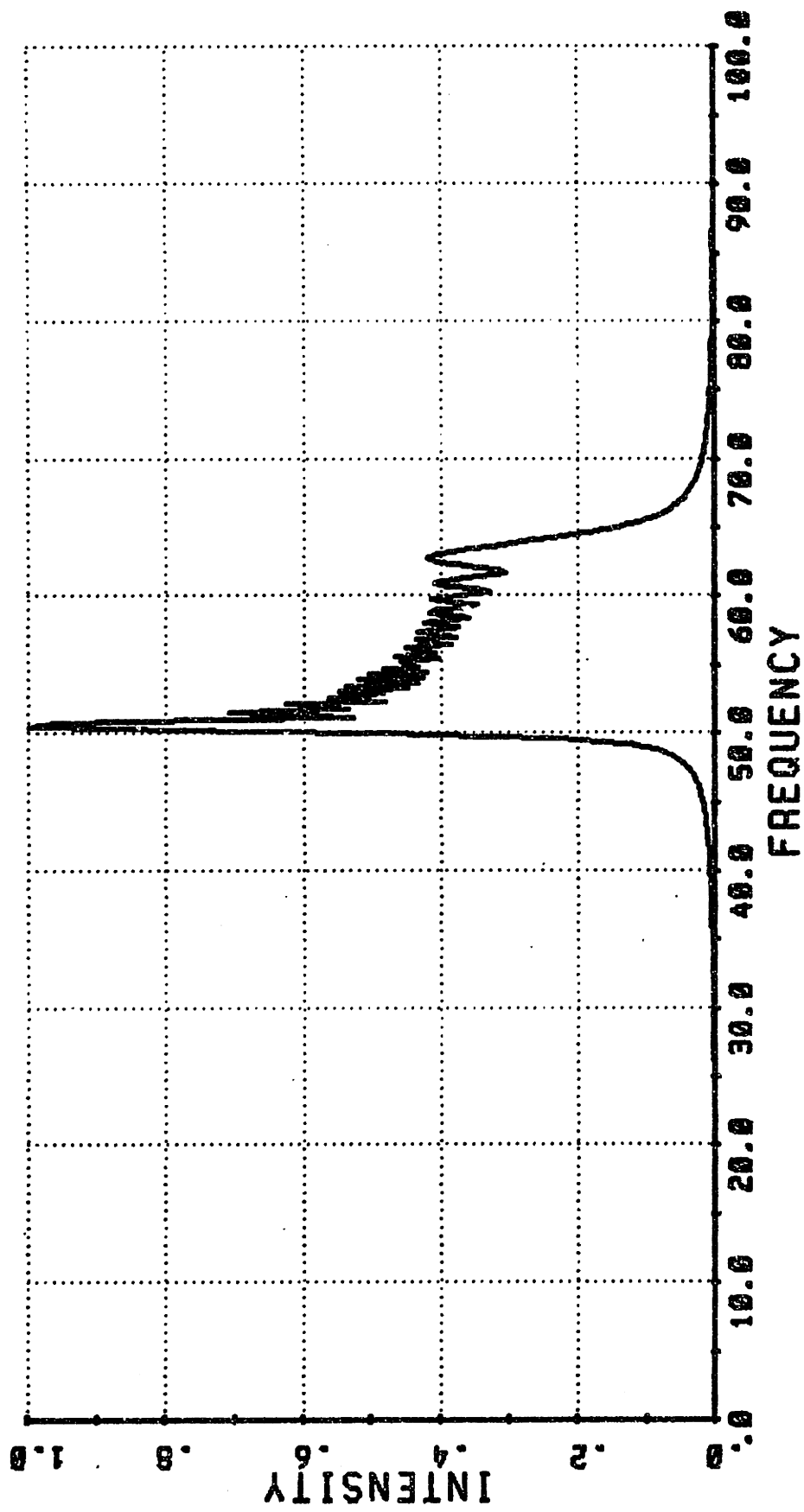


Figure 68c

SIGNAL AMPL. = 1.



CUBIC ERROR: AMPLITUDE = .66

SIGNAL FREQ = 50

Figure 68d

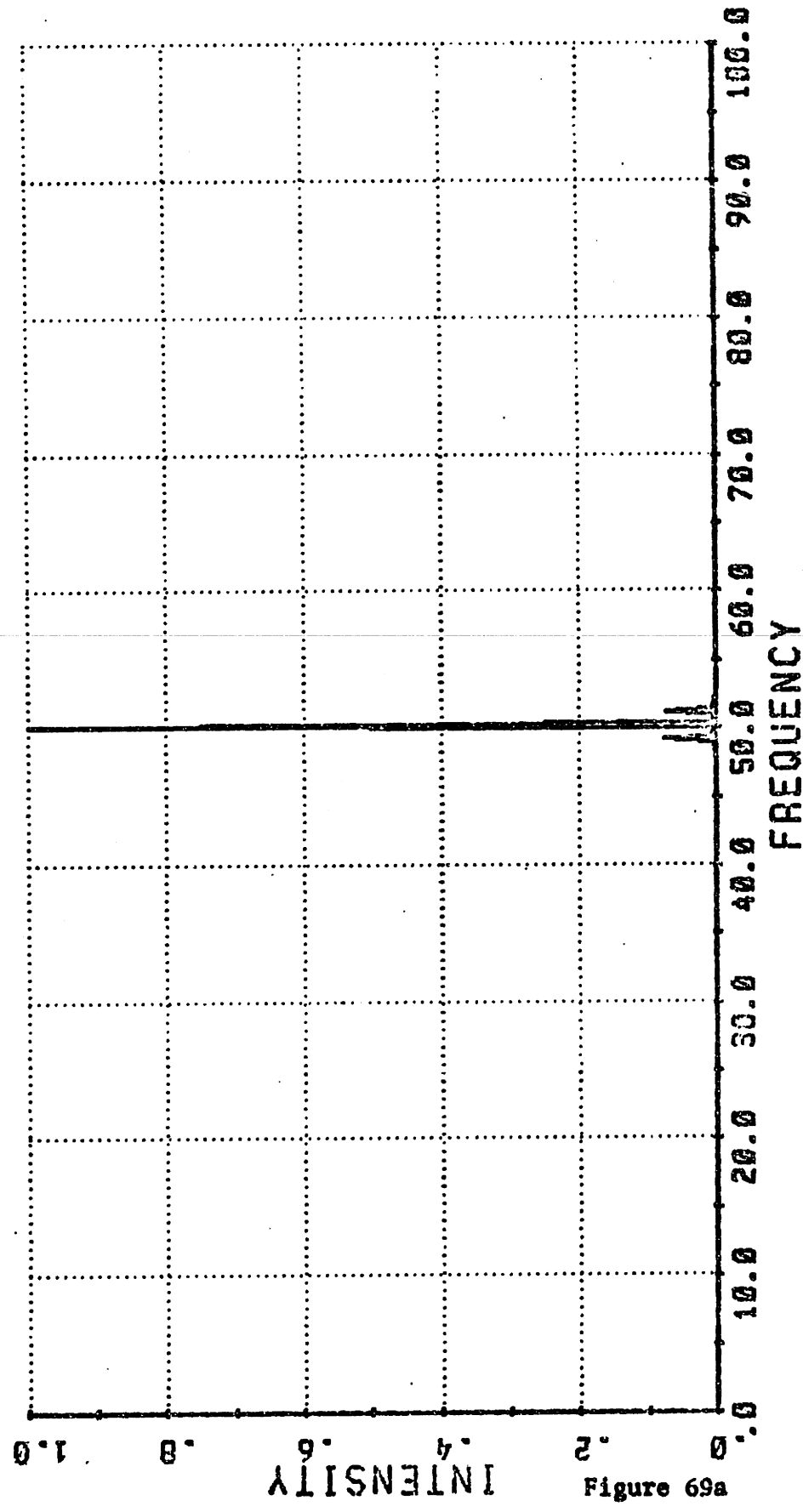
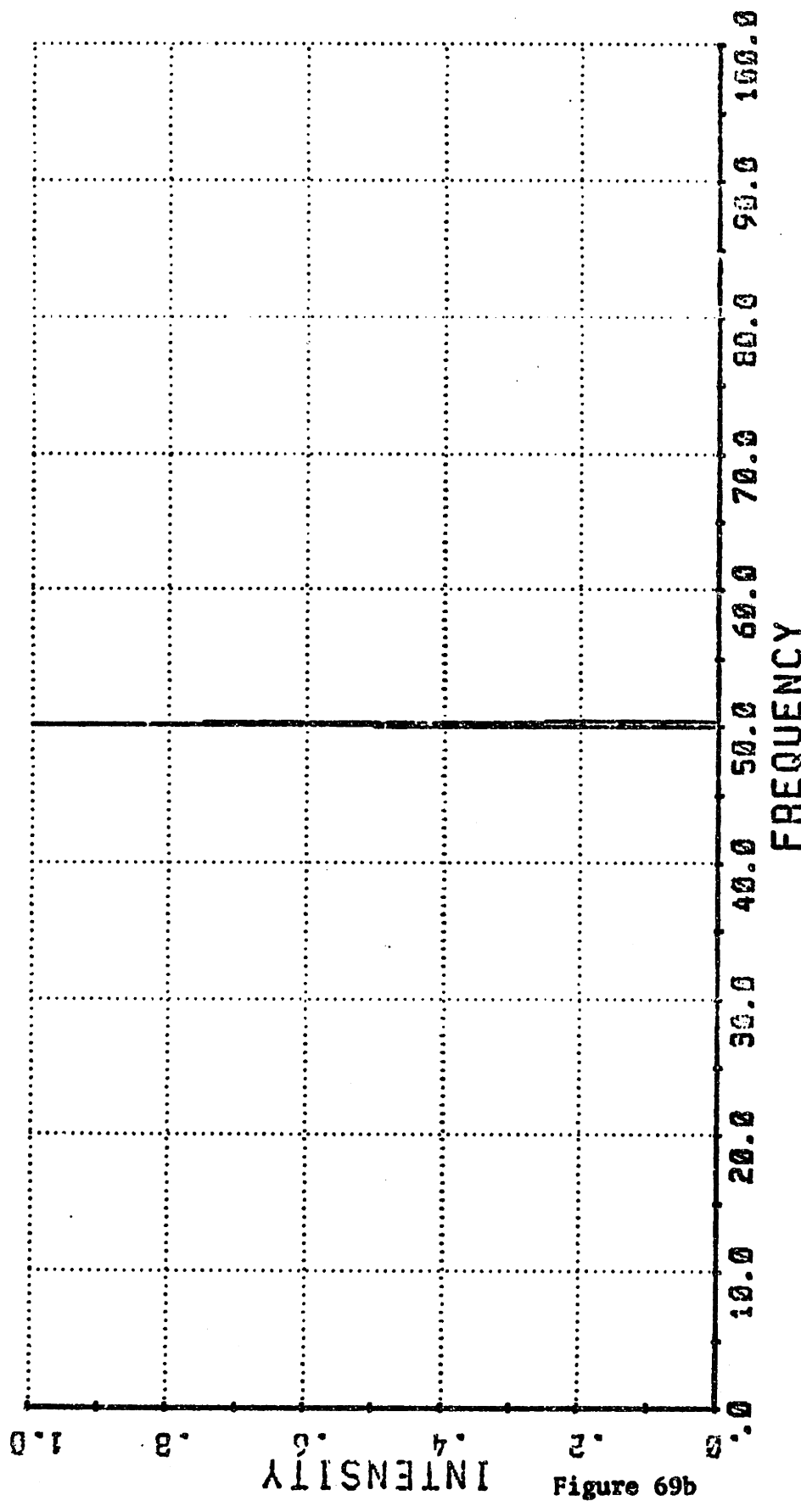


Figure 69a

PERIODIC ERROR; AMPL. = .1. FREQ. = 1.. PHASE = 0.

SIGNAL AMPL. = 1.



SIGNAL AMPL. = 1.

PERIODIC ERROR: AMPL. = .1 FREQ. = 1.0 PHASE = 90. DEG.

APPENDIX: INDIVIDUAL OPTICS TESTS

The parabolic mirrors M1 and M2 were tested by illuminating with a point source, returning the collimated beam to the parabola, and imaging the source at the focal point. The position of the focal point was determined by finding the minimum return spot size. For M1, the spot was returned without noticeable distortion at a distance of 14 cm. This is the specified focal length. For M2, the best image was found at 44 cm., and was considerably larger than the source. At 40 cm, the specified focal length, the image showed a great deal of coma.

This coma could cause two problems. If the angle of the beam leaving the mirror is too steep, the shear in the beam will limit the resolution. The angles implied by the return spot size are on the order of 2×10^{-2} radians. This gives a solid angle of 1.6×10^{-3} sr, and a limit on resolution of .1 icm at 100 icm. This does not compromise the design. The other possible problem is spillover of the beam due to lack of tight focus.

APPENDIX: POLARIZER CONSTRUCTION

The polarizers have to be reasonably efficient up to 100 icm. Calculations show that a periodicity of 50 microns with the wire diameter half the spacing would be satisfactory.

Because of limitations imposed by the winding lathe and availability, a spacing of 53 microns (480 lines per inch) and a wire diameter of 20.3 microns (.0008 inch) were chosen. The wire (from Sylvania Electric) is gold coated Tungsten wire for high electrical conductivity and tensile strength. Its breaking tension was measured to be between 55 and 80 grams x g; there are some sections of wire which are tucked under following turns, and this weakens the wire and leads to the large range of strengths.

The wires should be as taut as possible to prevent sagging, but not so close to failure as to make them difficult to handle. A tension of 55 grams x g was chosen. The polarizer is made by winding a continuous strand of wire around a rectangular frame, so the frame must be able to withstand a tension of $2x(\text{number of wires})(\text{tension/wire})$. The size of the frame was chosen to be 6.5 inches wide by 7.5 inches tall so that the evenly distributed tension is 753 pounds. We require that the deflection of the crosspieces be small with respect to the length, and that the material be hardened to provide a smooth, rugged surface for the wires.

Using the formula

$$d = 64 W l^3 / 384 E$$

where

W = total load

l = length

E = modulus of elasticity

= maximum deflection

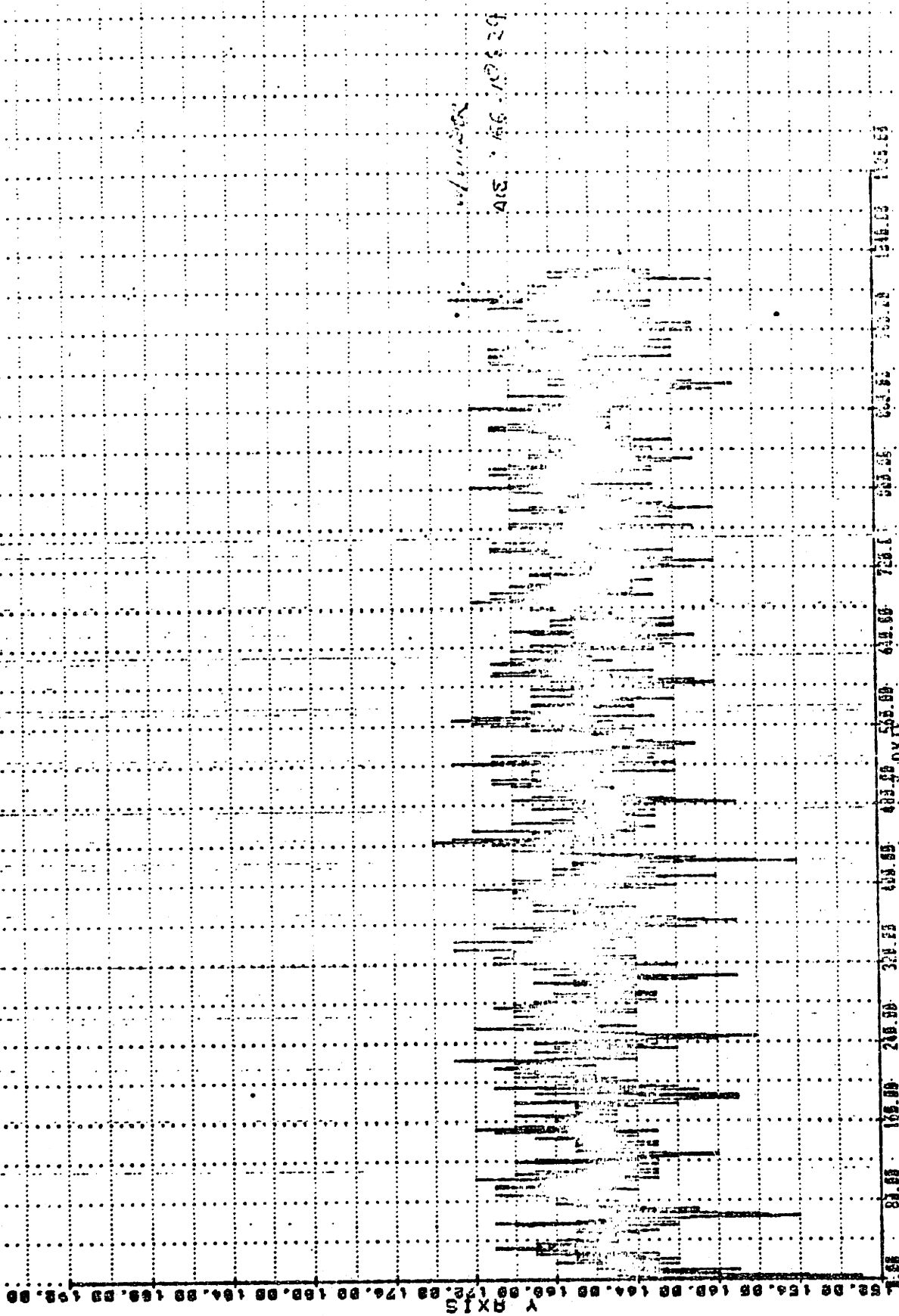
For the diameter of a uniformly loaded beam of 15 mils deflection we choose 1/2 inch diameter rod for the crosspiece. Since the prototype polarizers are designed to be usable at liquid He temperatures, the verticals must be chosen with their temperature coefficient of contraction in mind. For tungsten, the integral over shrinkage from 300 degrees to 4.2 degrees is about 1×10^{-3} ; Invar, the chosen material for the frame sides, has an integral of 5×10^{-4} . This means that the tension in the wires increases slightly when the polarizers are cooled.

Another important property of the polarizer frames is flatness. In the text, a desired flatness of 5 microns overall is indicated. This requires straightness of the horizontals as well as accurate right angles at the joint to the sides. In the prototype, the bearing rod was initially held with screws to the verticals and then soldered while on a flat (less than 1 micron deviation) table.

The winding was performed on a South Bend Lathe, using the lead screw to advance the winding jig. To determine the accuracy

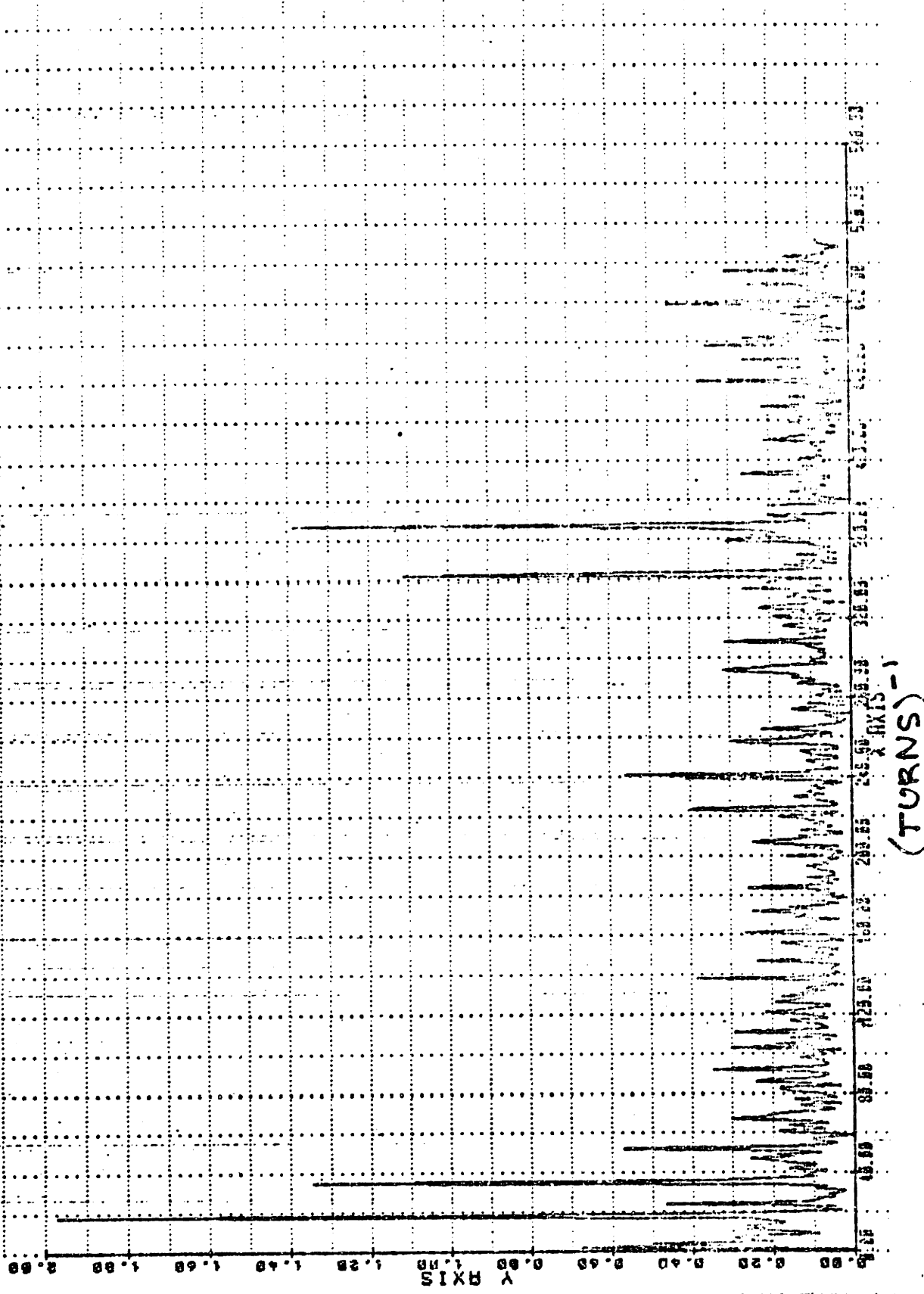
Lathe Lead Screw Regularity

TURNS



RINGS/TURN

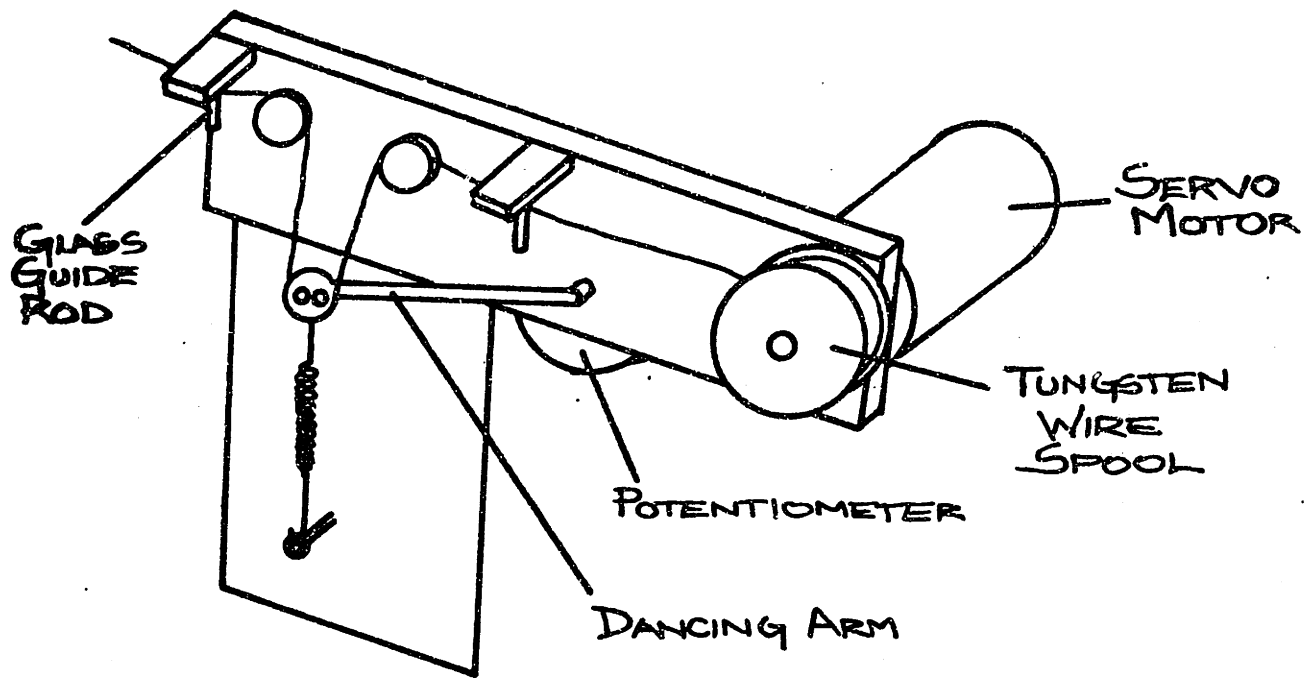
Figure 70



FRINGES

Figure 71

Lathe Lead Screw Spectrum



WINDING JIG

Figure 72

of the screw, a laser interferometer was mounted on the lathe, with one arm on the carriage. Data on the number of fringes per turn of the headstock was analyzed in time and frequency, using a computer program developed for the purpose (LATHER). There are some periodic variations in the speed of the carriage due to slightly out of round gears. The RMS deviation from the average is about 1 part in 166 or .6%; the peak deviation sampled is 10 parts in 166, or 6%. The fourier transform shows sharp peaks corresponding to periods of 60,30,20,3, and 2.9 turns. All of these peaks are less than two fringes in peak amplitude (see figures 70,71). It was concluded that the lead screw is satisfactory.

Because the tension on the wire needs to be maintained close to the breaking point over a wide range of feed rates, the tension is servo controlled. The jig (see figure 72) uses a dancing arm with its pivot a potentiometer acting as the sensing element; to make its position a function of tension, the variable to be controlled, it is spring loaded. The output voltage from the dancing arm pot is compared with a reference and sent via a power amplifier to a servo motor upon which is mounted the spool of wire. In this fashion, the tension is kept constant to within 4gr x g. A synchronous motor mounted on the headstock drives the lathe at 10 RPM, leading to a peak wire speed for the full size polarizers of 10 cm/sec.

To wind a polarizer, a frame is mounted in the head and tailstocks with jobs. The carriage is set at the left hand edge of travel and the wire strung and taped to the frame. The servo gain is turned up, carriage engaged, and synchronous motor turned on. If all goes well, about 5 hours later a polarizer is wound.

The next step is to solder the wires where they meet the bearing rod. An acid flux is applied just to the bearing rod end to be soldered. The end of the frame is preheated until the flux bubbles, and then placed in a trough of solder as deep as the diameter of the bearing rod and left until the solder flows. It is important when dipping the polarizer in the solder to protect the faces of the polarizer from spitting flux; cardboard is sufficient. Repeated fluxing and dipping may be necessary. The polarizer is allowed to cool slowly after soldering is completed, and then washed in clean water and than alcohol.

Despite precautions, adjacent wires may become clumped; a one mil stainless steel shim stock "pick" can be used with a stereo microscope to pluck and comb out these nonuniformities. Finally, one side of the polarizer is cut away with a razor blade.

APPENDIX: ALIGNMENT OF THE INTERFEROMETER

The two fundamental tools for aligning the interferometer are a HeNe laser and a transit. The laser is used with an attachment to allow interferometers to be easily set up and return beams to the laser to be observed. It consists of a beamsplitter with all angles exact and a mirror on one side of the beamsplitter, both securely mounted on the laser. The beam out of the laser is split; one half continues, and one half exits at 90 degrees to the original beam. The straight beam is reflected from an external mirror to be aligned, returns to the beamsplitter, and is superposed on the 90 degree beam. Used coarsely, the colinearity of the return beam and 90 degree beam are an indication of the perpendicularity of the mirror to the beam. Observed carefully, the fringes of the resulting interference can be a very sensitive measure of the relative motion between the laser and the external mirror.

The transit has the important feature that as the focus is changed, the focus point remains colinear with the optical axis. This, along with the ability to translate the transit vertically and horizontally, allows the transfer of optical axis. It is also possible to rotate the transit a predetermined angle so that the optical axis can be set up at angles to each other.

The philosophy of alignment is to first identify the fundamental defining axis and points of the instrument, then to determine what constraints already exist to determine these referents, and finally to generate them in a noncontradictory sequential process.

The fundamental axis and points in this instrument are:

- 1) The position of one DH vertex center
- 2) The axis of carriage motion through the DH vertex center
- 3) The plane of the BS polarizer center
- 4) The line 29.4 degrees (the M2 off axis angle) from the axis of carriage travel, and the point on that line which lies at the distance of the focal length of M2 from the DH vertex center.

There were some already established positions and axis at the time of alignment; a linealy independent subset of these were chosen as the basis for the alignment, and the others forced to conform. This included the axis of carriage translation, the position of the vertex center of one DH, and the M2 focal length and off axis angle.

The procedure than followed in a orderly fashion:

- 1) A vertical mirror was placed parallel to the axis of carriage translation. This was determined by setting up a laser interferometer with the mirror as one arm, and then adjusting the mirror until translating the carriage caused less than 10 fringes

net for a one inch translation.

2) A vertical mirror was set perpendicular to the axis of carriage motion, roughly at the plane of M2. The laser jog and a second BS were used. First, the laser beam was set perpendicular to the carriage axis (by seeing the return beam superposed on the input). Then the second BS was inserted, and rotated until the return beam from the internally reflected 90 degree beam was superposed on the other beams. Finally, the new mirror was aligned to return the BS beam coaxially with all the others.

3) The second DH vertex center was determined to be along the line of carriage translation from the first. Pointed jigs were placed in the mounting holes in the carriage. The transit was placed parallel to the carriage translation (by focussing on the back and front of the mirror). Then the transit was translated to the DH axis and the focus shifted from one to the other DH.

4) The separation between the DH mounting holes was measured to be correct. This distance is the cosine of the off axis angle of M2 times the focal length of M2.

5) One DH was set at 29.4 degrees. Method: The transit was set parallel to carriage translation and rotated by 29.4 degrees, and the DH set to return the transit image.

6) A mylar BS was inserted perpendicular to and at the center of the carriage when the carriage was centered in its travel.

Method: The perpendicularity was insured by setting the transit

perpendicular to the carriage mirror, and then the front and back of the BS were focussed upon.

7) The other DH was placed at the correct angle. Method: The first DH was viewed through the mylar BS with the transit, and the image of the second DH made to superpose on the first.

8) A second mirror perpendicular to the carriage axis was placed in the same plane as the vertex center of one DH. Method: The perpendicularity was determined by looking at multiple reflections between the two parallel mirrors, and the correct plane determined by measuring from the center line (determined by the BS position).

9) The other mirror perpendicular to the carriage motion was placed in the plane of the other DH, using the methods above.

10) A second mylar BS was placed at the position of the IPOP polarizer, and made parallel to the BS by focussing on the front and back of each element.

Here a check was made of the alignment accuracy. A laser beam was inserted along the axis of the output of M1 and adjusted in angle until all of the spots everywhere superposed. The input angle for which this occurred was 29.5 degrees, 11 degree away from the intended input angle; this is 2×10^{-3} accumulated error. The output beam was parallel to the input beam plus or minus 20 arcsec.

11) The focal point of the M1 mirrors was determined by using the

sun as a parallel source. The input-output holder was placed at the correct height.

12) An M₁ was placed at the focal point of M₂, and adjusted so that a horizontal input beam (as in the check above) appeared at the focal point.

13) The second M₁ was placed so that an input beam vertically down at the first M₁ appeared at the output focal point.

14) One of the flats at the position of M₂ was removed, and an M₂ substituted. It was adjusted until the laser spots again superposed.

15) The other M₂ was placed as above.

16) Finally, the mylar B₅ and IPOP were removed and replaced with the polarizers. Their position was determined by setting the transit to be perpendicular to the carriage mirror, and focussing on the front and back of the polarizers.

This alignment led to the high frequency response and efficiency shown in the body of the text.

APPENDIX: INSTRUCTION MANUAL

This is an instruction manual for the COBE mockup interferometer. This fourier transform spectrometer can make measurements in the range from about 1.5 to 100 wavenumbers. It can be used in a step and chop mode or in a rapid scan mode. The manual describes the use of the instrument in these two modes. The first section describes the characteristics of the two modes concurrently so that a choice between them can be made. The second section deals with the mechanical and electrical details of preparing the interferometer to take data. The third section deals with the specifics of running in the two modes.

SECTION I: PLANNING THE RUN

The first decisions that need to be made in using the interferometer are the selection of wavelengths of interest and the resolution required. The resolution is equal to the reciprocal of the total scan length. The maximum delay available, as limited by the carriage travel, is 10 cm. The shortest scan in the rapid scan mode is 1.75 cm.; in the slow scan mode, an arbitrarily short scan is possible. Hence the best resolution is .1 wavenumber (1cm), and the coarsest easily 10 icm.

In the slow scan mode, the only detector system constraint on the highest optical frequencies measurable is the passband of the optical filters in the dewar. The source is chopped at an audio frequency well above the point where i/f noise in the detector and amplifier is appreciable, and the carriage is moved slowly enough so that the highest modulated frequency (meaning the frequency in hertz of the modulated intensity of the beam by interference) is lower than the chopping frequency. At the low end of optical frequencies detector noise (at the chopping frequency) can become a problem. The sources available, a black body at temperatures as high as 1000 degrees centigrade and a mercury vapor lamp, have outputs that fall at longer wavelengths. The interferometer response is also falling at long wavelengths, with the corner frequency at about 3 icm. With no losses outside

of the interferometer, and with the BB as the source, detector noise (at about $1*10^{-13}$ NEP) is not a limitation.

In the rapid scan mode, the noise characteristics of the detector system need to be more carefully considered. When rapid scanning, the chopper is not used and the modulation of the signal comes from the movement of the carriage alone; optical frequencies are translated into modulated frequencies directly. It is apparent that the thermal time constant of the detector as well as the optical filters in the dewar will determine the highest modulated frequency that is detectable. Routines allow for the correction of the rolloff due to the detector, but since the signal to noise goes down with the detector response there is a limit to the highest practical frequency. The corner frequency of the detector ($=1/2*\tau$) is a reasonable choice; the carriage speed should be set so that the highest modulated frequency (equal to the carriage speed in optical cm/sec times the highest optical frequency of interest in icm) does not greatly exceed the detector limit. The present detector has a time constant at .5 volts detector bias of about 8 ms, and hence a corner frequency of 20 hertz.

The low frequency detector imposed limit is due to i/f noise in the detector-amplifier-dewar system. This should be carefully measured, and the carriage speed chosen high enough so that the lowest modulated frequency lies above the bulk of the noise.

Practically, one can measure the noise with the rapid scan operating program by covering the detector and taking a scan, collecting some data at the same speed, and directly comparing the signal to noise. One then selects a scan speed that gives the desired signal to noise. Presently there are problems with microphonics from the carriage servo that introduce excessive low frequency noise with scan speeds faster than 1 cm/sec; furthermore, the servo will not run faster than 3 cm/sec. There are no apparent problems with running the carriage at very slow speeds.

Another fact which must be considered when choosing speeds and wavelengths is the absorption of the signal radiation in the interferometer path by water. At the high end, the primary problem is the loss of signal. Above about 35 icm the water lines are so closely spaced and so strong that with the available resolution and normal humidity the signal to detector noise is small. By purging the box that surrounds the interferometer with dry nitrogen (by filling a container inside the box with liquid nitrogen) the vapor pressure can be reduced by a factor of ten or better; it must be kept in mind that any ancillary optics must be equally well purged. The purging introduces another problem: the fluctuation of humidity. This makes ratios of files taken at different times sensitive to the quality of the purge. One must be careful to keep the purging container at a more or less

constant level of liquid nitrogen, and to take files to be ratioed in close temporal succession.

At the low end, the fluctuations in overall transmission of the atmosphere due to changes in the humidity (whether or not the box is purged) appear as low modulated frequencies in the interferogram, and hence as excess signal in the spectrum. This noise, which is $1/f$ in character, dominates over the BB signal below about .2 hertz depending on the weather. Modulated frequencies of interest should be made to lie above this frequency, suggesting rapid scan mode for most low frequency measurements.

Other constraints on the measurable wavelengths are due to the interferometer itself. Two phenomena at low optical frequencies are significant: rolloff of the response below 5 icm, and geometric modulation of the beam at large optical delays. The first problem is caused by diffraction losses; the response is down to .5 at 2 icm and probably falling rapidly at longer wavelengths. The other error is due to shifting of the image at the detector as the carriage is moved. It grows roughly quadratically with the delay, and influences primarily the first few points in the spectrum.

At high frequencies, the primary limitation appears to be the polarizers. The fineness of the wire spacing is one

determining factor; when the wavelengths become comparable to the periodicity of 50 microns, the polarization begins to drop and the efficiency of the interferometer with it. The constraints on overall flatness are also severe. The beamsplitter can only deviate by $\lambda/8$ for destructive interference of wavelengths λ . As measured, the response is .5 at 70 icm and is usable to 120 icm.

Once the mode and carriage speed have been determined, electrical filters to condition the signal for the computer must be selected. For the slow scan mode, the first concern is with the lockin that demodulates the chopped detector signal. The signal tuned amplifier Q should be low enough to allow the post multiplier filter to limit the bandwidth so that filter whitening can be easily analytically removed. (The BW of a tuned filter is $f_0/Q = f$.) The time constant of the latter filter should be selected so that the highest modulated frequency will not be severely attenuated, but it must be long enough to integrate over a chopping cycle. The signal line from this point on should be DC coupled to the computer. At the computer, some LP filtering will be necessary to reduce AC hum, and to ensure that no noise picked up can cause aliasing in the transform.

For the rapid scan mode, the detector output is AC coupled at the interferometer end of the line, buffered, and sent into the computer room. Again the LP filtering is chosen to allow the signal of interest through while attenuating unwanted hum and

noise. The detector time constant will also be acting as an LP filter.

In both modes of operation, care must be exercised to ensure that aliasing will not occur. For the rapid scan, the highest optical frequency and hence modulated frequency is a function of the scan length L, and is equal to about 250 L Hz if L is in cm. This is because the sampling periodicity is adjusted so that 1024 points are always taken. The filters should be chosen so that there is virtually no signal at (or above) this modulated frequency. The slow scan mode allows the choice of two different periodicities: 50 or 100 samples per mm of carriage travel (1 cm of mechanical carriage travel results in 3.49 cm of optical delay). This corresponds to 71.5 or 143 μ cm full scale in the spectrum. The carriage speed chosen (by selection of micrometer drive motor) determines the modulated frequencies, and LP filters are required to eliminate the signal above the fourier folding frequency as before. For the motor speed given in RPM, the modulated frequency is given by $RPM \times 3.69 \times 10^{-3}$ hertz/ μ cm.

SECTION II: SETTING UP

Connections between rooms: The Teledyne urley position transducer outputs p and q are input to A-D channels 000 and 001 respectively. The sign of the feedback is set by this arrangement, so it must be correct. The TDG box in the interferometer room is differentially received in the computer room to eliminate ground loops. The glitch is sent on cable A to the computer room, received differentially, and input to A-D 011. For the rapid scan mode, the signal from the detector is buffered with a battery powered amplifier in the interferometer room and sent out on cable B. The signal lead must not be grounded anywhere in the interferometer room to avoid ground loops; in particular, the dewar must not be connected electrically to the interferometer. For the slow scan mode, the signal is demodulated by the lockin and sent out on cable B. The signal cable in the computer room is buffered if necessary, and filtered as required. Cable C is fed by the Y DAC via its buffer, received in the interferometer room differentially, and either input to the servo box in the case of rapid scanning, or fed to a strip chart recorder for slow scanning.

The power amplifier has a BNC input, and a banana output. The output is current sensing (1 volt in gives 1 amp out), and the white binding post does not lie at ground. The white post is connected to the + terminal on the linear motor; this must be

correct for the servo feedback to be right. The power supplies for the servo box, glitch, and TDG should be kept a reasonable distance from the rest of the system to avoid pickup.

The TDG must be checked for alignment before running. It has two outputs which are in quadrature. If the ruling has moved with respect to the sensor the pulses may be missing or in poor phase relation over some part of the carriage travel. To check this, use the offset in the servo box to smoothly move the carriage while observing both TDG channels simultaneously on an oscilloscope. Turn the overall gain to 20%, the AD gain to 0, and set the VEL gain to 570. Turn on the power amplifier, and then the split supplies. Finally, turn on the power at the switch on the servo box. The carriage will now travel at a velocity proportional to the DC offset and in a direction determined by the sign of the offset. With practice, one can scan the carriage back and forth while observing the two TDG outputs. If its signal is missing or is badly phased, the grating has probably moved away from the sensor and must be realigned (swing around its axis of attachment to the carriage). Do not allow the carriage to sit at an end with a large offset, as the power amplifier will overheat; balance the offset while making adjustments. Always balance the offset before turning down the gain.

In either mode, the first task is to align the input and output optics for maximum signal. This is most easily done by chopping the source and observing the signal strength on a lockin amplifier. The input presently used is angled 9.5 degrees from the vertical. Both of the standard sources can be mounted at this angle; if auxillary optics are used, they must inject at this angle. The $\Delta\Omega$ is not limited at the input at present with $\Delta\Omega = .5$. The position and angle of the input is determined by an aluminum reference block mounted on top of the input mirror holder.

The output beam is vertical and on the other side of the interferometer. The usual detector dewar is down looking and sits on a mount above the output mirror. This mount is slid about on a horizontal plane at the focus of the output mirror until the signal is maximized. An alternative mount is available which allows the insertion of optical filters perpendicular to or at 45 degrees to the beam in a light pipe above the output focus. Its position is peaked similarly. For rapid scanning, a steel can surrounds the dewar to shield the detector/amplifier from magnetic pickup from the linear motor.

One can at this time also optimize the angle of the beamsplitter polarizer. First the micrometer screw is mounted and the carriage position of the central maximum located by

observing the lockin output as the center of the carriage travel is manually scanned. With the carriage carefully placed for maximum signal, the B5 adjusting screw is turned to further peak the signal. Some interaction between the carriage position and the B5 is necessary, although interaction is minimal. The B5 angle is not a perfectly smooth function of the adjusting screw, so it is advisable to approach the peak from either side, starting about one full turn from the peak.

SECTION III: TAKING DATA

A. Rapid scan

To run the rapid scan program, first set the overall gain to 0. Set the ADC gain to 700, and the VEL gain to 578. Run the program ZERO; it sets the DAC to 0 (only necessary if the program crashed, or if the DAC was offset for some other reason). Now set the overall gain to the point indicated on the servo box. The program assumes that the carriage is at the right hand end of its travel as viewed from the input-output end of the interferometer, and that there is sufficient DC offset to slew it to that position from the center of travel in about 30 seconds. Ensure that this is so.

The rapid scan program may be operated from the interferometer room if desired. Type BOCT RKMFB to the usual monitor, and once it has finished its awakening, type SET TT CONSOL=1. The system consol is now the teletype, and will remain so until SET TT CONSOL=0 is typed.

Run NEWPH. It will ask if the concise version is desired; for this, and all other yes/no questions, a carriage return or 0 acts as a no response, and 1 is interpreted as yes. The program will ask for the desired scan length (which is quantized in units of 1.75 cm because of the sampling algorithm), the scan speed,

the trigger frequency (which should be 2000. Hertz for best results), and the distance that the carriage sits from the central maximum. As it is now set up, this distance (to the accuracy which it is required) is 1.8 cm. These setup questions will not be repeated unless the program is left, so to change these parameters the program must be rerun from scratch.

At this point, the number of cycles of data taking and the decision to apodize the interferogram are required. The interferogram can be saved, so the choice of apodization is not irreversible. When the carriage return is given after the apodization question, the carriage should start out for the center of travel. If it does not move or slams into the far stop, SLOWLY turn the overall gain to 0 and look at the servo troubleshooting guide before proceeding. If all goes as planned, when the scan is finished the computer outputs servo error data in the format.

NCYCLE SUM OF ERRORS SUM OF ABS. VALUE OF ERRORS NCYCLE
The errors are given in units of the finest TDG division, which is 1/200 mm of carriage travel or 17.5 microns of optical delay. These numbers should be even if the glitch is stationary in position, by the nature of the driver. The errors are corrected each cycle gradually over the length of the cycle. If the size of the error is comparable to the wavelengths of interest, the servo operation must be improved before proceeding.

The computer will also print out the peak value of the interferogram as sampled, and the peak value of the spectrum; the normalization is such that the peak amplitude of a sine wave input is indicated.

Next, the computer (if requested) will print out a menu of options for processing the data. If the interferogram is to be saved, this should be done first. All subsequent processing affects only the spectrum, and the interferogram remains unsullied. The program NNEWFF can be used to transform and manipulate interferograms after a run.

SERVO TROUBLESHOOTING GUIDE

First, turn the overall gain to 0 slowly, put 666 into the switch register, and then control -C out of the program. Run ZERO to remove any offset in the DAC. Then identify the problem and rectify it; there is usually a clear cut reason for servo failure.

| MODE OF FAILURE | POSSIBLE CAUSE |
|--|--|
| No motion of carriage upon commencement of scan | Gain low or zero Y DAC circuit not complete No clock Start at wrong end of travel |
| Carriage runs rapidly to end of travel and stops | No TDG signal Incorrect TDG phase Gain too high |

| | |
|-----------------------------|----------------------|
| In middle of scan, carriage | Gain too high |
| loses control and runs | TDG out of alignment |
| into stop | Computer crash |
| Oscillation of carriage | VEL gain too high |
| during scan | |

B. Slow scan

The same connection scheme is used for the slow scan inputs to the computer. However, the DAC Y output is now a monitor of the sampled interferogram, which can be sent back to the interferometer room while running. This arrangement has a number of advantages. Firstly, it allows a single operator to be sure that the system is operating. Secondly, since the plotting routines also use the Y DAC, it allows one to identify the end of a data run and synchronize the taking of multiple runs with the computer.

The way the slow scan program coadds cycles is to take a slightly longer scan than is desired, align with previous scans using the glitch as a fiducial, and truncating the excess data from the end of the record. For this scheme to work, the operator must measure the distance from the flitch to the central maximum with the micrometer screw and supply the computer with this information, and must know where the desired scan starts so that the cycles can be started somewhat (say 10 mils) further away from the CM than that point. The first piece of information can be obtained by watching the glitch (from the monitor output) and noting the transition point, and then observing the lockin and noting the position of the CM. The scan starting point can be calculated once the scan length, in carriage travel, has been determined.

The scan length is a function of the parameters; the TDG periodicity chosen, and the number of points desired. The periodicity is either 50 or 100 samples or "lines" per mm, as noted before; this corresponds to .002 or .001 cm of carriage travel per point taken. The number of points is restricted to powers of 2 (because of the fast fourier transform algorighm) and has a maximum at present of 1024 points. The distance obtained has to be converted to inches for the micrometer screw, and it works out conveniently to be about 128 points per .1 inch for the 50 lpmm choice, and 256 points per .1 inch for the 100 lpmm choice. One turn of the screw beyond the end of the scan is more than sufficient to ensure that enough extra scan is included for coadding.

To get the slow scan program goind, turn on the servo electronics (servo box, TDG and glitch, power amplifier) and adjust the gain and offset as though checking the TDG (the DAC gain should be 0); one wants the offset such that a gentle pressure is maintained against the micrometer screw. Make the measurement of glitch to CM, and set the carriage to the right (as viewed from the input-output end of the interferometer) of the CM, outside of the desired scan as described above. A chart recorder should be connected to the Y DAC as a monitor. In the computer room, the trigger to the ADC should be 500 hertz. The x-y recorder on the computer should be set at 2.5 v/cm y and 1

v/cm X, with the zero at X=4 cm, and Y=10 cm. Have a piece of paper in the recorder, and the servo of the recorder on.

Run FIRALL, the data taking program, and answer the periodicity, point number, and glitch-cm questions. Choose the number of cycles; when the carriage return is given, the computer starts looking for data. Start the carriage motor. When the scan is finished, the DAC output will go to +10 volts momentarily to signal the end of the scan. The motor can be disconnected, and the screw wound back to the starting point. Since the computer watches the rewind so that it can know when to start the next scan, there is a maximum speed allowed for the reqind (with the 500 hertz sampling rate, the ADC must catch every TDG) which is about ten turns per second, not a severe restriction. In a multiple scan, the Y DAC will give a -10 volt spike when the carriage has been reqound for enough. On completion of the scan, the computer will have made a recording of each interferogram on the X-Y recorder, aligned as they were when the coadding was done. The coadding should be checked by looking for lineup of significant features. The peak and end values of the interferograms are indicated on the spectrum is given for an equivalend input sinewave. The option of writing the interferogram on the disk is given; this is the best way to store the data. A collection of manipulative options is then

presented. To transform interferograms after a run, run FIRALL and tell it that 0 points are to be collected. The program will then prompt for a file to be transformed. The program DATALL has a more extensive list of options than FIRALL, but requires a spectrum written by FIRALL as input.

OPERATING MANUAL DIAGRAM

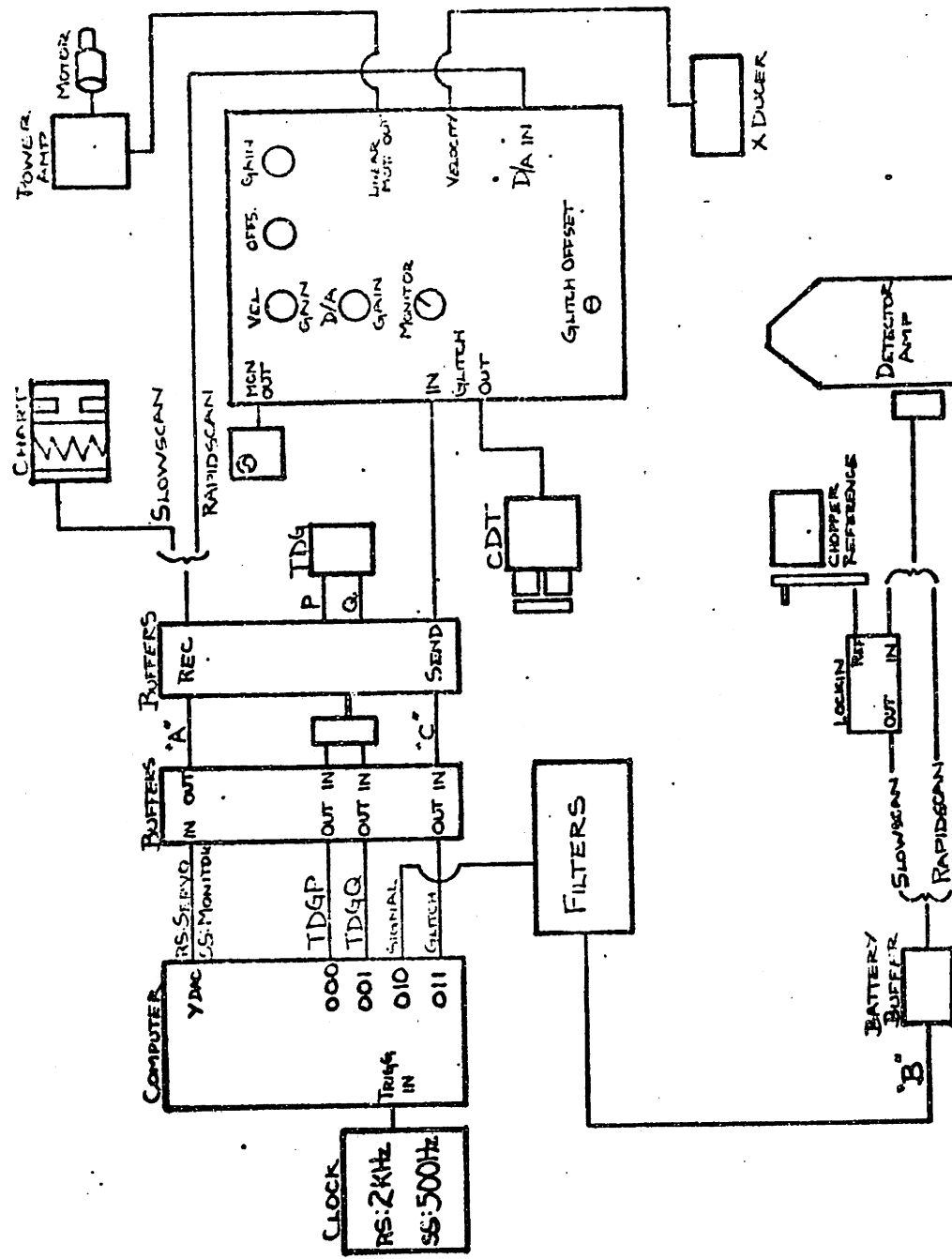


Figure 70